DESIGN AND DEVELOPMENT OF AN EXPERIMENTAL APPARATUS FOR HARDWARE-IN-LOOP TESTING OF SOLAR ASSISTED HEAT PUMP SYSTEMS

by

George Benzion van Arnold

A thesis submitted to the faculty of
The University of North Carolina at Charlotte
in partial fulfillment of the requirements
for the degree of Master of Science of
Applied Energy and Electromechanical Systems

Charlotte

2020

Approved by:

_____
Dr. Weimin Wang

_____
Dr. Aidan Browne

_____
Dr. Wesley Williams

ABSTRACT

GEORGE BENZION VAN ARNOLD. Design and Development of an Experimental Apparatus for Hardware-in-loop Testing of Solar Assisted Heat Pump Systems. (Under the direction of DR. WEIMIN WANG)

Growing concerns related to the environmental impacts of rising global energy consumption compel the continued development of low-emission technologies for the building sector. In the United States, space conditioning and domestic hot water generation account for over half of residential energy end use, with natural gas as the predominant fuel source for heating in much of the country. Solar-assisted heat pump (SAHP) systems offer a promising alternative to meet these demands more sustainably. In combination with thermal storage, these systems utilize renewable solar energy to enhance the performance and range of application of heat pump technologies. SAHP systems include a variety of design configurations and functionalities.

In this thesis, a concept for a multifunction, indirect, solar-assisted heat pump (MISAHP) system is presented which relies on the utilization of the solar collector array both to absorb and reject thermal energy to deliver both heating and cooling functions for a residential structure. An experimental apparatus is designed and built to facilitate the study of this concept using a hardware-in-loop (HIL) methodology, which combines major advantages of computer simulation and field testing.

The apparatus includes an 11.6kW (3.3ton) capacity water-to-water heat pump, 409L (108gal) thermal storage tank, 288L (76gal) domestic hot water tank, two variable speed circulation pumps, and emulation hardware representing a solar collector array and conditioned building space. Each emulator utilizes a pair of brazed-plate heat exchangers, connected to plant heating and chilled water loops, to provide a thermal source and sink for laboratory testing. The salient feature of this design lies in its flexibility. A complex network of piping and electronic diverting

valves are used to create various energy flow paths to support fifteen different operational modes for space heating, space cooling, domestic hot water generation, and energy storage charging. This design is intended not only as a platform for research of the MISAHP system concept, but also allow for similar testing of less-complex related SAHP configurations. The apparatus is heavily instrumented for temperature and flow measurement, including thermocouple probes installed at the inlets and outlets of all major components, specialized thermocouple probes used to monitor thermal stratification in both tanks, and induction-style flow meters to accompany both circulator pumps and at the discharge outlet on the domestic hot water tank. Control and data acquisition are predominantly managed using National Instruments hardware and LabVIEW software.

The experimental apparatus is installed, commissioned, and tested in the E.P.I.C. Solar Lab at the University of North Carolina at Charlotte. Basic functionality of control and operation is verified for significant elements of the laboratory setup. As demonstrated through testing of four different operational modes and domestic hot water withdrawal emulation, the experimental apparatus is ready to support future research of SAHP systems.

ACKNOWLEDGEMENTS

The completion of this thesis would not have been achievable without the support and guidance of my family, friends, instructors, and colleagues. To those as follow, I would like to express my deepest appreciation and gratitude:

To the AOSmith corporation and Michael Giordano of McKenny's Inc. for their generous donations of materials for this project.

To Bryan Fagan of Murray Supply Co. for his exceptional customer service and patience with returns and exchanges, and to Robin Moose of UNCC for her time and efforts in ordering and receiving equipment.

To the faculty at UNCC, particularly Dr. Aidan Browne, Dr. Maciej Noras, Dr. Jerry Dahlberg, and Franklin Greene for their thoughtful instruction, expert advice, and troubleshooting assistance at various stages in this project, and throughout my graduate school experience.

To my long-time friend Kyle Jonson for his encouragement (and commiseration), and to my colleague Don Gariepy for his comradery and efforts to include me in industry networking and educational activities.

To my parents for raising me to value science and hard work in the pursuit of knowledge.

To my advisor, Dr. Weimin Wang, for his compassionate guidance and remarkable dedication to my success, both academically and personally.

And finally, to my wife, Jacqueline, for her infallible patience, unconditional love, and unwavering support which, above all else, made this endeavor possible.

TABLE OF CONTENTS

LIST OF TABLES

LIST OF FIGURES

CHAPTER 1: INTRODUCTION

1.1 Overview/Energy Outlook

Population growth and the rise of urbanization have contributed to an accelerated increase in energy demand. In 2018, worldwide energy consumption grew by 2.3%, a rate of increase nearly double that of the average over the preceding decade (IEA 2018). Throughout recent history, fossil fuels such as oil, natural gas and coal have consistently supplied the dominant share of the world's energy, accounting for greater than 80% of overall consumption as recently as 2015 (Schiffer, Kober, and Panos 2018). These resources are considered non-renewable, and despite the historically steady increase in their production, concerns related to the finite nature of their supply are growing as demand continues to rise. Additionally, the scientific community has reached the consensus that emissions resulting from the combustion of fossil fuels are contributing to changes in the composition of the earth's atmosphere, with dire consequences immanent. Energy-related CO2 emissions rose by 1.7% in 2018, following an established trend of exponential growth since the industrial revolution (IEA 2018). Greenhouse gasses (e.g. carbon dioxide and methane) trap heat in the atmosphere. Increasing concentrations of GHGs have caused a gradual increase in average global temperatures, accompanied by augmented regional weather extremes. Although the dynamics of climate change are inherently complex and the effects are not yet fully understood, serious implications are already apparent. Recent evidence suggests that even radically aggressive efforts to reduce emissions will not prevent a significant rise in average global temperature over the next 30 years (Aijazi and Brager 2018). As the world's oceans warm, polar ice is melting at an alarming rate, and coastal communities across the globe are beginning to experience the effects of rising sea levels and conditions that favor increasing severity and frequency of extreme weather events. Changing climate patterns have altered critical ecological structures, threatening biodiversity as habitat degradation influences

deviated migratory patterns and accelerated extinction rates for sensitive species. Furthermore, these effects are compounded as the destruction of plant life weakens the planet's primary mechanism for natural regulation of CO_2.

1.2 Motivation for Research

With climate change representing arguably the most significant challenge faced by modern society, mounting evidence affirms the need for expedient and comprehensive action to counteract its effects. While advances in renewable energy technologies offer a cleaner alternative to fossil fuels; political, economic, and practical considerations will continue to impede the transition. Acknowledging the intermittent availability of solar and wind resources, and the strain they place on energy infrastructure, it is theorized that a successful strategy to mitigate the effects of climate change must include not only a shift to renewable power production, but also substantial efforts to improve the efficiency of energy consumption across all sectors.

Globally, energy use in buildings may account for as much as 40% of total consumption, recently surpassing demands from industrial and transportation sectors in many developed nations (Pérez-Lombard, Ortiz, and Pout 2008). Similarly, roughly 40% of global greenhouse gas emissions can be attributed to buildings (Aijazi and Brager 2018). As modern technology and standards of comfort have evolved contemporaneously, space conditioning has claimed a growing share of total energy end-use. In 2015, the EIA reported that residential dwellings accounted for 55% of the energy consumed by the building sector in the United States. Furthermore, roughly half of that energy was used for space conditioning or DHW preparation (EIA 2015).

Due to the fundamental relationship between energy demand for space conditioning and environmental factors such as temperature, humidity, precipitation, and insolation, future

trends in building energy use will be directly influenced by the effects of climate change, forcing the adaptation of building design to increasingly extreme and variable environmental conditions.

Overall, greater than 50% of U.S. households use natural gas for heating, a trend which is even more pronounced in regional data excluding the southern United States, where winters are generally mild (EIA 2015). Given the prevalent use of natural gas, and the associated environmental concerns, innovative alternative technologies that utilize renewable energy sources without sacrificing occupant comfort are of great interest. In this regard, solar-assisted heat pump systems represent a promising solution, coupling the high electrical efficiency of heat pumps with renewable solar energy. Previous studies of SAHP systems have indicated their potential to significantly reduce the consumption of fossil fuels for space heating and domestic hot water preparation in many regions, including colder climates (Chu and Cruickshank 2014). Furthermore, SAHP systems with thermal energy storage capacity are ideal candidates for the implementation of innovative load shifting strategies made possible by the contemporary evolution of smart energy grids and Internet-of-Things (IoT) technologies. Load shifting with heat pumps and thermal energy storage offers economic benefits associated with peak-demand shaving, enhanced grid stability without costly infrastructure changes, and an increased potential for self-consumption in microgrids (Laveyne et al. 2014).

In recent years, increasing attention has been given to the development of an integrated concept for SAHP systems to perform multiple functions, including space heating, space cooling, DHW preparation and electricity generation. The inherent complexity of a multi-function system creates substantial challenges for performance evaluation, which is necessary to justify investment costs for consumers. Any innovative SAHP design and associated controls, once developed, must be tested and validated before being deployed in the field at scale. This thesis

intends to develop an experimental apparatus to address the need for laboratory testing of SAHP systems.

1.3 Scope of Study

The delivery of this thesis includes a review of the literature and existing research related to the various components and configurations utilized by solar-assisted heat pump systems. SAHP system classification, functionality, and application are investigated to inform design decisions in the development of a concept for a multifunction, indirect solar-assisted heat pump system for residential space heating, cooling, and DHW preparation. The design concept includes novel characteristics intended to enhance system performance. An experimental apparatus has been constructed using commercially available equipment to demonstrate the operation of the proposed system concept under simulated boundary conditions. The laboratory setup utilizes existing building thermal plant facilities as an energy source and sink for the physical emulation of a simulated hydronic space conditioning load and solar collector assembly. DHW tapping profiles are simulated by using flow-regulated discharge. System control and data acquisition are managed using LabVIEW. Although automated control, quantitative performance evaluation and optimization are beyond the scope of this thesis, ample consideration has been given to facilitate future laboratory testing of the proposed system in various operational modes using a hardware-in-loop methodology, including extensive instrumentation to measure temperature development, thermal stratification in storage, and fluid flow rate.

CHAPTER 2: LITERATURE REVIEW

2.1 SAHP Functionalities and Applications

For residential applications, SAHP systems may be configured to perform any or all of three basic functions, including domestic hot water preparation, space heating and space cooling. If photovoltaic-thermal (PVT) collectors are used, electricity is generated as well. In a survey conducted between October 2011 and September 2012, participants of T44A38 reported that among commercially available SAHP systems for residential applications, a relatively small proportion of SAHP systems surveyed were designed for DHW preparation exclusively. In contrast, a vast majority featured both space heating and DHW functionalities. Furthermore, over half of those systems were reported to feature a capacity for space cooling, roughly split between active and passive designs. It is worth noting that 123 out of the 132 systems included in the survey featured multiple energy sources, in addition to the solar collector. Although not expressly stated by the authors, this suggests that the reported cooling functions were largely accomplished using parallel ground-source or air-source heat pump operation, not by using the solar collector as a heat sink (Ruschenburg, Herkel, and Henning 2013).

2.2 Major Components of SAHP Systems

2.2.1 Heat Pumps

A heat pump is a device that transfers thermal energy from a lower temperature reservoir to a higher temperature reservoir. This function requires external energy input, the form of which separates heat pump technologies into two basic categories requiring either mechanical or thermal energy to drive operation. Heat pump technologies in the first category utilize a vapor compression cycle, while those in the second category take advantage of adsorption or chemical reaction cycles. Heat pumps are unique in their ability to recirculate both environmental and

waste heat into the production process, enabling them to achieve heating and cooling of thermal loads with unrivaled efficiency (Chua, Chou, and Yang 2010).

Vapor compression heat pump systems include four basic components; a compressor, condenser, expansion valve, and evaporator. The compressor is a type of pump used to push a refrigerant working fluid through the system. The refrigerant enters the condenser in a gaseous state, where it condenses into a liquid, changing phase as heat energy is released to the surroundings. Next, the refrigerant passes through the expansion valve, which causes a significant drop in pressure and temperature. The low temperature, low pressure refrigerant then moves through the evaporator, where it vaporizes into a gaseous state as heat energy is absorbed from the environment. The thermochemical properties of refrigerants enable this process to move latent heat energy in opposition to the natural flow from hot to cold. Many heat pump systems include a four-way reversing valve, allowing the evaporator and condenser components to perform alternating functions to move heat energy in either direction (Demirel 2016).

Heat pumps are used to exchange heat energy between a variety of thermal reservoirs. Energy sources and sinks for heat pumps include air, liquids, and the ground. For building systems, typical applications include energy transfer to or from a conditioned interior space or thermal storage vessel. Evaporator and condenser designs vary depending on the source medium utilized, for example an air-cooled radiator for air-source heat pumps, submerged water-cooled heat exchanger for water-source heat pumps, or subterranean ground loop for ground-source heat pumps (McQuiston, Parker, and Spitler 2005).

Many heat pump systems incorporate a supplementary heat source to assist in meeting demand under high load conditions. These systems are called bivalent, while systems in which the heat pump alone is responsible for meeting demand are called monovalent systems. Bivalent systems

are typically designed with a heat pump capacity sized for just 20-60% of the maximum anticipated heating load, often drastically reducing their initial cost while still allowing the heat pump to cover a substantial portion of annual heating demand. Common supplementary heat sources include electrical resistance heaters and oil- or gas-fired furnaces (Chua, Chou, and Yang 2010).

In the past two decades, innovations in heat pump component designs have shown great potential for reducing energy use in buildings. Chua et al. (2010) presented a review of advancement in heat pump technologies with a focus on efficiency improvements for mechanical vapor compression designs. Traditionally, heat pumps of this variety employ a single compression stage. Compound or cascaded systems that include two or more compression stages have demonstrated performance advantages over single compression stage systems. Benefiting from smaller compression ratios and higher compression efficiencies at each stage, a multistage heat pump delivers a greater refrigeration effect. As a result, multi-stage compression systems are capable of efficient operation at lower temperature extremes. Multi-stage evaporation has also been investigated, where refrigerant vapor exiting the condenser is split into high- and low-pressure streams and delivered to multiple evaporators, increasing the physical area available for heat transfer. Experimental results have suggested substantial improvements in efficiency with the addition of a second evaporator. Compressor efficiency is another key factor affecting system performance. Various alternatives to conventional reciprocating compressor designs have been introduced in recent years, including scroll and revolving-vane compressors, which offer improved efficiency and reliability. (Chua, Chou, and Yang 2010).

HCFC, also called R-22, is the most commonly used refrigerant in modern heat pump systems. R-22 has a relatively low potential for environmental harm as compared to refrigerant compounds

utilized in the past; however, it still contains chlorine, which is a known catalyst for ozone depletion. For this reason, efforts to identify replacements with comparable thermochemical properties are ongoing. In addition to addressing environmental concerns, alternative refrigerant compounds such as R410A, R33A, and HFC mixtures including R170/R290 have demonstrated a potential for improved energy efficiency in operation (Chua, Chou, and Yang 2010).

Better designs and alternative refrigerants have enhanced the performance of heat pumps over a broader range of operating conditions, giving license to a multitude of new and exciting applications. The coupling of heat pumps with renewable energy sources including solar and geothermal systems, as well as novel concepts for industrial and agricultural drying processes, desalination, and cogeneration can contribute significantly to future reductions in energy consumption and greenhouse gas emissions.

2.2.2 Solar Collectors

Energy from the sun reaches the earth in the form of electromagnetic radiation. Solar radiation in the spectrum of wavelength from 0.1 to 100 microns creates a heating effect and is classified as thermal radiation (McQuiston, Parker, and Spitler 2005). Solar thermal collectors absorb thermal radiation and transfer the resulting heat energy to a working fluid (e.g., water or air), which is used to transport that energy for immediate use or storage. A variety of solar collector designs exist, many of which can be effectively integrated with SAHP systems.

The most basic solar collector design is the unglazed collector. In an unglazed collector, a working fluid contacts or passes through the device, which is constructed from a material that readily absorbs thermal radiation from the sun. As a fundamental characteristic of unglazed collectors, thermally conductive elements of the device are exposed to ambient air and are subject to relatively high convective heat transfer with their environment. As a result, the

operational performance of unglazed collectors is heavily dependent on the relative temperature of the working fluid to that of the ambient air. Unglazed collectors experience diminishing solar gains for operation above ambient temperatures, and improved performance for operation below ambient. For this reason, unglazed collectors are appealing for applications with moderate to low heating demands, and are most suitable for SAHP designs which utilize collectors as air source heat exchangers in the absence of solar irradiance (Hadorn 2015).

Glazed flat-plate solar collectors consist of a thermally conductive manifold or network of piping enclosed in an insulated housing and covered with a transparent glazing. Thermal radiation penetrates the glazing, where it is absorbed by the conductive elements which transfer heat energy to a working fluid as it passes through the device. Because the conductive elements are insulated from their environment, glazed flat-plate collectors experience far less convective heat loss as compared with unglazed collectors, contributing to superior efficiency at operating temperatures significantly higher than the ambient. Glazed flat-plate collectors are desirable for applications with greater heating demands such as direct space heating and DHW preparation (Hadorn 2015).

Evacuated tube solar collectors utilize a liquid-vapor phase change material to capture solar heat energy. U-shaped copper pipes containing the phase change material are enclosed in vertically pitched glass tubes that connect to a horizontal header pipe at the top of the assembly. Absorbed solar energy vaporizes the phase change material, carrying it upwards through the evacuated tube to the header. The vapor condenses in the header, where heat exchangers extract energy for delivery to the load. The glass tubes of the collector are evacuated to insulate the absorber elements from the environment, and feature a selective absorbing surface coating. These features allow evacuated tube collectors to deliver high heat extraction efficiency at temperatures above 80^{o}C, making them very useful to supply higher

heating loads required for DHW preparation and space conditioning in residential systems (Sarbu and Sebarchievici 2017a).

Photovoltaic-thermal, or "PVT," collectors combine photovoltaic and solar thermal components to produce electricity and useful heat simultaneously. Photovoltaic cells convert a portion of incident solar radiation into electricity. Two semiconductors are formed in a junction. When the component is exposed to light, photon energy excites electrons in the top semiconductor, developing an electric potential across the junction which can be used to drive an electric current. This effect occurs only for electromagnetic radiation in a particular range of wavelengths, as determined by the characteristics of the semiconductor material in use. A typical photovoltaic cell may convert only 4-17% of incident solar radiation to electricity, while the remainder is converted to heat, raising the operating temperature of the cell. Due to the thermochemical properties of semiconductors, higher operating temperatures are associated with lower electricity generation efficiency in photovoltaic cells. PVT collector designs utilize air or liquid cooling to transfer excess heat from photovoltaic cells to a working fluid, improving electricity yield while simultaneously harvesting heat energy to be distributed for use elsewhere. Thermal performance is inherently lower for PVT collectors than conventional thermal collectors due to the portion of absorbed solar energy which is converted to electricity, however electricity generated serves to offset the electrical demands of associated system components. Particularly in applications where heating demand is low, this factor may reflect an overall advantage from the perspective of whole system performance. (Chow 2010).

Thygesen and Karlsson (2013) compared the performance of solar-assisted heat pump systems for space heating and DHW preparation with different collector types. Numerical models were developed in TRYNSYS based on an existing near-zero energy residential building located in Sweden featuring radiant heating and a ground source heat pump. Using these models, cost and

energy savings were estimated for three scenarios: PV panels only, flat-plate solar thermal panels only, and both PV and thermal panels. Additionally, three energy billing schemes were considered, including instantaneous metering, daily net metering, and monthly net metering. TRYNSYS simulation results showed that irrespective of the metering scheme, the scenario incorporating the addition of solar PV collectors outperformed those incorporating flat-plate solar thermal collectors, delivering a superior solar energy utilization and more considerable long-term cost savings. The scenario including both solar PV and solar thermal collectors demonstrated competitive energy savings, however higher equipment and installation costs limited the potential return on investment. Recognizing the performance limitations highlighted in this study as an example of a potential application for PVT collectors, further investigation is necessary to assess the potential for their integration with SAHP systems (Thygesen and Karlsson 2013).

Some solar collectors, specifically engineered for use with SAHP systems, are designed to function directly as the evaporator of the associated heat pump. In these collectors, a refrigerant is used as the working fluid, and the body of the collector is designed to facilitate heat exchange to ambient air in addition to conversion of solar thermal energy. SAHP systems where the refrigerant is circulated through the collector are referred to as direct-expansion systems. In contrast, those utilizing more conventional collector designs with a working fluid such as water, brine, or antifreeze solutions are called indirect-expansion systems, referring to the indirect coupling of the heat pump to the collector. It is worth mentioning that direct-expansion systems have high up-front investment costs due to the use of specialized equipment and the labor associated with field connection of refrigerant lines, which must be performed by specially trained refrigeration mechanics (Bridgeman 2010).

Solar thermal collectors are primarily used for heating applications; however, they can also be utilized for cooling. Under certain conditions, mostly dependent on the local moisture content of the atmosphere, the rate of heat loss from a thermal mass to the night sky by long-wave radiation in the range from 8-13 microns (known as the atmospheric transparency region) can exceed the rate of conductive and convective absorption, resulting in cooling of the mass to sub-ambient temperatures. In most regions, the average tropospheric temperature is well below 0^{o}C year-round, allowing for effective nocturnal radiative cooling even in summer months under clear sky conditions (Sun et al. 2017). Solar thermal systems can be designed to take advantage of this principle to deliver a cooling function by circulating a working fluid through the collectors at night, rejecting heat energy accumulated during the day to the night sky. While research related to radiative cooling with SAHP systems is lacking, numerous studies have investigated this technique for conventional solar thermal systems, with some experimental results demonstrating cooling power delivery in the range of 20-80 watts per square meter of collector surface (Xu, Niu, and Guohui 2015). The integration of radiative cooling techniques and SAHP systems could enable even further potential for energy savings in cooling.

2.2.3 Thermal Energy Storage

Energy storage provides a means of balancing energy demand and production, a critical consideration for efficient solar thermal systems given the time-dependent nature of solar irradiance and an inverse relationship with ambient temperature. Energy demand for space conditioning is determined by the rate of heat transfer through the building envelope, which is mostly influenced by the differential of indoor and outdoor ambient temperatures. Inherently, energy demand for space heating is higher when ambient temperatures are low, and similarly, energy demand for space cooling is higher when ambient temperatures are high. Hourly and seasonal variation in ambient temperatures is mainly dependent on incident solar irradiation,

contributing to the infamous mismatch between energy production and demand timing in solar energy systems.

These concerns are mitigated in solar thermal systems through the integration of thermal energy storage. Heat energy captured by solar collectors may be transferred utilizing a working fluid to a storage medium for later use, thus allowing the system to take advantage of solar energy when it is available, independent of concurrent heating and cooling loads. A myriad of thermal storage methods are available to satisfy a wide range of design specifications for capacity and storage period. While thermal storage devices most commonly store energy sufficient to meet the demand for several hours, larger systems have been engineered to address the imbalance between supply and demand over weeks or even months for seasonal storage (Sarbu and Sebarchievici 2017b).

Heat energy can be stored in sensible, latent, and chemical forms. Sensible thermal energy storage is the most straightforward approach, where the stored thermal energy is proportional to the mass and temperature of the storage medium. In contrast, for latent thermal storage, heat energy is absorbed or released by a storage medium as it changes phase, while the temperature of the medium remains constant. Phase-change materials, or PCMs, for thermal energy storage utilize the transition between solid and liquid states. Liquid to gas phase-change processes are impractical for energy storage due to the high degree of variation in volume and pressure of the medium. Chemical energy storage involves the capture and release of heat as part of a chemical reaction resulting in a change in the internal energy of the medium. (Demirel 2016).

Thermal storage devices used in SAHP systems are primarily based on sensible heat storage, although phase-change and thermochemical processes have also been utilized. Water is by far the most common storage medium for these systems, a trend that can be attributed to the

minimal cost, high specific heat, and nontoxicity of this medium. In the range of temperatures typical for domestic applications, water has a sensible heat storage capacity of 70 kWh/m^3 (Ruschenburg, Herkel, and Henning 2013). Water for thermal energy storage is typically contained in pressurized metal tanks. Sacrificial anode rods, dielectric unions and protective linings are standard features to inhibit corrosion, a common cause of failure for storage tanks. Insulation is an important design consideration, as the rate of heat loss from the storage medium to the ambient has significant implications for the efficiency of a system. U-values from 0.3-0.5 W/m^2K are standard for water tank insulation, and thermal bridges are avoided where possible (Ruschenburg, Herkel, and Henning 2013).

Charging and discharging of thermal storage can be accomplished directly by circulating the water through the storage tank, or indirectly via a heat exchanger, located either inside or outside of the tank. While components used for direct transfer are simpler in design and typically lower cost, indirect transfer is required for installations that use non-potable water in the collector for freeze protection (Hadorn 2015).

In a most SAHP systems, thermal storage is utilized for DHW preparation as well as for space conditioning. Due to the discrepancy in operating temperature ranges for these subsystems, many configurations involve distributed thermal energy storage, with one dedicated tank for DHW preparation and a separate auxiliary storage tank often referred to as 'buffer' or 'float' storage. The user-defined setpoint for hot water draw, typically around 50^o C, is maintained in the DHW tank or accomplished with a tempering valve at the storage outlet by mixing hot water from the tank with cold water from the potable supply. Temperature levels in the auxiliary storage tank float up and down with fluctuations in solar radiation and load demand as control strategies work to capture solar energy whenever available. An alternative storage configuration commonly selected for space-restricted applications involves the use of a single thermal storage

vessel to serve DHW and space-conditioning demand. These combined, or 'combi-storage', devices rely heavily on thermal stratification to achieve the desired outlet temperatures corresponding to the two functions served (Hadorn 2015).

Stratification occurring in thermal storage tanks is characterized as the natural development of a vertical temperature gradient driven by the dependency of fluid density on temperature. Thermal stratification in storage is highly beneficial for solar thermal systems, allowing for lower collector inlet temperatures with the heat-carrying fluid supplied from the bottom of the storage vessel. Similarly, heat energy transferred to the storage accumulates in the upper region, increasing thermal capacity, and providing a high-energy reservoir from which to extract useful heat for space conditioning or DHW preparation. The stability of thermal stratification has a pronounced impact on the charging and discharging efficiency of the storage tank, with more significant disturbances contributing to substantial degradation in overall system performance. For this reason, the physical characteristics of thermal storage devices that influence the stability of stratification are an important consideration in solar thermal system design (Li et al. 2018).

For configurations where the working fluid is circulated through the storage device directly, inlet velocity has a substantial effect on the disruption of thermal stratification. Perforate or slotted inlet structures and internal baffles made with plates or porous mesh have been shown to assist in limiting the magnitude of disturbance. In contrast, for systems utilizing internal immersed heat exchanger coils, convection is the primary driver for disturbance of the temperature gradient. Both the form and positioning of internal heat exchanger coils affect the stability of stratification (Li et al. 2018).

Li et al. 2018 investigated the thermal stratification characteristics of six water storage tanks with different shapes. Heat energy was delivered to each of the tanks through an internal heat

exchanger coil. Experimental results indicated that circular-truncate-cone shaped tanks performed better than cylindrical tanks, and spherical tanks performed worst. Notably, while increasingly uniform temperature distribution consistently delivered reduced charging efficiency, storage devices which developed the highest levels of thermal stratification did not always achieve greater performance, indicating contributing factors affecting charge efficiency in addition to thermal stratification (Li et al. 2018).

2.3 SAHP Configurations

A wide variety of SAHP system concepts have been proposed and discussed in the literature, including several excellent review papers (Buker and Riffat 2016, Chu and Cruickshank 2014, Kamel, Fung, and Dash 2015, Mohanraj et al. 2018, Wang et al. 2020). As mentioned previously, a primary distinction based on the coupling of the heat pump to the solar collector separates system concepts into two categories; direct and indirect expansion types. In direct expansion systems, the refrigerant is circulated through a specialized solar collector, which acts directly as the heat pump's evaporator. In contrast, indirect expansion systems feature water, brine, or antifreeze as a working fluid, with the evaporator of the heat pump indirectly coupled to the solar loop. Further distinctions among SAHP systems reflect the broad range of individual component designs utilized, various configurations, differing modes of component interaction, and operational utility performed. Frank et al. (2010) examined the defining features of existing SAHP system concepts and suggested several approaches for systematic classification. While recognizing that additional aspects of the examined systems could be used to differentiate them further, the study identified critical parameters for system classification, including the energy sources and sinks of the heat pump (e.g., water, air, and ground), solar collector type (e.g., unglazed thermal collectors, flat-plate thermal collectors, and PVT collectors), and storage concept (e.g., single tank, dual tank, and borehole). Additionally, Frank et al. (2010) reported

three distinctive types of interaction among system components, namely serial, parallel, and regenerative. It is worth noting that these characteristics are non-exclusive, with many system concepts supporting operation in more than one of these interactive modes (Frank et al. 2010). For indirect SAHP systems, serial operation refers to configurations where the solar collector acts as the source for the heat pump. Solar heat energy is delivered to the evaporator of the heat pump through the solar loop, or by way of an intermediate thermal storage device. Parallel operation refers to configurations where energy is delivered to the load from multiple sources. For example, the heat pump may supply energy from a ground or air source heat exchanger to the load, independent of additional energy supplied from the solar collector. In a parallel configuration, the heat pump is not used when available solar energy is sufficient to meet the heating demand. Regenerative operation, found mostly in ground-coupled systems, refers to configurations where the solar collectors supply energy to the main source of the heat pump (Hadorn 2015).

2.4 Approaches to Study SAHP Systems

Computer simulation is a common approach to evaluate the performance of dynamic systems. Numerical models are developed through individual component testing and are used to estimate system response under various operating conditions. Many valuable analytical studies using computer simulation have been conducted in recent years related to performance and thermoeconomic optimization, as well as life-cycle cost evaluation of SAHP systems (Calise et al. 2016, Cai et al. 2016, Wang et al. 2011, Torres R, Picon Nuñez, and Cervantes de G 1998, Razavi, Ahmadi, and Zahedi 2018).

Several software platforms such as TRNSYS and EnergyPlus are available to support computer simulation of SAHP systems (Huang et al. 2018). Numerical models developed using these platforms have previously been validated for many SAHP system components and building

structures, facilitating the development of simulation models for assembled systems. Once developed, these models can be used for system design, control strategy development, and system performance assessment. Although computer simulation has the advantages of low cost and excellent repeatability, model fidelity is of some concern. In many cases, single-component testing of solar collectors, heat pumps, and boilers may not be adequate for predicting transient behavior in assembled building systems. Factors such as on-off cycling of auxiliary heaters, efficiencies of pumps and motors, runtime and standby losses, control strategies, and quality of installation practices have been shown to impact overall system performance substantially, and are not easily anticipated in simulation (Haller et al. 2013).

Field testing is another approach to evaluate dynamic systems. The performance of a complete installed system is monitored on-site under real operating conditions, and the data analyzed. Many researchers have utilized field testing in the study of SAHP systems (Kong et al. 2018, Besagni et al. 2019, Kuang and Wang 2006, Shan, Yu, and Yang 2016). Field testing can be very costly to implement, and the repeatability and comparability of results are extremely limited due to the change of boundary conditions over time and the unique characteristics of any particular installation. Nevertheless, because field testing provides the most accurate and reliable performance data possible, this method is widely used in product development (Huang et al. 2018).

The methods of field testing and simulation can complement each other by synergistically combining hardware and software in hardware-in-the-loop (HIL) simulation. HIL involves the operation of real physical components in connection with real-time simulated components. Depending on the experimental needs, the hardware can be a controller, a single piece of equipment that performs specific physical tasks (e.g., water movement by a pump or solar energy collection by a solar collector), or an integrated system. A successful experiment using

hardware-in-loop methodology combines many of the desirable aspects of pure simulation and field testing, delivering a high level of accuracy and repeatability, at a relatively low cost. Following extensive utilization in the automotive and power electronics industries, HIL testing has recently gained popularity among researchers of building systems and controls (Haller et al. 2013).

Controller-in-the-loop testing, or CIL, is an application of HIL methodology where the controller is only hardware component tested. In the context of building systems, CIL testing involves a simulation model of an entire building, including building shell, internal loads, and HVAC components coupled to a test controller through an interface in a closed loop. The interface performs the data conversions necessary for the control hardware to communicate with the simulation. Digital signals representative of the test conditions are output from the simulation, converted to analog, and supplied to the sensor input terminals of the controller, while analog signals from the controller are converted to digital and fed back into the simulation (Huang et al. 2018).

HIL experiments incorporating other system components in addition to controllers are more complicated. Relevant parameters such as water temperatures and flow rates must be replicated physically based on outputs from the simulation. Additional devices such as pumps, heat exchangers, mixing valves, and resistance heating elements may be incorporated into test equipment for this purpose, and appropriate measurements must be obtained to confirm that accurate test conditions are produced. (Haller et al. 2013).

Whole system testing, or WST, is a highly comprehensive subset of HIL methodology that tests complete systems under simulated boundary conditions representative of the full range of potential operating conditions. Results from WST can be used to extrapolate transient behavior and energy consumption of a complete system for nominal boundary conditions throughout an

entire year. In the context of WST for building systems, hardware-in-the-loop is comprised of all system components typically installed inside a building, including storage tanks, pumps, valves, controllers, auxiliary heating units, and all devices related to DHW preparation. For systems utilizing air source heat pumps, the air source heat exchanger may be installed in a climate chamber. Solar collectors are not included as hardware-in-the-loop. Instead, solar collector behavior is simulated and emulated, allowing for reproducible test conditions. Per EN12975-2, collector simulation models must account for collector reference area, zero loss efficiency, linear and quadratic heat loss coefficients, specific heat capacitance, incidence angles, pressure drop, mass flow rates, and the effects of condensation or frosting where applicable. WST follows a test sequence comprised of a set number of consecutive test-days, which each correspond to a real day of the year, based on one climate profile and one definition of DHW and space conditioning loads. Additional run time may be desirable for system pre-conditioning or post-check, to insure against potentially misleading discrepancies in the state of energy of the system at the start and end of the test period, which would otherwise necessitate a comprehensive evaluation of the internal energy balance of the system. WST results are valid only for the climate and load profile tested. Subsequent tests involving alternative system configurations or climate profiles should use identical load definitions to facilitate comparison. Energetic performance of a system is determined from test results, including the total electricity and fuel consumption and the ratio of useful energy output divided by total consumption of purchased energy. Additionally, fractional energy savings are evaluated as compared to a comparable reference system not incorporating renewable energy sources (Haller et al. 2013).

Typically, HIL experiments have utilized a hardware interface, consisting of analog-to-digital and digital-to-analog converters; however, an alternative method employing software interface may offer some advantages. Simulation processing speed and hardware sampling frequency are

critical considerations for HIL testing because the characteristics of the interface limit the rate of signal exchange, which seeks to approximate real-time operation. A mechanism for effective time synchronization between hardware and simulation is imperative, such that the data exchanged is updated at the same time interval. This may be very challenging for some applications. A software interface eliminates the need for physical A/D or D/A converters, offering the potential for improved processing speed and simplified time synchronization, as suggested by Huang et al. (2018), who presented an HIL simulation framework utilizing a software interface based on the open-source software platform VOLTTRON. This serves as an example of a generic, scalable solution for HIL testing of building systems and components which supports high volumes of data exchange with various existing simulation programs. Because VOLTTRON has low CPU, memory, and storage requirements, this framework can be implemented at low cost using small-form-factor computers (e.g. Raspberry Pi) (Huang et al. 2018).

2.5 Relevant Experimental Work

The study of heat pump systems has received notable research investment in recent years. In this section, details of pertinent interest are presented for a selection of relevant experimental work. Their review as follows is intended to summarize consequential findings, exemplify effective research practices, and illuminate practical considerations applicable to the endeavors of this thesis.

Many studies about the development of various building heating and cooling systems have utilized whole system testing, and as such, provide relevant examples for laboratory design and experimental practice. In particular, the methodologies used for the emulation of building heating and cooling loads are of interest to this thesis.

Macdonald et al. (2015) presented a methodology for hardware-in-the-loop testing of HVAC equipment using TYRNSYS for simulation and LabVIEW for data acquisition and control. A test bench was developed to emulate a range of operating conditions typically experienced in small scale commercial hydronic systems. The set up involved a complex hydronic network forming two auxiliary loops used for source and load emulation. Three-way valves allowed for the integration of various heating and cooling devices individually or in series combinations to achieve the desired conditions. A water-to-water heat exchanger fed by the laboratory building's chilled water loop served and an energy sink, and a 54kW capacity electric boiler supplied heat energy for source and load emulation. An additional water-to-water heat exchanger and a non-reversing 100kW nominal capacity water-to-water heat pump were connected for heat energy transfer between the two auxiliary loops. An insulated storage tank of 974L was also included for each of the loops, adding thermal mass to improve temperature stability. A pair of variable-frequency-drive circulation pumps were employed to provide flexible mass flow rates up to 7.6L/s to each loop. Several PT-100 platinum resistance sensors provide feedback to the test bench controller for temperature regulation in each of the auxiliary loops. A turbine flow meter with magnetic pick-up on the inlet to the test equipment, and PT-100 platinum resistance sensors on the inlet and outlet provided measurement data of test equipment operation. Experiments were performed to verify the operation of the test bench independently and to demonstrate the imposition of simulated building loads on hardware-in-loop equipment. Results demonstrated a successful reactionary response of the simulation to measurement data, with some discrepancies in setpoint and return temperature attributed to imperfect control strategies (Macdonald et al. 2015).

In another study, De La Cruz et al. (2017) presented an HIL test bench for investigation of double service (DHW and space conditioning) air-to-water heat pump system performance. The

experimental set up included both the indoor and outdoor units for the heating system under test, and a DHW tank equipped with a backup electrical resistance heater and coupled to the system via an immersed internal heat exchanger coil. A hot tap water bench was connected to the DHW outlet to simulate DHW tapping behavior. Electronic valves regulated the hot tap water bench operation using feedback from energy and water mass flow rate sensors to achieve emulation of a DHW tapping scenario based on a profile obtained from field test data. A cooling water bench was connected to the heat pump to emulate a thermal load. A 50L mixing tank was employed for tempering of the space heating water stream exiting the heat pump with cold water from the cooling water unit to achieve setpoint temperatures corresponding to dynamic conditions in a virtual building, which was simulated with Modelica software using BuildSysPro library models. An indoor air thermostat was emulated featuring typical dead-band operation, and outdoor air temperature and solar radiation sensors installed at the location of the outdoor unit under test supplied real-time weather data inputs to the simulation. An OPC (Object linking and embedding for Process Control) server enabled communication between Modelica and a LabVIEW program responsible for physical control of the test bench. Additionally, a control management interface utilizing TCP/IP and Modbus RTU connections allowed the test bench to operate the heat pump controller as a Modbus RTU slave to modify and evaluate various system control parameters. Instrumentation to monitor system operation included water temperature sensors at the inlet and outlet of the condenser and DHW tank, three temperature sensors on the surface of the DHW tank to monitor stratification, air temperature sensors upstream and downstream of the evaporator, a power meter to monitor electricity consumption, a backup heater activation sensor, valve position sensor, and a water mass flow rate sensor. Experimental results were successful in identifying performance impacts of various control parameter

settings, demonstrating the importance of adapting heat pump control strategies to occupant behavior and building thermal profile (Tejeda De La Cruz et al. 2017).

Some studies utilizing whole system testing methods similar to those described previously have focused on SAHP systems specifically. Results from these studies have highlighted advantages and disadvantages for various system concepts and control strategies, and have revealed critical considerations for future experimentation.

Wang et al. (2011) investigated a concept for a novel indirect expansion solar assisted multifunction heat pump for space heating, space cooling, and DHW preparation. In this configuration, the solar collector directly feeds an outdoor insulated water tank. The tank is coupled to a water-cooled plate heat exchanger connected in parallel with two air-cooled fin tube heat exchangers (the indoor and outdoor coils of the heat pump). A refrigerant receiver installed on the high-pressure side of the heat pump enables refrigerant flow through the expansion valve in the proper direction for seven different operational modes, including space heating, common space cooling, common solar water heating, heat pump water heating, solar-assisted space heating, space cooling, and heat pump water heating, and energy-saving defrosting. An experimental test unit was constructed to evaluate system performance in the laboratory. All seven operational modes functioned successfully, and the system was able to transition between modes smoothly. Experimental results demonstrated highly efficient system performance for outdoor temperatures from 5-8^{o}C, indicating a great potential for energy savings as compared to conventional solar thermal systems with electrical resistance auxiliary heating in regions with abundant solar radiation throughout autumn, winter and spring (Wang et al. 2011).

Wagar (2013) developed an experimental test unit to investigate single- and dual-tank configurations of a dual-side indirect heat pump assisted solar domestic water heater system in

a thesis presented at the University of Waterloo. “Dual-side” refers to a configuration that operates in two primary modes, the first transferring energy from a solar collector to storage by way of a heat exchanger, and the second by way of a water-to-water heat pump. The test unit included a 300L DHW storage tank, 450L float tank, brazed plate heat exchanger, variable speed circulation pump, and water-to-water non reversing heat pump with a compressor rated at approximately 1-ton refrigerating capacity and dual coaxial refrigerant-to-water heat exchangers oversized with about 1.5-ton capacity to accommodate a broader range of source and load flow rates. An electrical resistance heating element in the DHW tank served as an auxiliary heat source. Two- and three-way electronic valves were used to select between the two operational modes, and to include or exclude the float tank. A floating two-way valve was utilized to regulate hot water draw from DHW storage. An electric circulation heater with a rated capacity of 6kW was employed to simulate the operation of the solar collector. Output power was controlled through a duty cycle to mimic a solar collector area of $4m^2$. Instrumentation included custom-built Type T thermocouple probes for process temperature measurement and in-tank thermal stratification monitoring, paddle-wheel style fluid flow meters, and transformer devices for measuring voltage and current delivered to the heat pump and the auxiliary resistance heating element. Control and data acquisition were accomplished using LabVIEW, with a custom virtual instrument feeding simulation parameters such as weather data and DHW draw profiles into LabVIEW from Microsoft Excel spreadsheets to provide setpoints for system control. Custom TRYNSYS models were developed in an attempt to replicate experimental performance results in simulation. Four tests were conducted to represent realistic operating conditions of the system for one day of each season in the geographic region of Ontario, Canada, and the experimental and simulated results compared and analyzed. The TRYNSYS model created was appreciably successful in predicting

experimental performance for days exhibiting lower solar irradiation; however, simulation error grew as solar fraction increased. Simulation error was most apparent for operation in heat exchanger mode, corresponding to more considerable disruption of thermal stratification. Notably, these simulation errors were compounded by the effects of control decisions based on storage temperatures. Experimental results collected also revealed significant practical limitations of the proposed system. In this configuration, the heat pump was not able to extend solar energy collection into the evening as expected. During testing, temperatures in the bottom of the storage tank were always above 45°C by late afternoon, exceeding the maximum inlet load temperature tolerance of the heat pump, preventing its operation (Wagar 2013).

Banister and Collins (2015) developed an experimental test unit to study the performance of an indirect dual tank SAHP system for DHW preparation. The test unit included a float tank, a DHW storage tank, two circulation pumps, electronic valves, and a water-to-water heat pump with a nominal capacity of 3.8kW. An electrical resistance heating element in the DHW tank served as an auxiliary heat source. Solar collector behavior was emulated with an electric circulation heater. A TRYNSYS simulation model of the system was created to assist in the development of a control strategy to select an operational mode based on source and load conditions to meet demand with the least consumption of electricity. The proposed system configuration performed energy exchange between the solar loop or float tank and DHW storage by way of a heat exchanger or water-to-water heat pump, with the solar loop charging the float tank directly at times of available solar energy in excess of demand. In all, six operational modes were enabled, including solar-DHW, solar-HP-DHW, float-DHW, float-HP-DHW, solar-float, and auxiliary DHW heating. Experimental performance results were used to tune the TRYNSYS model of the system. The calibrated model was then used to simulate the annual performance of the system for a residential application with a daily DHW draw of 300L following common use

patterns. Results suggested that with a collector area of 5m^2, the dual tank system could deliver a 6% reduction in electricity consumption as compared to a comparable Solar-DHW system with an electric auxiliary heater. Additionally, whereas conventional solar-DHW systems experience diminishing returns for increasing collector area above 7.5m^2, simulations demonstrated significant energy savings for SAHP systems with larger collector areas by comparison, which can be attributed to the additional thermal storage capacity of the dual tank system. Simulation results indicated that for a collector area of 10m^2, the dual tank SAHP system achieved 12% greater electricity savings than comparable solar-DHW systems. Impressively, this demonstrated a total reduction in electricity consumption of 75% as compared to traditional electric DHW tanks (Banister and Collins 2015).

As shown, preceding studies featuring hardware-in-loop test methodology has laid much of the groundwork to facilitate the development of the experimental set up presented in this thesis. Various communication profiles linking simulation software such as TRYNSYS or Modelica with LabView data acquisition and control have been successfully implemented to achieve source and load emulation in a laboratory. Heat energy was most commonly supplied using an electric circulation heater or boiler, and water-cooled heat exchangers were utilized for heat extraction. DHW tapping profiles were consistently simulated by controlled discharge using electronic valves. Experimental test equipment was either commissioned to design specifications, or assembled from commercially available components. System performance and efficiency were calculated from temperature, fluid flow rate, and electrical power consumption data acquired using readily available instrumentation, with pertinent attention to thermal stratification in storage.

CHAPTER 3: SYSTEM CONCEPT AND EXPERIMENTAL APPARATUS DESIGN

3.1 Functional Analysis and Description of Concept

The goal of this project is to design and build an experimental apparatus to facilitate the study of a multifunction, indirect, solar-assisted, heat pump (MISAHP) system. The underlying concept for the MISAHP system relies on the utilization of a solar array as an energy source and sink to deliver space heating, space cooling and domestic hot water generation, either directly or with assistance from a water-to-water heat pump as required to meet the needs of a residential structure and its occupants. Thermal energy storage extends the practical applications of this system by addressing the intermittence of the solar resource. Figure 1 illustrates the major components included in this concept and the energy transfer paths employed to perform the required functions in various seasonal conditions and climate regions. In addition to the configuration as shown, the MISAHP system may be coupled with PVT collectors, generating electricity to offset power consumed by the pumps, compressor, and other system components.

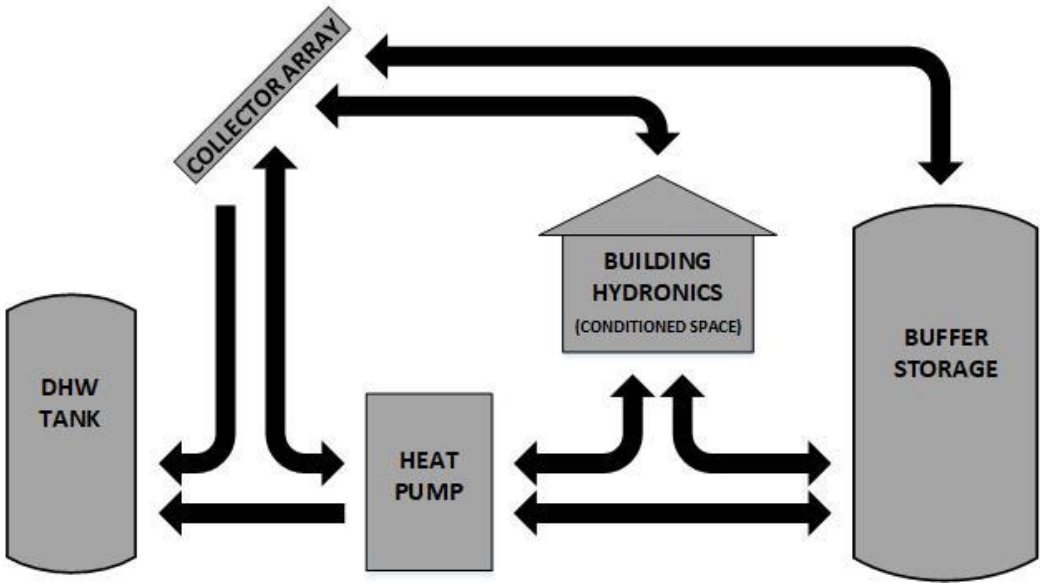

Figure 1: MISAHP System Concept

In the proposed system, major components are connected by a network of water piping. Electronic valves divert the path of the water through the various branches of system piping to allow for 15 different operational modes. The MISAHP system utilizes these modes to deliver heating and cooling functions as required for thermal comfort and domestic hot water consumption of building occupants, transferring thermal energy bidirectionally between components. The solar collectors are used both to absorb and reject thermal energy, and buffer storage extends the system's space conditioning capacity when outdoor conditions are not favorable for energy transfer at the collector.

Operational modes utilized by the MISAHP system are listed below, categorized into four groups based on primary function including DHW generation, space heating, space cooling, and energy storage. All modes are named to indicate the direction of energy transfer from left to right. Thus, for each mode, the thermal source is named first, and the thermal sink is named last. The heat pump is named between the source and sink if used to assist in the transfer of energy for that mode.

<u>DHW Generation Modes:</u>
Collector Array–> DHW Tank (CA-DHW)
Buffer Storage -> Heat Pump -> DHW (BS-HP-DHW)

<u>Space Heating Modes:</u>
Collector Array -> Conditioned Space (CA-CS)
Collector Array -> Heat Pump -> Conditioned Space (C-HP-CS)
Buffer Storage -> Conditioned Space (BS-CS)
Buffer Storage -> Heat Pump -> Conditioned Space (BS-HP-CS)

<u>Space Cooling Modes:</u>
Conditioned Space -> Heat Pump -> DHW Tank (CS-HP-DHW)
Conditioned Space -> Collector Array (CS-CA)
Conditioned Space -> Heat Pump -> Collector Array (CS-HP-CA)
Conditioned Space -> Buffer Storage (CS-BS)
Conditioned Space -> Heat Pump -> Buffer Storage (CS-HP-BS)

Energy Storage Modes:
Heating Season:
Collector Array -> Buffer Storage (CA-BS)
Collector Array -> Heat Pump -> Buffer Storage (CA-HP-BS)
Cooling Season:
Buffer Storage -> Collector Array (BS-CA)
Buffer Storage -> Heat Pump -> Collector Array (BS-HP-CA)

In this thesis, an experimental apparatus is developed to facilitate the use of hardware-in-the-loop and whole system testing methodologies to study variants of the MISAHP system concept described. The experimental apparatus is not intended to demonstrate a real residential application. Instead, it is designed to offer flexibility for testing and performance evaluation, with potential applications including component testing for validation and calibration of numerical simulation models, and hardware-in-the-loop simulation for the development and optimization of control strategies for different operating conditions, physically emulated using laboratory hardware.

The apparatus is installed in a designated portion of the solar lab in the EPIC building on The University of North Carolina at Charlotte campus. MISAHP system components, including storage tanks, circulator pumps, and the water-to-water heat pump, are installed as hardware-in-the-loop. Boundary conditions are emulated using heating and chilled water loops supplied from the university campus' plant hydronic distribution system. Plant water loops are coupled with the experimental apparatus by large capacity water-to-water heat exchangers to enable testing for a broad range of thermal load profiles. With this set-up, a simulated thermal response can be produced in the laboratory to represent solar collectors and buildings with various sizes and design characteristics. Additional considerations made in the construction of the experimental apparatus are intended to allow for future changes in system configuration to replace or modify components, incorporate additional functions, or simplify the design as deemed appropriate for continued study.

3.2 Experimental Apparatus Components

In this section, components of the experimental apparatus are described in the sequence of heat pump, buffer storage tank, DHW tank, circulator pumps, conditioned space emulator, collector array emulator, piping and mechanical accessories, instrumentation, and National Instruments (NI) hardware and software for controls and data acquisition.

3.2.1 Heat Pump

A 5-Series WaterFurnace heat pump (Catalog number: NSW040G12RCSS0AA) is used for this experimental set up. This water-to-water type package unit generates hot water in its heating mode and cold water in its cooling mode. The heat pump is designed for geothermal heating and cooling applications with a ground-coupled source loop (utilizing boreholes, trenches, surface water etc.). Although not intended by the manufacturer for use in the configuration investigated by this thesis, this unit is suitable for research of MISAHP systems, which operate based on the same underlying principles as geothermal systems. Figure 2 shows the front of the heat pump as installed in the apparatus.

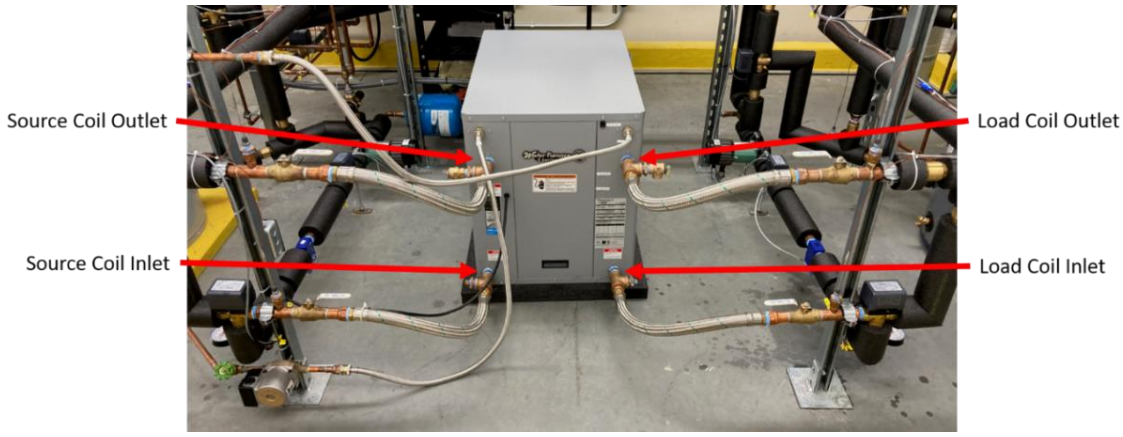

Figure 2: Water-To-Water Geothermal Heat Pump

For residential applications, the desired capacity of the heat pump is around 10.5 kW (3 tons). The WaterFurnace 5-series line includes two models in close range of this capacity: a 7.3 kW (2.5 ton) model and an 11.6 kW (3.3 ton) model. An auxiliary hot water generation feature,

described later in this section, was available only for the larger of the two heat pumps, and influenced the selection of the 11.6 kW (3.3 ton) capacity model for this project.

Table 1 provides the performance of the heat pump at rated conditions according to the ISO/AHRI/ASHRAE Standard 13256-2 (ISO 1998). Table 2 lists the operating limits of the heat pump as presented in the product manual (WaterFurnace 2020). The performance map relating the operational efficiency and capacity achieved to various source and load-side water temperatures and flow rates is provided in APPENDIX A: HEAT PUMP PERFORMANCE TABLES

Table 1: Heat Pump Performance at Rated Conditions

Application	Rating Condition	Capacity (kW)	EER for Cooling (Btu/h/W)	COP for Heating (-)
Water Loop Heat Pump	Cooling (30°C Source, 12°C Load)	10.5	15.5	NA
	Heating (15°C Source, 40°C Load)	14.0	NA	4.8
Ground Water Heat Pump	Cooling (15°C Source, 12°C Load)	12.0	23.4	NA
	Heating (10°C Source, 40°C Load)	11.5	NA	3.9
Ground Loop Heat Pump	Cooling (25°C Source, 12°C Load)	11.0	17.5	NA
	Heating (0°C Source, 40°C Load)	8.9	NA	3.1

Table 2: Heat Pump Water Temperature Limits (WaterFurnace 2020)

Operating Limits	Water Temperature (°C)	
Source-side	Cooling	Heating
Min. Entering	-1.1	-6.7
Max Entering	43.3	32.2
Load-side	Cooling	Heating
Min. Entering	10	15.6
Max Entering	32.2	48.9

The heat pump is pre-charged with environmentally friendly R-410A refrigerant. A variable-speed compressor is desired for this project; however, a variable-speed model of the appropriate capacity was not available from the manufacturer at the time of purchase. Therefore, the selected model features a single-speed, scroll-type compressor. The heat pump is equipped with an optional soft-start accessory called IntelliStart (Figure 3). IntelliStart can reduce the standard starting current (LRA) of the compressor up to 60% (WaterFurnace 2020). This feature is of interest as a tool for peak load reduction in a future investigation of power management of the MISAHP system. Coaxial refrigerant-to-water heat exchangers are used in the condenser and evaporator. According to the product manual, these heat exchangers are oversized to reduce the pressure drop and improve efficiency at low flow rates. The heat exchangers are encased in Thermashield foam insulation to prevent condensation in low-temperature loop operation. A balanced port bidirectional thermostatic expansion valve is used for precise refrigerant metering. Built-in safety mechanisms are used to prevent equipment damage as a result of improper operating conditions, including thermistors monitored for freeze protection in the heat exchangers, pressure switches for high- and low-pressure protection of the refrigerant loop, and a self-resetting under/over-voltage shutdown (WaterFurnace 2020).

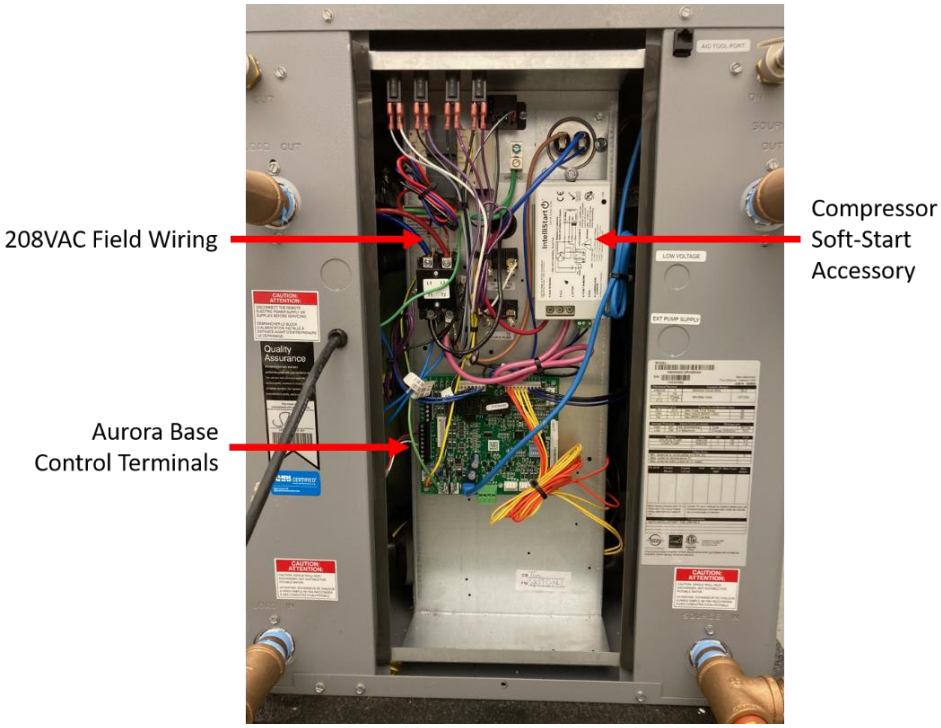

Figure 3: Heat Pump Control Box

As mentioned previously, the heat pump also features heat-reclaiming hot water generation using a factory mounted desuperheater, which is essentially a heat exchanger located between the compressor and the condenser to enable the use of superheated high-temperature refrigerant gas for DHW generation. As shown in Figure 4, a tee installed at the cold water inlet of the DHW tank supplies low-temperature water to the desuperheater loop, pulling either from the dip tube opening at the bottom of the tank or from the building mains if in-tank water pressure is reduced due to active DHW demand. A circulator pump, installed at the outlet of the desuperheater, moves hot water to the bottom of the DHW tank through a tee installed at the drain valve fitting. A temperature limit switch is installed to contact the copper pipe near the

inlet to the desuperheater and breaks the circuit powering the circulator pump when the temperature limit is met.

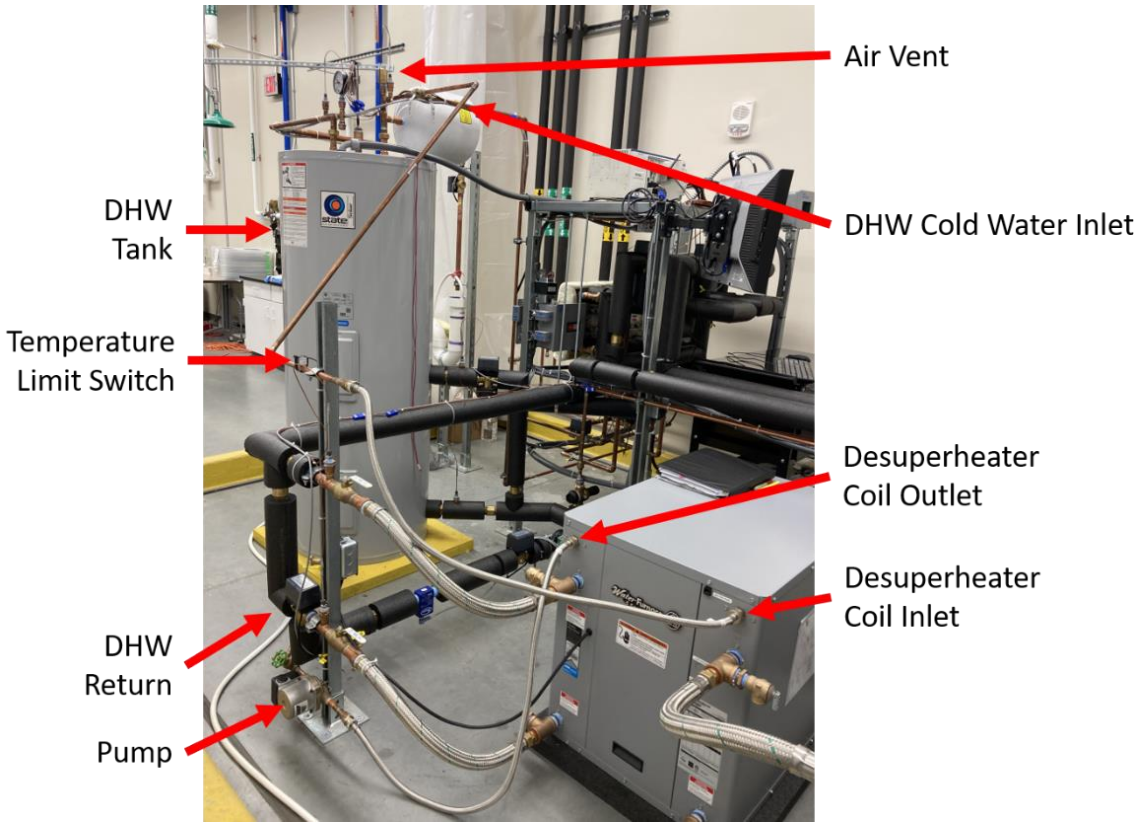

Figure 4: Heat Pump Desuperheater Loop

The heat pump is factory wired for compatibility with 220VAC power supplies. Necessary accommodations were made for the 208VAC supply available in the lab space, accomplished by switching the blue and red wires at the 24V transformer as specified in the installation manual (Figure 3). Factory wiring was also modified to disable circulator pump control, otherwise managed from a proprietary controller available from the manufacturer. Following with the installation manual instructions, the black/white wire on the load pump relay was moved from the N/C terminal to the N/O terminal.

The heat pump is equipped with *Aurora Base Control* (Figure 3), which is the entry-level control option from the manufacturer. This control platform is 24VAC activated, with terminals for typical thermostat control wiring. A 2-pole compressor contactor is energized 10 seconds after a

control input is received at the Y1 terminal on the control board. The reversing valve coil is energized in response to a control input at the O terminal, triggering cooling operation for heat transfer from the load-side coil to the source-side coil.

Because all testing conducted on the MISAHP system utilized emulated conditions rather than an actual space conditioning load, a remote thermostat cannot be used for control of the heat pump. Furthermore, due to the piping configuration between major components, some MISAHP heating modes require that the heat pump operates in cooling mode to move energy in the desired direction intended. In place of a remote thermostat, electronic relays are used to control the heat pump. A Honeywell Spyder 24VAC controller (Relay Controller), generously donated for the project by Michael Giordano from McKenny's Inc., was programmed to energize two relays from Functional Devices Inc. (RIBUIC) in response to voltage signals generated in LabVIEW and output from NI hardware (Figure 5). The relays are used to open and close circuits at the heat pump control board. Both are fed from the heat pump's 24VAC control output terminal (R), and the N/O wires are connected to return the signal to the compressor (Y1) and reversing valve (O) terminals of the Aurora Base control board when the relay is closed (Figure 3). By energizing the relays from the controller, the operation of a basic thermostat is recreated to cycle the heat pump compressor on and off, and to energize the coil on the four-way reversing valve for modes requiring load-to-source energy transfer.

Figure 5: Relay Controller and Relays

3.2.2 Buffer Storage Tank

Because of the inherent nature of solar intermittence, and the mismatch between solar irradiance and thermal loads, both in timing and magnitude, energy storage considerations can be critical for the effective use of the solar resource. In this thesis, thermal energy storage is utilized by the MISAHP system; however, electrical storage may be of interest for future work involving the integration of PVT panels. Water storage tanks like those used in the MISAHP system are the most prevalent example of thermal storage used in the field. Existing literature on solar thermal systems with water storage generally stresses the importance of maintaining thermal stratification for efficient energy transfer. In this context, thermal stratification refers to the naturally occurring vertical temperature gradient driven by buoyant forces caused by the temperature dependency of water density. In a typical solar thermal system, cold water from the bottom of the storage tank is circulated to the collector while hot water is delivered to the load from the upper portion of the tank. Water circulation is prone to destroy thermal

stratification in the tank, which reduces the thermal efficiency of the system. To alleviate the disturbance of stratification, as is a common practice in solar thermal systems, storage tanks with internal heat exchanger coils are preferred. The use of immersed coils also isolates the water used in the collectors from the potable water supply, enabling the replacement of water with brine or glycol solutions for freeze protection, as is necessary for many climates.

Recall from the functional analysis that the MISAHP system is intended to provide cooling as well as heating functions. Accordingly, the buffer storage tank is used to store hot water in the heating season and cold water in the cooling season. Because a single internal coil heat exchanger could not harness the temperature gradient in the storage tank effectively for both functions, an alternative configuration using two immersed coils is investigated for this application. The dual-coil design facilitates effective heat transfer in either the upper or lower portion of the tank, used for thermal storage in cooling or heating modes respectively (Figure 6). A Bock EnviroStor Tank (119SKDC) was selected. This model features a glass-lined steel tank, foam insulation, and two separate heat exchanger coils. Two magnesium anode rods are employed for corrosion prevention. Table 3 summarizes the major technical parameters of the buffer storage tank (Bock Water Heaters 2020). Figure 7 shows the buffer storage tank as installed in the MISAHP system, and illustrates the alternative utilization of the dual coil design, which was originally intended for applications involving solar thermal primary heating and hydronic auxiliary heating in combination with a gas-fired boiler. Arrows indicating the path of water through the coils are color-coded to illustrate the temperature change achieved.

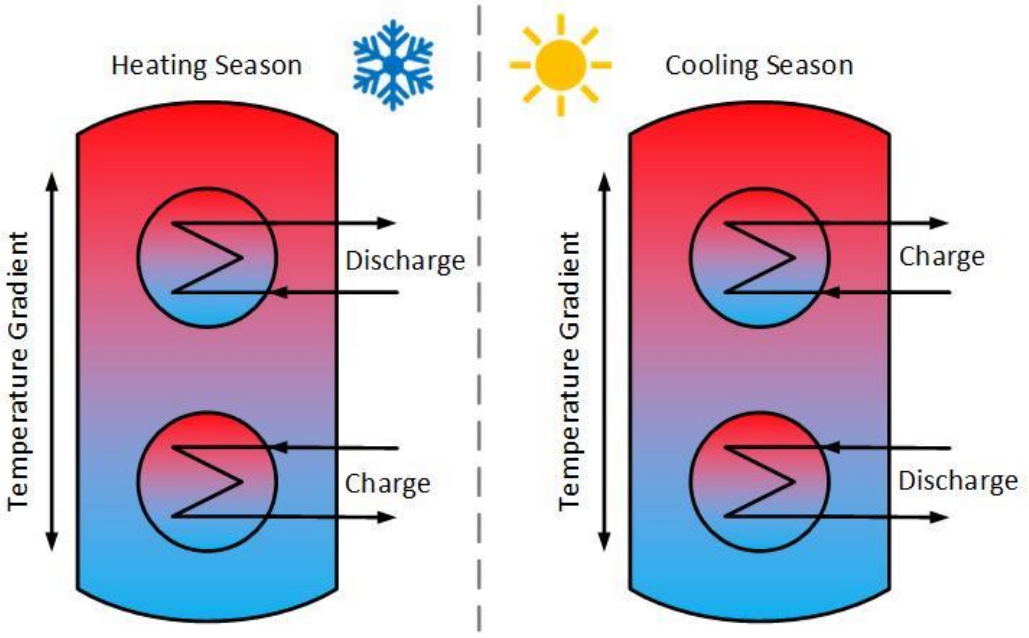

Figure 6:Buffer Storage Concept for Efficient Energy Exchange in Heating and Cooling Modes

Figure 7: Buffer Storage Tank with Dual Immersed Heat Exchanger Coils

Table 3: Buffer Storage Tank Specifications

Parameter	Value	Unit
Tank Volume	409	L
Upper Coil Volume	7	L
Upper Coil Surface Area	0.88	m^2
Upper Coil Friction Losses - 0.88 L/s (14gpm)	1200	Pa
Lower Coil Volume	10.5	L
Lower Coil Surface Area	1.32	m^2
Lower Coil Friction Loss - 0.88 L/s (14gpm)	1800	Pa

Table 4: Buffer Storage Tank Dimensions

Dimension	cm	inch
A	71.2	28
B	165.1	65
C	146.69	57.75
D	146.69	57.75
E	131.45	51.75
F	124.76	49.12
G	98.43	38.75
H	85.73	33.75
I	41.28	16.25
J	22.23	8.75
K	16.51	6.5

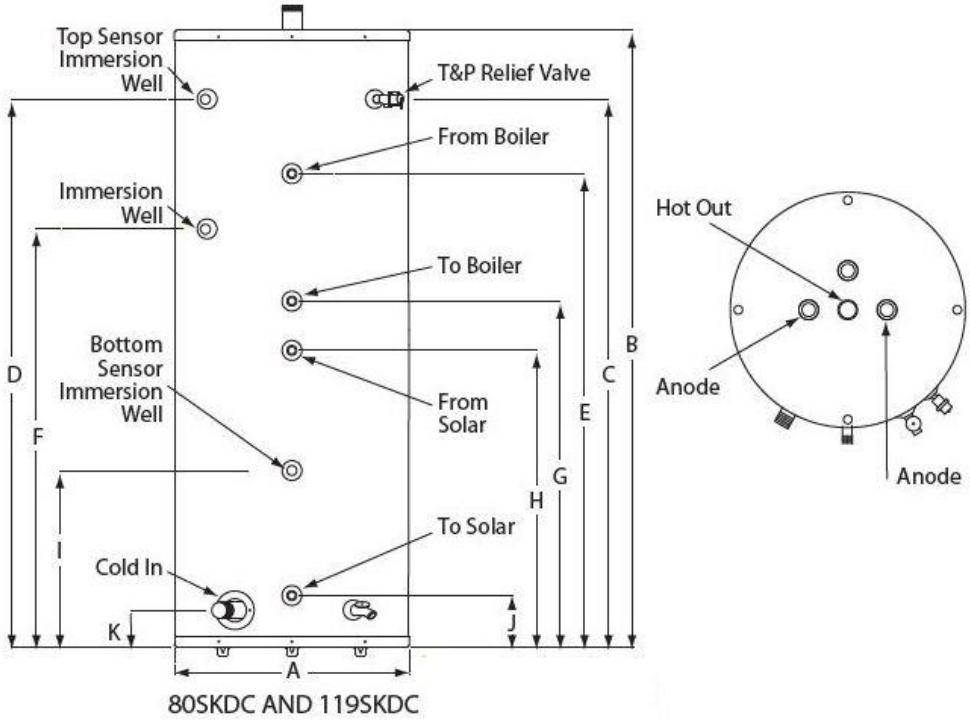

Figure 8: Buffer Storage Tank Dimensional Drawing (Bock Water Heaters 2020)

It is worth noting that the volume of this tank is relatively small for a real system. However, under ASME Boiler and Pressure Vessel Code, a tank with a volume greater than 450L is regarded as a pressure vessel and is required to meet higher standards for material construction, tensile strength and inspection procedure. Due to the substantial increase in the cost of ASME-certified tanks, the largest capacity not subject to the pressure vessel code was selected for this project.

3.2.3 Domestic Hot Water Tank

AOSmith Corporation donated the DHW tank (State Model SB680SOTXG) used for the experimental apparatus. This model is intended for use with indirect solar hot water systems and features a glass-lined steel tank with foam insulation, and a single immersed heat exchanger coil. In addition to the coil inlet and outlet ports, pressure relief port, drain port, and potable inlet and outlet ports, this model features two additional unused threaded ports (plugged from the factory) which offered flexibility for integration with the heat pump's desuperheater, as well as system instrumentation. A 4500W electric heating element is installed in a port on the side of the tank for auxiliary electric heating when available solar energy is insufficient to maintain the desired water temperature. The heating element is rated for 240V. Because only 208V power is available in the lab space, the heating element, when active, draws more current than intended by design. The heating element is thermostatically controlled, and the factory setting of 49°C is retained for testing conducted in this study. Table 5: DHW Tank Technical Parameters summarizes the major technical parameters of the DHW tank (AOSmith 2020).

Table 5: DHW Tank Technical Parameters

Parameter Name	Value	Units
Storage Volume	288	L
Coil Volume	2.8	L
Coil Surface Area	1.49	m^2

Table 6:DHW Tank Heat Exchanger Coil Friction Losses

Flow Rate		Friction Loss Through Coil	
L/s	gpm	ft.w.c	kPa
0.13	2	0.1	0.3
0.25	4	0.3	0.9
0.38	6	0.5	1.5

Table 7:DHW Tank Dimensions

Dimension	cm	inch
Height	160.66	63.25
A	12.7	5.375
B	76.2	30.125
Diameter	60.96	24
Insulation	5.08	2

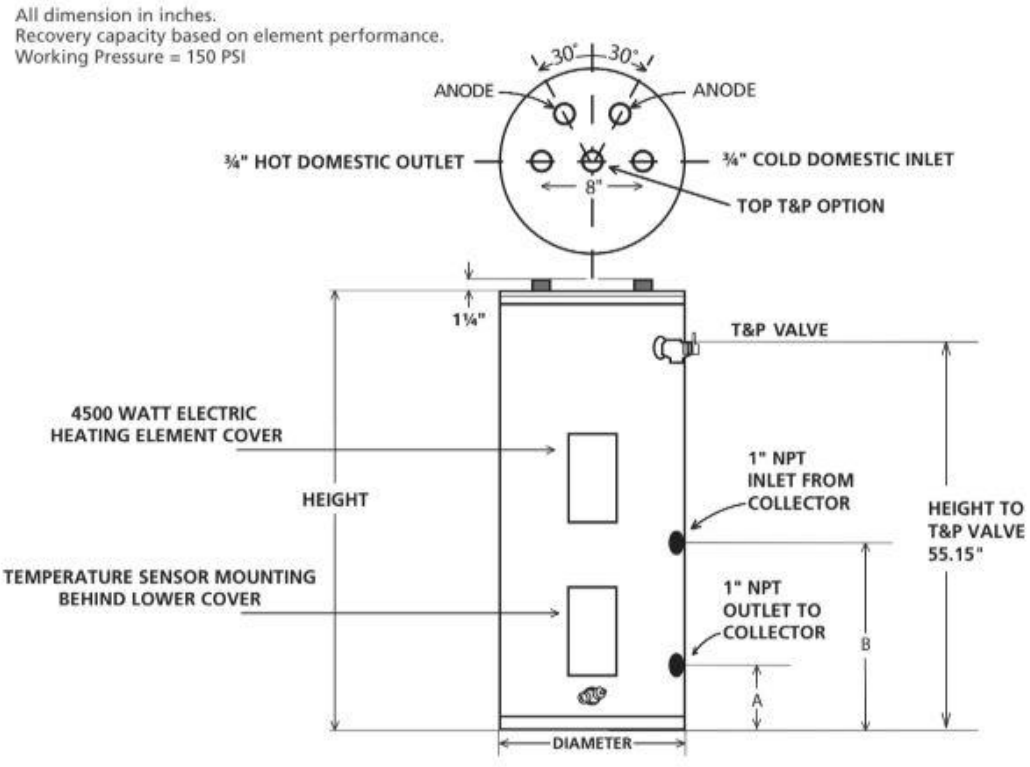

Figure 9: DHW Tank Dimensional Drawing (AOSmith, 2020)

3.2.4 Hydraulic Network and Mechanical Components

Type L copper pipe is used for water piping to connect the components of the apparatus. Soldered and Teflon-sealed threaded connections are used. Additionally, copper and brass union fittings are installed at various points in the piping network to facilitate disassembly of the apparatus if the need should arise in the future, either for the replacement of individual components, or reconfiguration of the piping network to improve performance or simplify system design. Generally, pipe sizing is ½-inch for water supply distribution, ¾-inch for plant water loops, and 1-inch for the MISAHP system. Foam insulation of 5/8-inch thickness is installed to reduce transfer and standby losses, and as a safety consideration for the user.

A ½-inch copper non-potable water line supplies water to the system. Fourteen shut-off valves and five drain valves are installed at various points in the apparatus piping to facilitate flushing, bleeding, isolation of individual sections of piping, and to meet future needs for system maintenance or modification. Shut-off and drain valves are numbered and shown in their relative locations in Figure 10. “S” and “D” designations accompany the numerical assignment for each of these valves to distinguish between shut-off and drain valves.

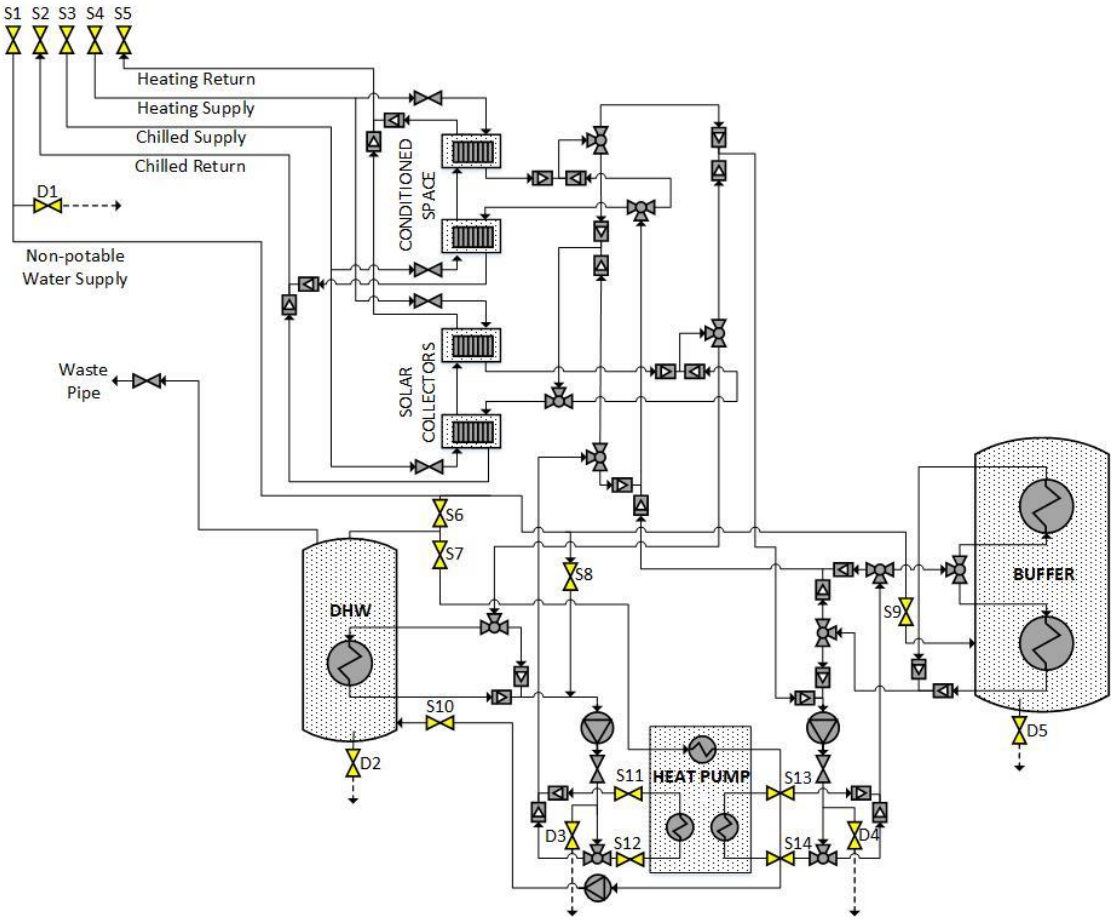

Figure 10: Shut-off and Drain Valve Locations

The MISAHP system piping network consists of multiple branches, used in various combinations for different operational modes to define the path of the water between major components of the system. Given that the system operates in 15 modes, has 11 diverting valves, and 22 check valves, to devise an organizational structure to differentiate between all possible combinations of piping branches utilized by the system would pose a formidable challenge, and would belabor the reader for no discernable benefit. For this reason, no attempt is made in this document to distinguish between all possible loop configurations by name or numerical designation. Instead, active loops are described loosely using “source-side loop” or “load-side loop.” This nomenclature is derived in reference to the circulator pumps installed adjacent to the source- and load-side water coil connection, Although the pumps themselves are named to describe

their connection to the source- or load- side coil of the heat pump, it is more appropriate reference the circulator pump because all possible loops include one, and never both, of the pumps in their circuit. In contrast, many of the loops do not involve the heat pump. This terminology is sufficient for most discussions, while any query related to the source-side and load-side loop configurations used by any mode can be easily cross-referenced with the experimental apparatus operational mode diagrams provided in Appendix C if additional clarity is required.

At the return junction of all piping branches in the MISAHP system, brass mechanical spring check valves are installed to ensure the proper flow direction for the active loops in all modes and isolate active loops from inactive branches.

A mechanical pressure-reducing valve is installed to reduce supply pressure feeding the storage tanks to 2.8MPa (40psi), specified to maintain system pressure below the cutoff maximum specified for the electronic valves, one of which must seal off the system at the DHW discharge line. While this value is below average for a typical utility-connected dwelling, it approximates the lower end of the typical household supply pressure range for a well-sourced dwelling and is therefore not unreasonable for this project. A second-tier pressure reducing valve is installed between the supply distribution lines and the MISAHP system piping network (Figure 11). This valve further limits the pressure supplied to the MISAHP system piping to 1MPa (15psi), to avoid exceeding the pressure limits specified by the heat pump at high flow rates.

Figure 11: Pressure Reducing Valve for MISAHP System Water Piping

Six mechanical dial gauges are installed to measure water temperature and pressure in the plant heating and chilled water loops, on the pressure side of the MISAHP source- and load- side circulator pumps, and for each of the water tanks. These gauges are used to verify pressure levels when filling, flushing, or bleeding the system.

To isolate the copper piping from vibrations produced by the heat pump compressor, flexible braided hoses are used at the connections of the MISAHP system piping to the heat pump inlet and outlet ports.

Three expansion tanks are installed to mitigate stress on system components from the expansion of water due to temperature changes. Because the apparatus design isolates the MISAHP system piping from the two water tanks, a separate expansion tank is provided for each closed portion of the system. Expansion tank sizing is 38L (10gal) for the buffer storage tank, 17L (4.5gal) for the DHW tank, and 8L (2.1gal) for the load-side loop, as shown in Figure 12.

Figure 12: Expansion Tanks -Buffer Storage (left), DHW Tank (top right), Load-Side (bottom right)

Water temperature changes are assumed to be highest for the load-side loop, which handles direct energy transfer from the collector to the DHW tank. It was expected that temperature changes would be more moderate on the source-side loop; therefore no expansion tank has been installed; however, a ¾-inch female threaded adapter is included in the construction of the source-side loop to accommodate the addition of a fourth expansion tank if later deemed necessary (Figure 13).

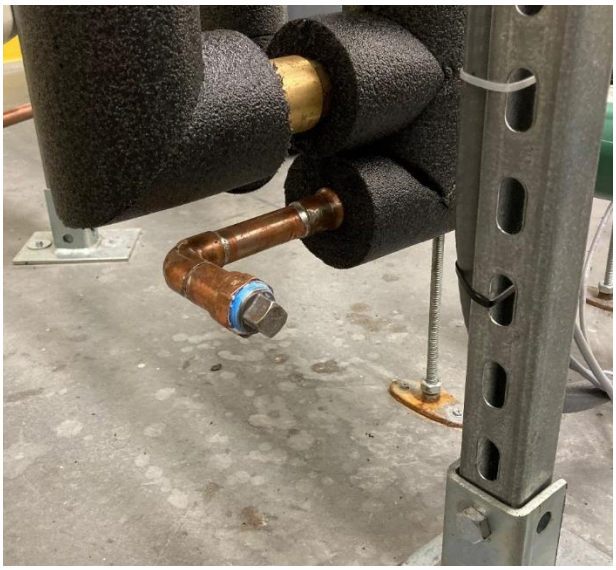

Figure 13: Future Installation Point for Source-Side Expansion Tank

A mechanical air vent is installed at the highest point in the MISAHP piping network to facilitate the removal of air pockets when filling the system (Figure 14). A second air vent is installed at the inlet to the DHW tank, as specified in the installation manual for the desuperheater kit supplied with the heat pump.

Figure 14: Mechanical Air Vent

A mechanical water-hammer arrestor is installed upstream of the 2-way electronic valve used for DHW discharge. The hammer arrestor dampens vibrations created when the valve is opened or closed. Prior to installation of the hammer arrestor, severe vibrations were observed to prevent accurate flow measurement from the flow meter on the discharge line

Mechanical temperature and pressure relief valves rated at 99°C/10.3MPa (210°F/150psi) are installed from the factory on each of the water tanks as a safety precaution. As recommended in the installation manual, two pressure relief valves rated at 2.1MPa (30psi) are installed at the source- and load-side outlets of the heat pump.

The general piping layout, including distribution lines and relative locations of all mechanical accessory components installed in the experimental apparatus, is shown in Figure 15.

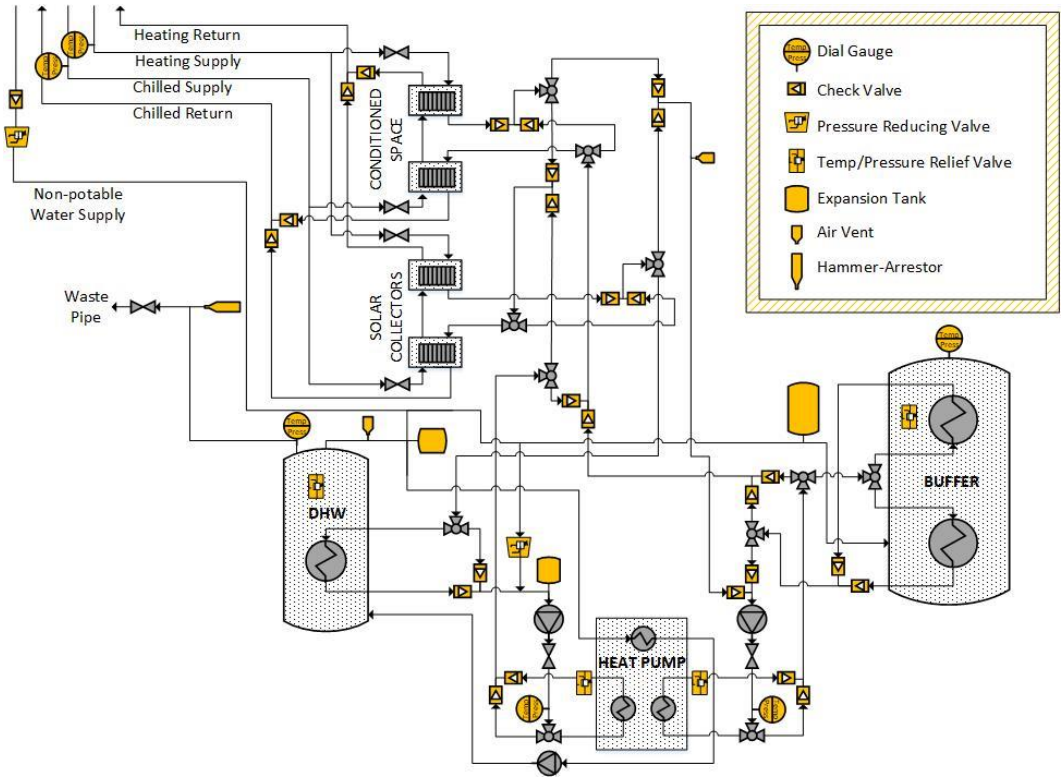

Figure 15: Experimental Apparatus Distribution Piping and Mechanical Accessory Components

3.2.5 Electronic Valves

Electronic zone valves are used to regulate water flow in the system. The valves selected from Dwyer Instruments (3ZV20424 for 3-way valves and ZV20424 for 2-way valves), are intended for use in conjunction with a thermostat in hot- and cold-water HVAC systems to regulate flow rate in response to room or zone temperature (Dwyer Instruments, 2020b, 2020c). As shown in

Figure 16, these feature a brass valve body and removable electronic actuator assembly with a manual override lever that also provides visual feedback for valve position. Inside the valve body, a short lever arm terminates in a rubber stopper, which travels between the two opposing ports of the valve, labeled “A” and “B.” The stopper forms a seal with the ports at the extremes of the lever stroke, directing flow to the opposing outlet pathway, and modulates the resistance to fluid flow across the range of intermediate positions. The lever arm movement in the valve body is driven by a shaft that connects to the bidirectional electric motor of the actuator assembly.

Figure 16: Electronic Valves - 3-way Valve (left), Lever-arm, Stopper, A/B Port Designations (center), and 2-way Valve (right)

Floating and modulating actuators are available. Initially, floating valves were selected for diverting the path of the water in different modes, with the expectation only 2 positions would be required; diverting the full volume of flow to either the “A” or “B” port, and that intermediate positions of the valve would not be used. However, preliminary trial operation of the valves before system installation revealed that the floating valve response is dependent on the time duration of the control signal received, creating the potential for improper operation due to compounding error after repeated use. Additionally, no mechanism is included in floating valve design to prevent damage to the valve actuator if the control signal timing is not externally controlled.

Modulating valves are equipped with a motor-timeout feature and are not dependent on external control timing. Modulating versions were, therefore, ultimately selected for both 2-way and 3-way valves. The modulating actuator adjusts the position of the valves in response to a control signal for a position. A set of four dip switches on the actuator control board allow for selection between four accepted control signal types (0-20mADC, 4-20mADC, 0-10VDC, 2-10VDC), and allow for an automatic calibration procedure to be initiated if necessary (Figure 17). Both 3-way and 2-way versions of these valves are installed in the apparatus. These are distinguished by the utilization of three available ports on the valve body, which is shared by both models. The 2-way valves have just two open ports, one inlet and one outlet at the opposing ends. 2-way valves lack the orifice that seals with the stopper on one of the ports. The 3-way valves utilize both opposing ports as outlets ("A" and "B"), while the third center port is used as the inlet.

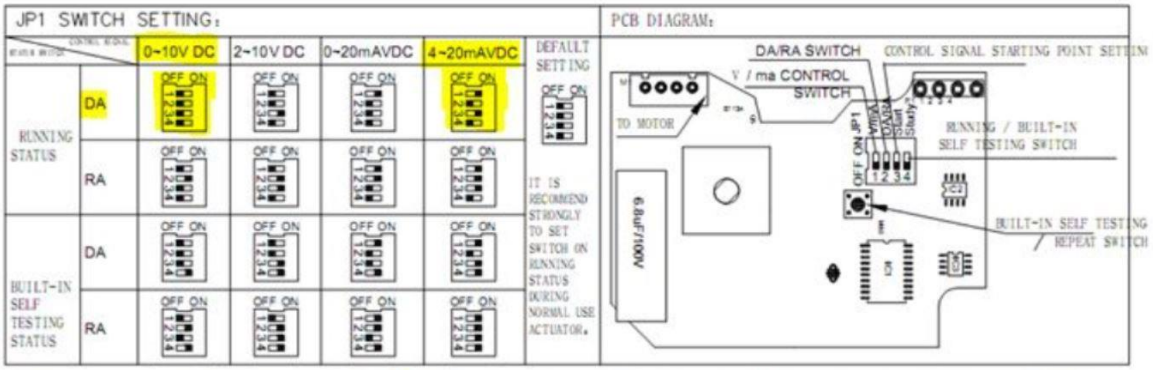

Figure 17: Modulating Valve Actuator Schematic and Dip Switch Legend

The 3-way valves are used to control the path of water flowing through the various branches of the MISAHP system piping network for different operational modes. Nine different valve position combinations are utilized in the operation of the system. Several modes share valve positions settings, utilizing the same flow path for heat transfer in the alternate direction (i.e., modes CS->CA and CA->CS). For the 3-way valves, 4-20mA control is selected, with a 4mA

control signal corresponding to the “A,” or default, position, and 20mA signal corresponding to the “B” position. As mentioned previously, it was not intended to utilize any of the intermediate positions allowed by the design of these valves; however, this feature proved useful in some instances. The relative locations of all 3-way valves (numbered 1-11) installed in the experimental apparatus and their orientation with respect to the A and B outlet ports are shown in Figure 18.

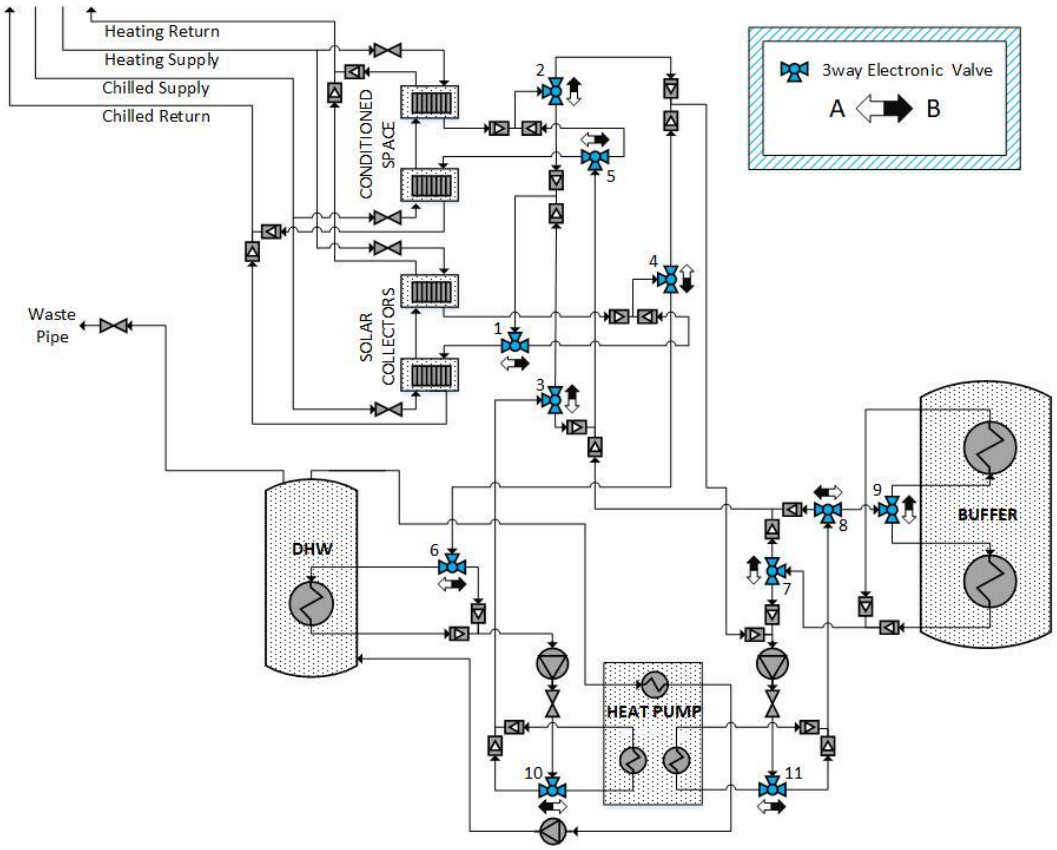

Figure 18: 3-way Electronic Valve Locations

The 2-way valves are used for flow rate modulation in the thermal source, sink, and DHW demand emulation. Additionally, a 2-way valve is installed immediately downstream from each of the circulator pumps for friction head tuning optimization of the pump circuits. For 2-way valves, 0-10VDC control is selected, with a control signal of 0V correlating to fully closed, and a 10V control signal correlating to the fully open position at the full stroke of the valve. The

relative locations of all 2-way valves (numbered 12-18) installed in the experimental apparatus are shown in Figure 19.

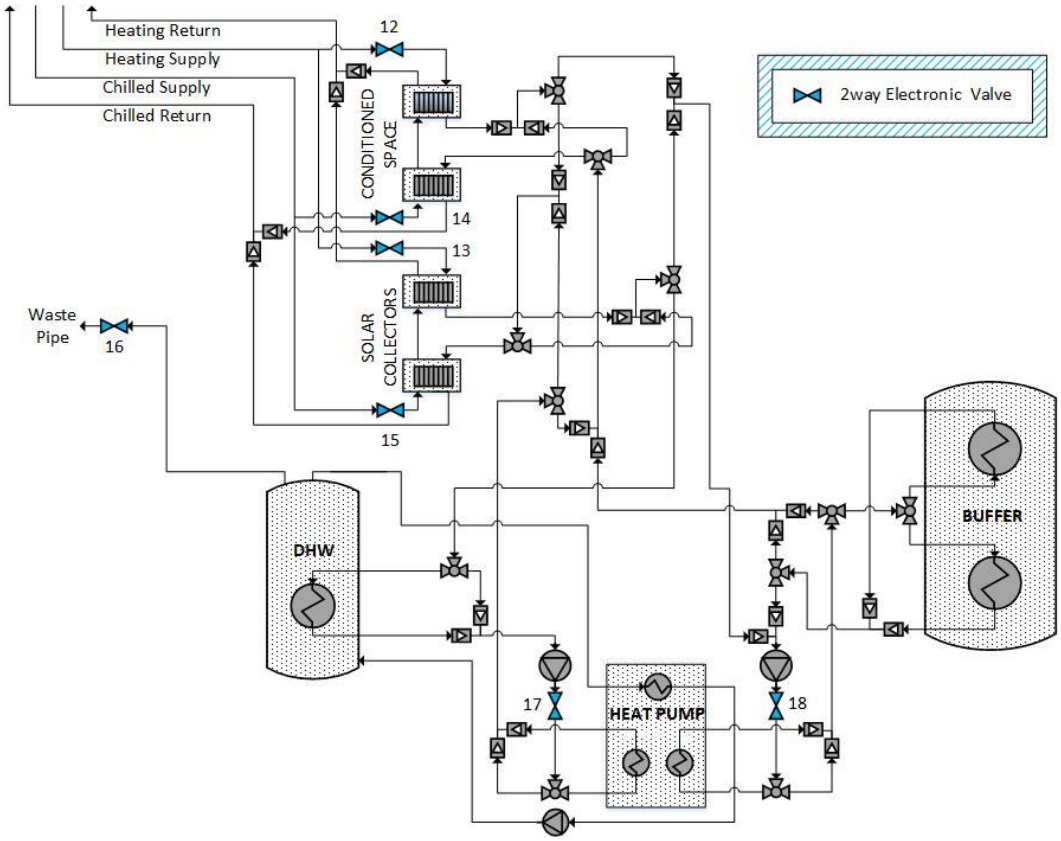

Figure 19: 2-way Electronic Valve Locations

All electronic valves operate on 24 VAC. A 100VA transformer meets the power requirements of all 18 valves, as well as the Relay Controller, which also operates on 24VAC supplied from the transformer.

3.2.6 Circulation Pumps

Variable-speed pumps are installed to accommodate testing at different flow rates to be optimized for various operating modes, setpoints, and environmental conditions. The operating requirements of the heat pump mandate a flow rate in the range between 0.32L/s (5gpm) and 0.76L/s (12gpm) for both the source- and load-side loops in all heat pump modes. A lower flow rate may be desirable for other modes.

Two identical Taco 00e Series pumps (Catalog number VR3452-HY1-FC1A01) are selected for water circulation in MISAHP water loops (Figure 20). The pumps are centrifugal type and use electronically commutated motors (ECMs). The pumps accept 0-10 V control signals for speed regulation and are capable of Modbus RTU interface for control and performance monitoring. Voltage control is employed at this stage in the project. These pumps are also equipped to operate in several self-regulating automatic modes, including constant speed, constant pressure, and proportional pressure, which are not used for the experimental apparatus. A user interface on the front of the control panel can be used to cycle through digital display options to report flow rate (gpm), rotational speed (rpm), pressure differential (ft.w.c), and power consumption (W). Figure 21 shows the performance curve of the Taco pumps (Taco Comfort Solutions, 2020).

Figure 20: Variable Speed Circulation Pump

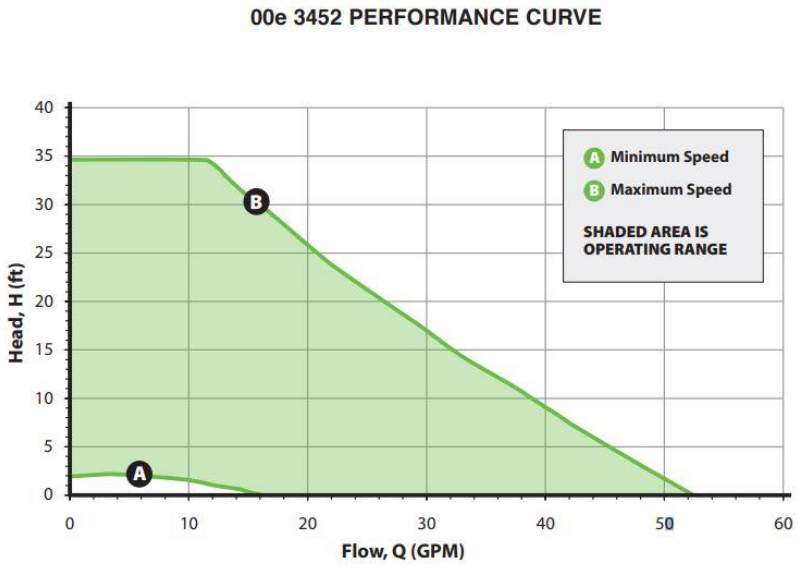

Figure 21: Performance Curve, Source- and Load-Side Circulator Pumps (Taco Comfort Solutions, 2020)

A Grundfos Comfort-Series circulator pump (UP15-18B5), supplied with the heat pump, is installed at the outlet of the desuperheater coil (Figure 22). This pump is powered from accessory terminals in the heat pump and controlled by a thermostatic switch on the inlet to the desuperheater coil.

Figure 22: Desuperheater Loop Pump

Figure 23 shows the three circulator pumps in their relative locations in the experimental apparatus.

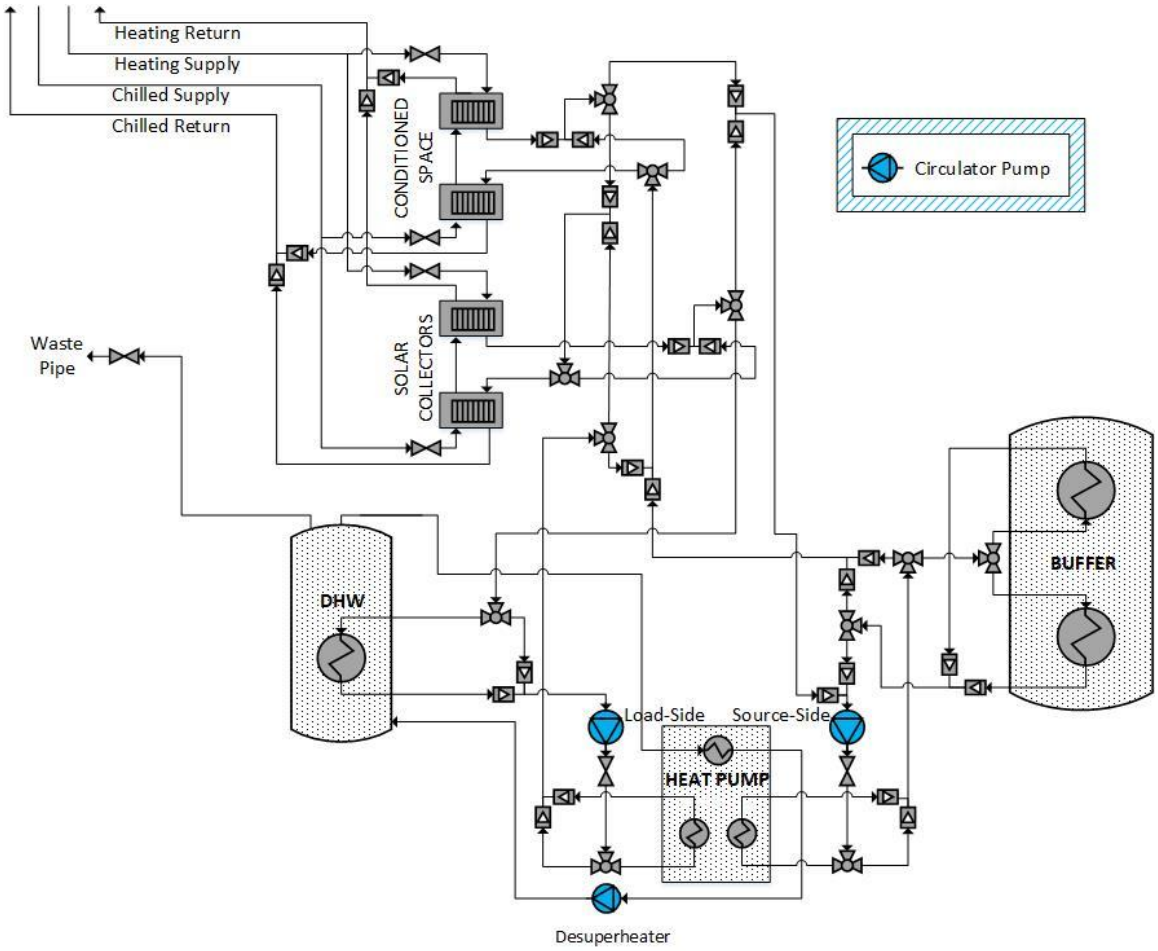

Figure 23: Pump Locations

3.2.7 Collector Array Emulator

The experimental apparatus is installed in a laboratory and is not connected to any real solar collectors. The thermal response of a solar collector array is emulated for all testing scenarios, allowing for flexible research and repeatable test conditions.

Two brazed plate type heat exchangers (Kelvion FP5X12-24), connected in series, take the place of the collector array in the MISAHP system (Figure 26). The thermal response of the collector array is emulated using the university campus' plant heating and chilled water loops, with one heat exchanger connected to each, providing both a source and sink for thermal energy transfer.

Table 8: Emulator Brazed Plate Heat Exchanger Specification provides the technical specifications for the heat exchangers used for emulation.

Table 8: Emulator Brazed Plate Heat Exchanger Specification

	Side A		Side B	
Capacity (BTUh)	Min. Required Flow Rate (gpm)	Pressure Drop (psi) at Min Flow Rate	Min. Required Flow Rate (gpm)	Pressure Drop (psi) at Min Flow Rate
250,000	5.5	1	17	5.2
300,000	6.7	1.3	20.4	7.3
350,000	7.8	1.6	23.8	9.7

The eventual goal of the experimental apparatus is to realize HIL simulation, a building load profile simulated in software (e.g., TRNSYS). At each timestep, based on the heating load and the temperature ($T_{sysSupply}$) of water supplied from the MISAHP system, the simulation software calculates the temperature ($T_{sysReturn}$) of water returned to the MISAHP system. The value of $T_{sysReturn}$ can then be communicated from the simulation software to the MISAHP controller, which uses that value to modulate position control of the 2-way valves installed on the plant water loops at the inlet to the heat exchangers, adjusting the flow rate of plant water through the emulator to deliver the appropriate return temperature. If the temperature of water return on the experimental apparatus side can be controlled to follow the value of $T_{sysReturn}$ obtained from the simulation software in real-time, the heat exchangers can successfully emulate the collector (Figure 24, Figure 25: Concept for Thermal Source Emulation).

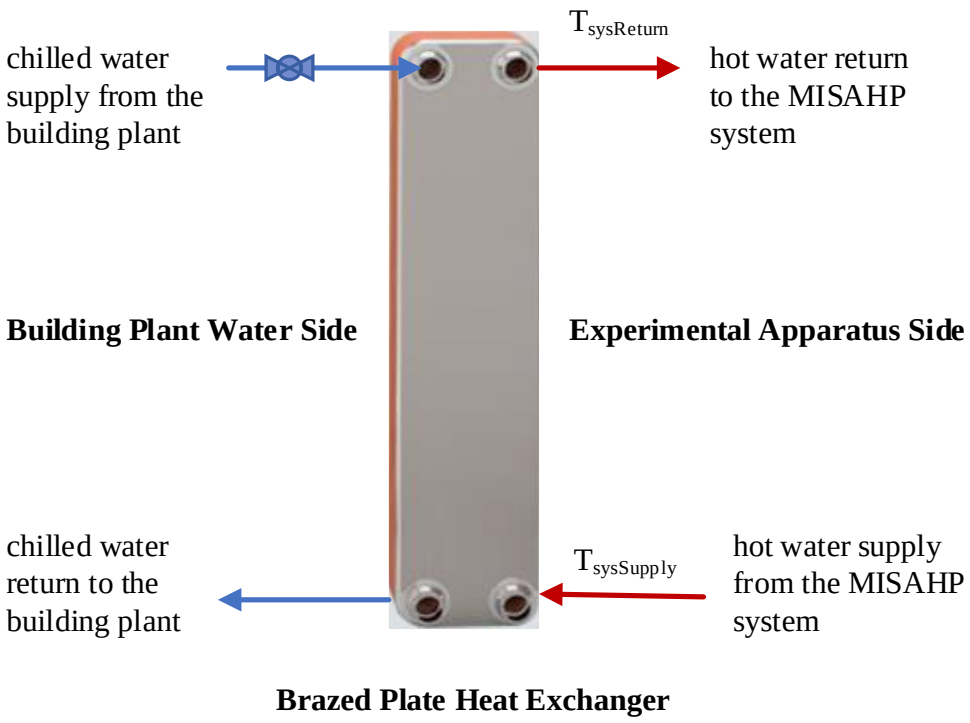

Figure 24: Concept for Thermal Sink Emulation

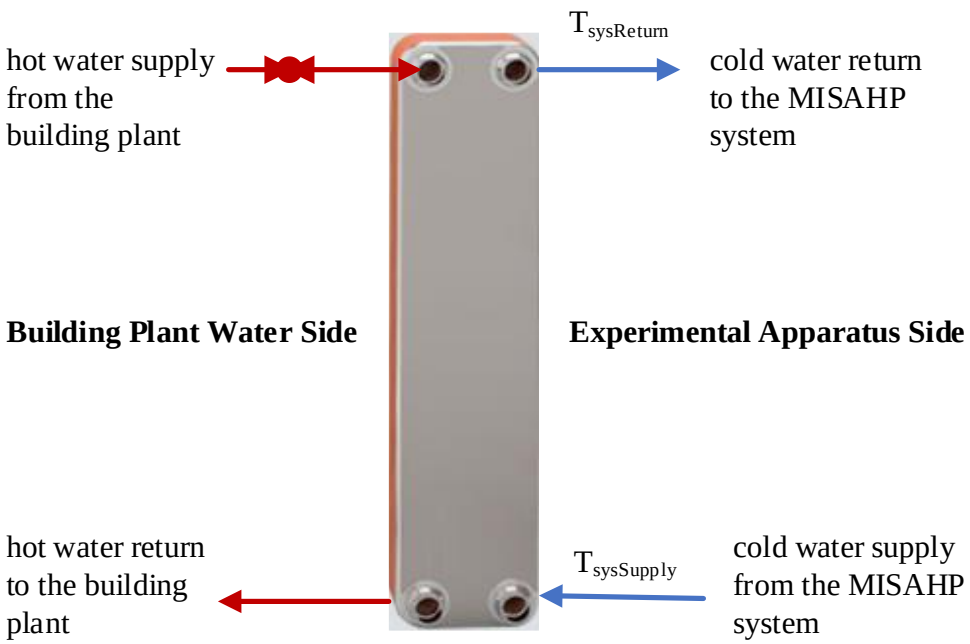

Figure 25: Concept for Thermal Source Emulation

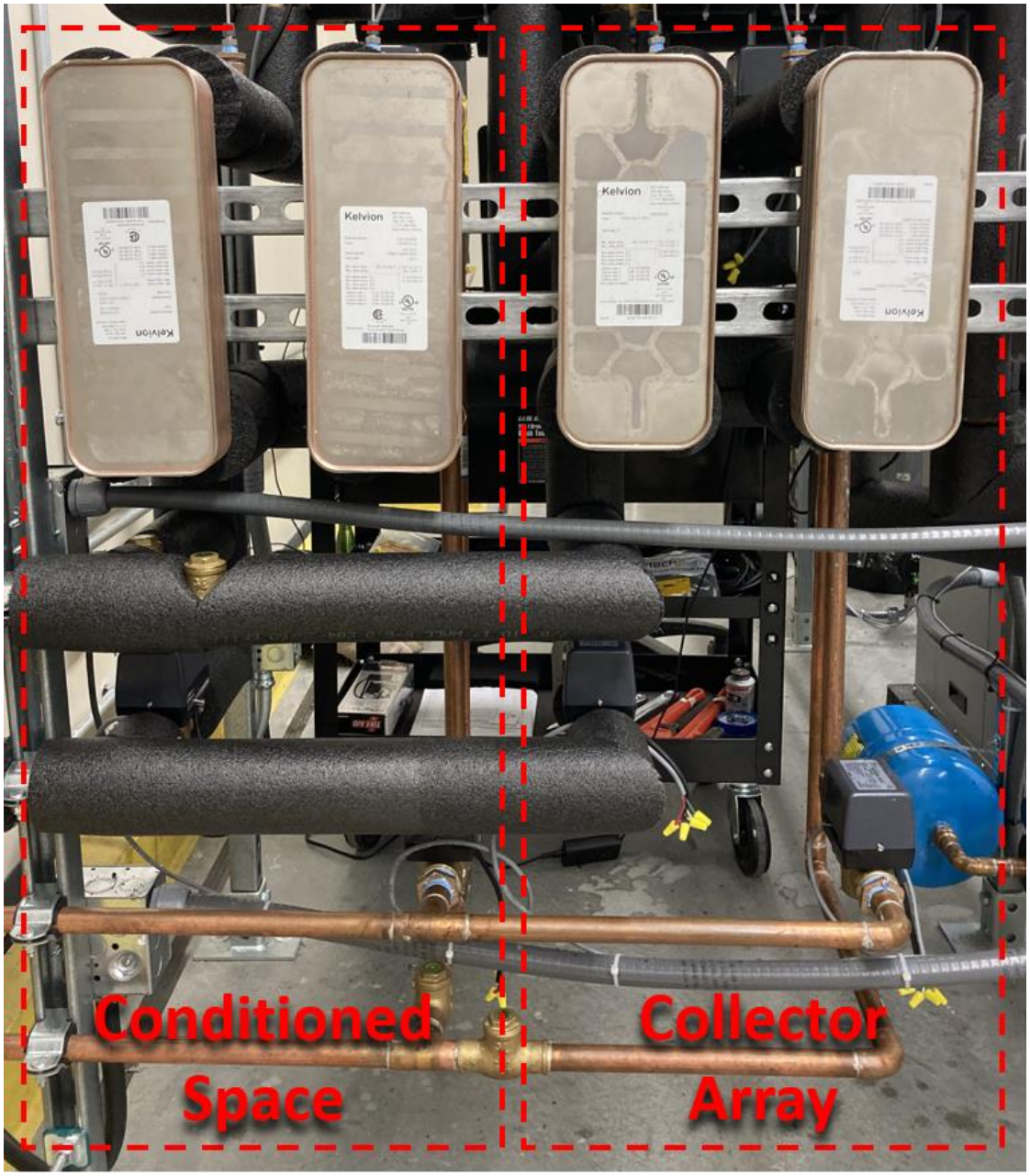

Figure 26: Conditioned Space and Collector Array Emulation Hardware

3.2.8 Conditioned Space Emulator

The experimental apparatus is not connected to a real building hydronic distribution system or domestic hot water fixture. Conditioned space heating and cooling loads and DHW demand are emulated for all testing scenarios. The same concept utilized by the collector array emulator is appropriate for conditioned space emulation. In an identical piping configuration, two brazed plate heat exchangers (Kelvion FW5X12-24) take the place of real hydronic distribution components in the MISAHP system (Figure 26). Heat exchangers used for this project were ordered at different times, two were purchased in 2017 and two in 2019. The second pair of heat exchangers, used for collector array emulation, is a direct replacement for the model used in the conditioned space emulator, which was no longer available at the time of the second order, having been discontinued by the manufacturer.

3.2.9 Domestic Hot Water Demand Emulator

A shown in Figure 27, occupant DHW demand is emulated using a 2-way electronic valve installed on the outlet pipe of the DHW tank. This pipe discharges water from the DHW tank to the laboratory waste drain. Feedback from the flowmeter installed on the DHW outlet is used for position control of the 2-way valve to regulate the timing, flow rate, and volume of hot water discharged as needed to achieve the targeted DHW demand schedule.

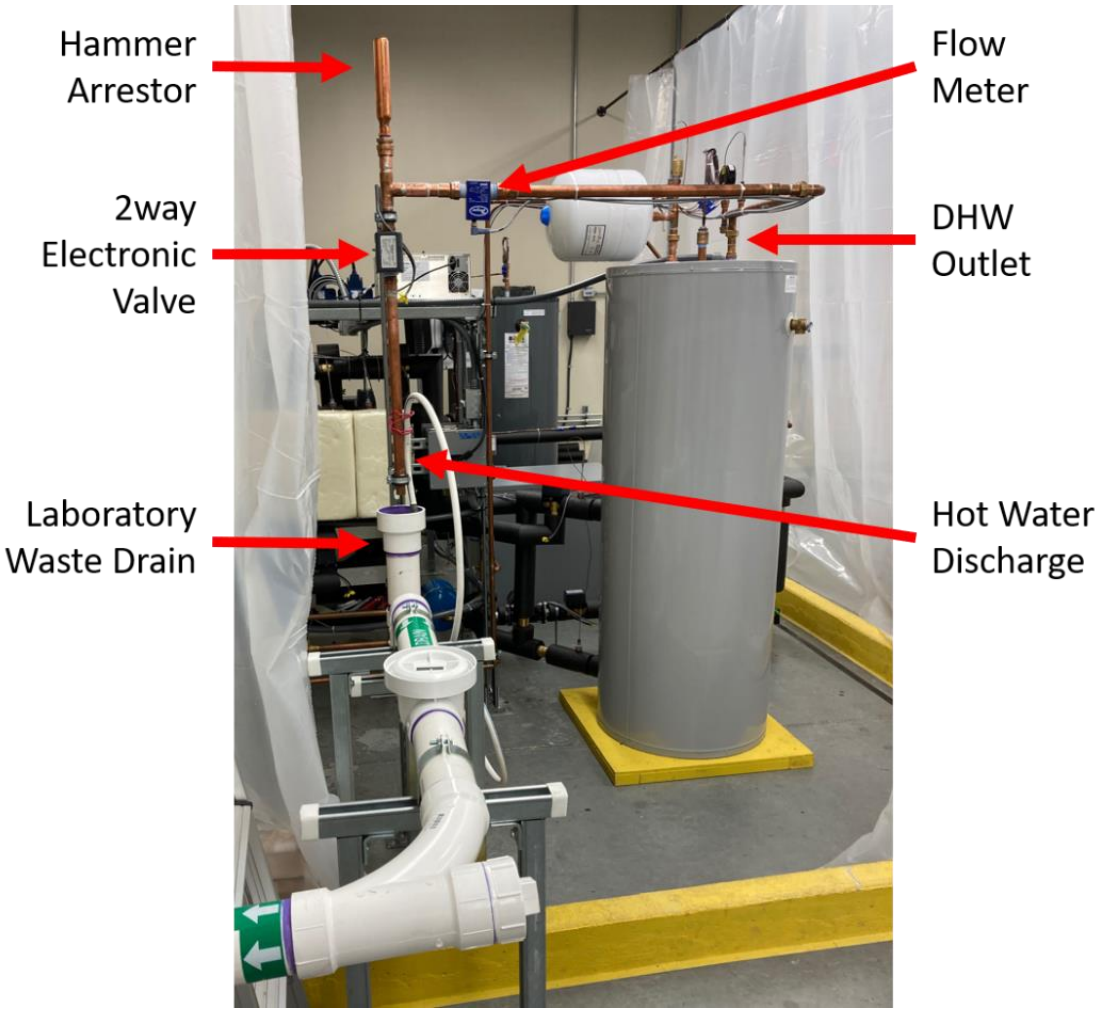

Figure 27: DHW Demand Emulator

3.2.10 Instrumentation

A total of twenty-eight Type T thermocouples are used for temperature measurement. All temperature sensors are connected to NI hardware using 24 AWG insulated Type T thermocouple wire. Type T miniature flat blade connectors are included near each thermocouple for ease of removal.

Eighteen rugged, heavy-duty transition joint thermocouple probes (OMEGA TJ36-CPSS-18U-6) are used for single-point temperature measurement close to the inlet and outlet of each major component of the experimental apparatus. Probes are installed using threaded thermowells and ¼-inch brass compression fittings as shown in Figure 28: Rugged Transition Joint Thermocouple

Probe. These thermocouples are made from special limits of error materials and have an accuracy of +/- 0.5°C in the range of temperatures expected for this system (OMEGA, 2020b).

Figure 28: Rugged Transition Joint Thermocouple Probe

Ten additional thermocouple sensors (OMEGA TC-GG-T-20-72) are used to monitor thermal stratification in the water tanks. Similar to the temperature probes used elsewhere in the system, these thermocouples are also made from special limits of error materials, and have an accuracy of +/- 0.5°C (OMEGA, 2020a). Special sensor wells and vertical thermocouple probes were designed and built to provide five temperature readings, evenly spaced along the vertical axis of each tank. The design and construction of these instruments are detailed in APPENDIX B. . Installed sensor wells and vertical thermocouple probes are shown in Figure 29.

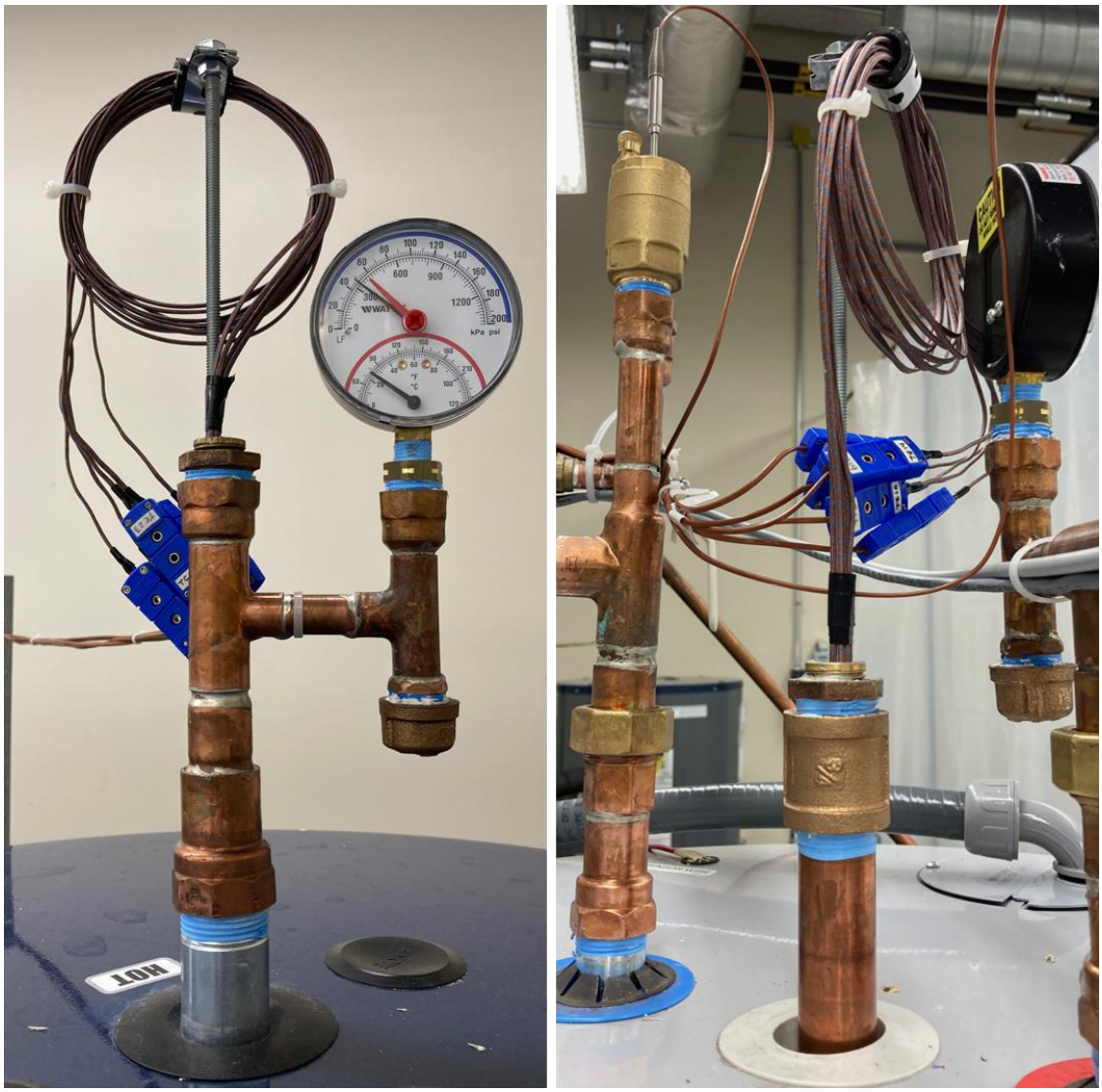

Figure 29: Specially Constructed Vertical Sensor Wells and Thermocouple Probes, Buffer Storage *(left), DHW Tank (right)*

Relative locations of all temperature sensors are shown in Figure 30: Thermocouple Locations, which includes labels indicating the associated channel of the PXIe-4353 Temperature Input Module for each thermocouple.

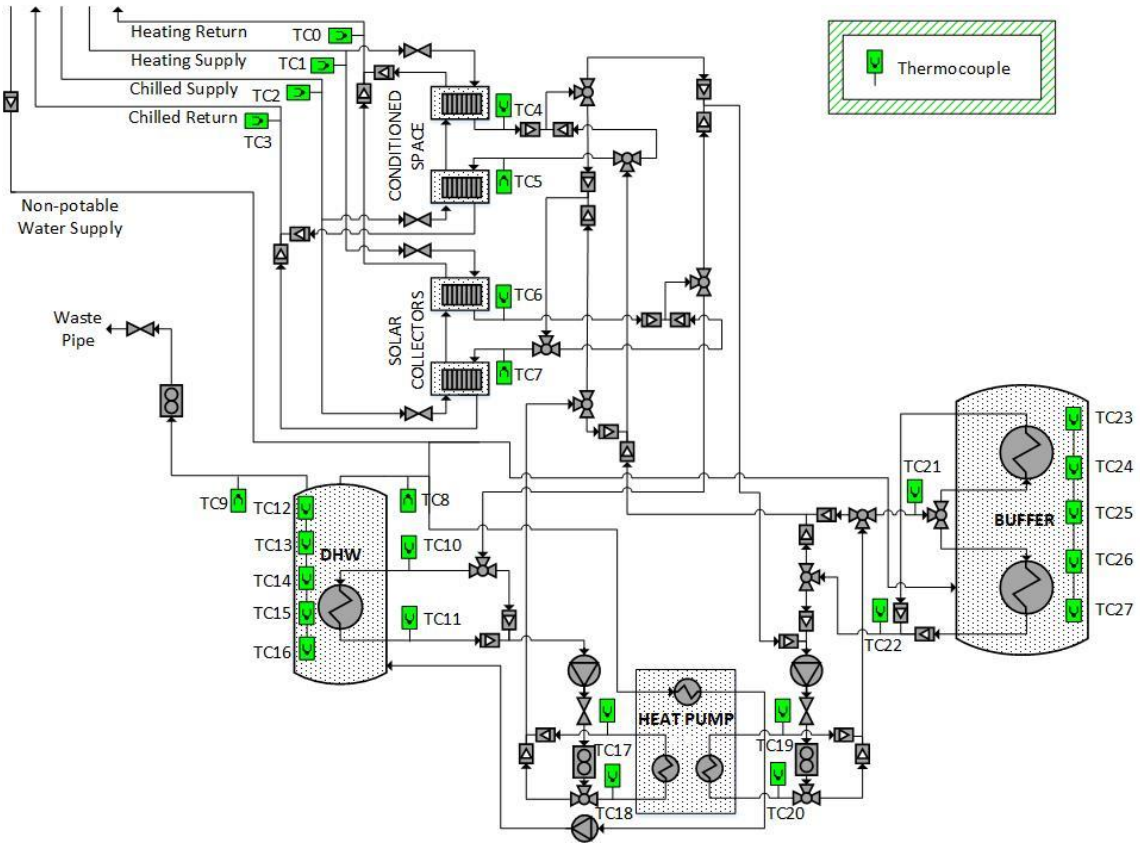

Figure 30: Thermocouple Locations

Water flow rates are measured using Dwyer MFS2-4 flow meters, shown in Figure 31: Induction-Style Flow Meter. These non-contact style instruments have no moving parts, and with minimal added flow restriction, offer +/-1% accuracy for a flow range of 0.1L/s – 1.7L/s (1.3gpm - 26.4gpm). The sensors operate on the principle of induction, producing a voltage proportional to the velocity of conductive fluid flow through the magnetic field generated internally by the sensor. This voltage is picked up by a pair of electrodes on opposing sides of the sensor measurement tube, and the device circuitry outputs a 24 VDC pulse signal at a rate of 750 pulses per gallon. Straight pipe runs of a prescribed length are included in the system at flow measurement points according to manufacturer recommendations for best accuracy (Dwyer Instruments, 2020a).

Figure 31: Induction-Style Flow Meter

As shown in Figure 32, 24VDC power used by the flow meters is supplied from a small power output module. The signal output from each sensor is routed through a multichannel optocoupler to step down the potential to a range of 0-5VDC for acquisition using the NI-PXIe6363 (DAQ). The optocoupler is supplied 5VDC from a power output on the DAQ terminal board.

Figure 32: Flow Meter 24VDC Power Supply and Optocoupler for Pulse Signal Voltage Conversion

Figure 33 shows the relative locations of the three flow meters installed in the experimental apparatus.

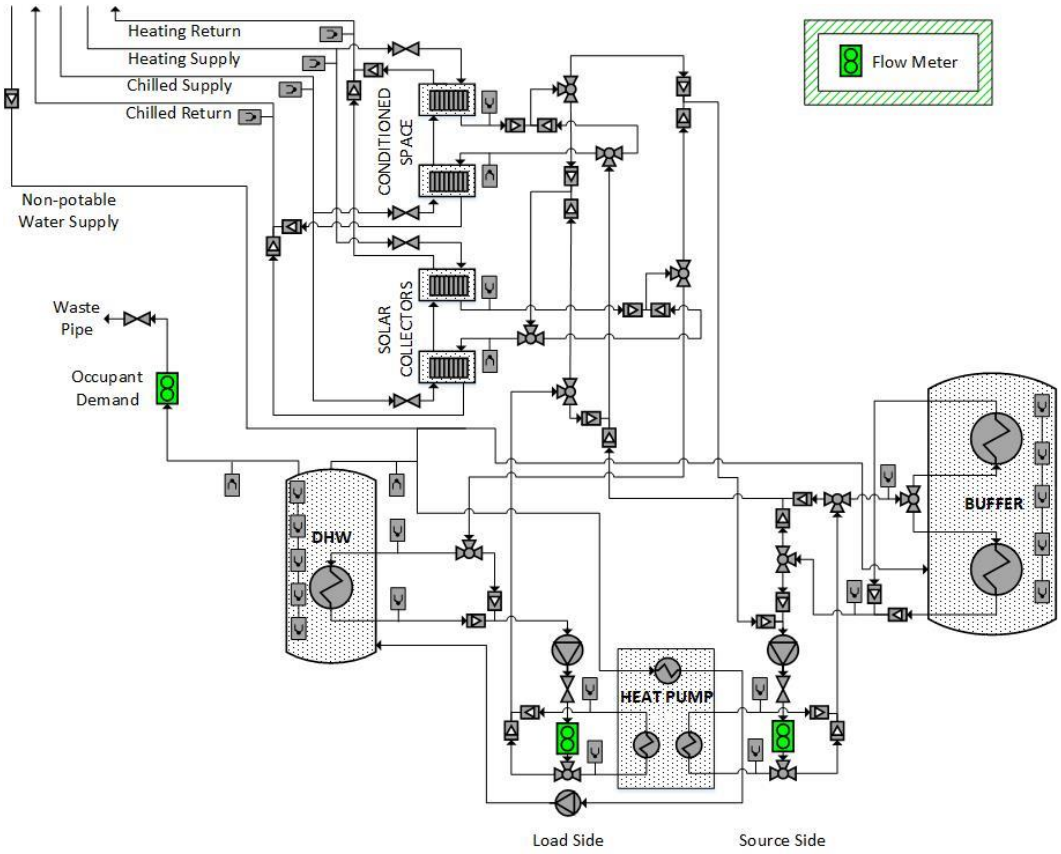

Figure 33: Flow Meter Locations

In addition to electronic instrumentation, six mechanical dial gauges, installed primarily to verify pressure levels in set-up, serve a secondary purpose as a safety precaution to monitor MISAHP system pressure during testing (see section 3.2.4)

3.2.11 LabVIEW Control and Data Acquisition

Data acquisition and control of the experimental apparatus is predominantly managed using NI hardware with LabVIEW and DAQmx software.

A PXIe-1078 chassis houses a PXIe-8840 Quad-Core express controller, and three additional NI modules for data and control signal input and output: a PXIe-6363 Multi-function In/Out Module, a PXIe-4353 Temperature Input Module, and a PXI-6704 Analog Output Module (Figure 34).

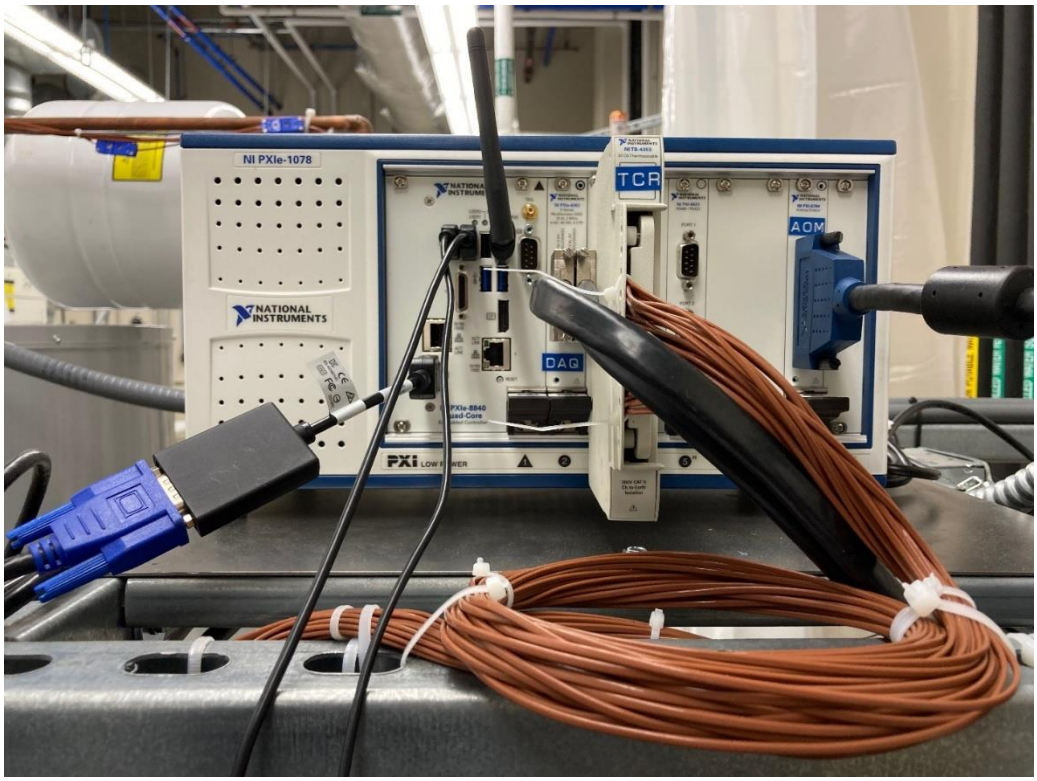

Figure 34: National Instruments Hardware

The PXIe-6363 Multifunction In/Out module (DAQ) is installed in Slot 2 of the chassis. Analog output channels of the DAQ are utilized for speed control of the source- and load-side circulator pumps. The DAQ is also used to acquire signals from the flow meters. Four programmable function interface (PFI) terminals are configured as counter channels: three for pulse-frequency measurement and a fourth for edge counting. Signal wires from each of the three flow meters are connected to a separate pulse-frequency channel. A jumper wire is placed between the edge counting terminal and the pulse frequency terminal used with the flow meter installed on the outlet of the DHW tank. This configuration allows simultaneous measurement of flow rate and discharge volume as required for the emulation of the DHW demand schedule (Figure 35).

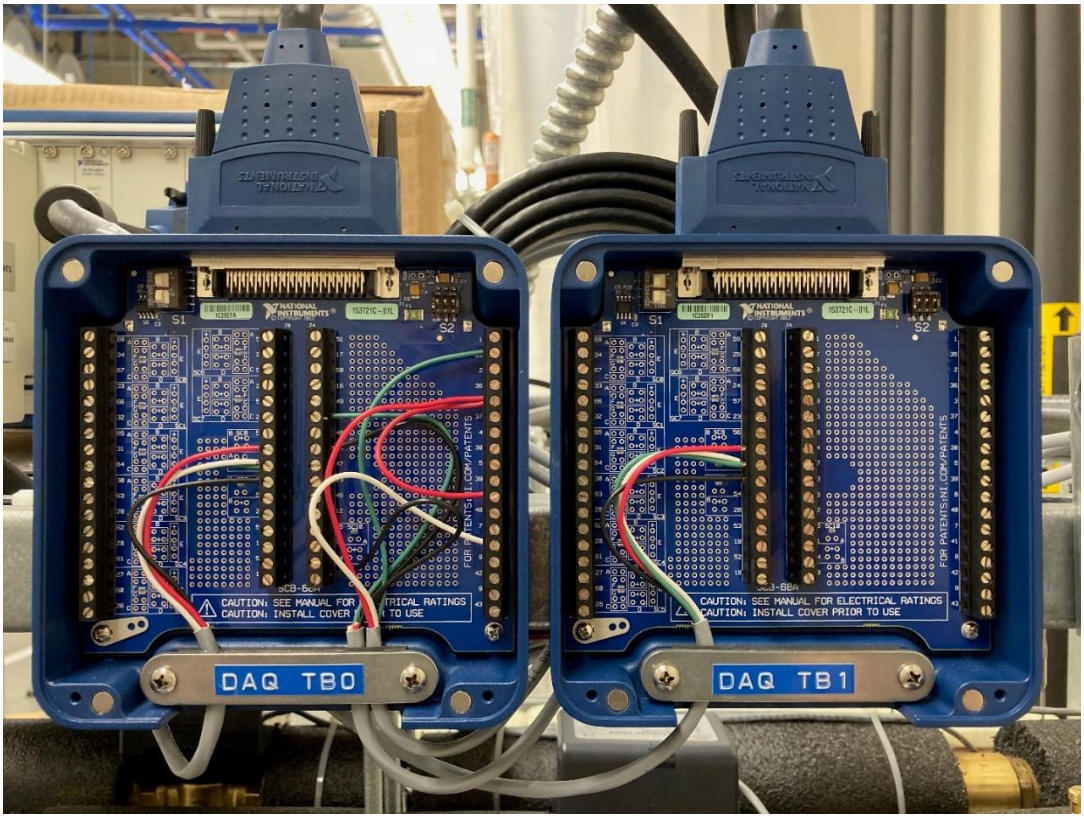

Figure 35: PXIe-6363 Multifunction I/O Module Terminal Block Wiring

The PXIe-4353 Temperature Input Module (TCR) is installed in Slot 3 of the chassis. This module is coupled with an NI Isothermal Terminal Block that optimizes thermal conductivity between the thermocouples and built-in thermistor cold-junction compensation (CJC) channels. A total of 28 thermocouples are connected for temperature readings (Figure 36).

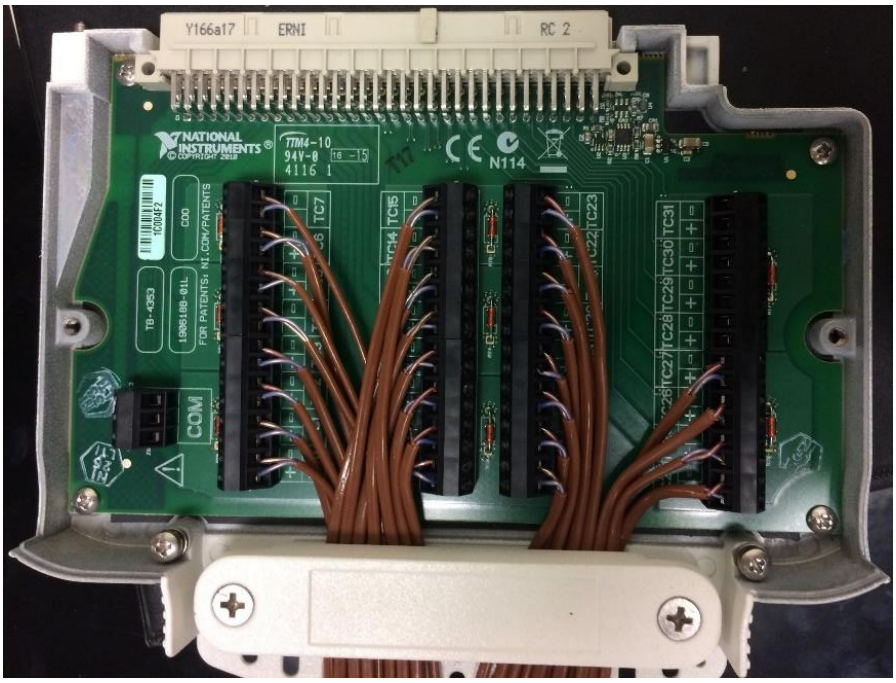

Figure 36: PXIe-4353 Temperature Input Module Isothermal Terminal Block Wiring

The PXI-6704 Analog Output Module (AOM) is installed in Slot 8 of the chassis. Seven voltage output channels are utilized for control of 2-way valves, and eleven current output channels are utilized for control of 3-way valves. Three additional voltage output channels are used to provide reference signals to the relay controller for switching of heat pump control signals and power supplied to the 2-way and 3-way electronic valves (Figure 37).

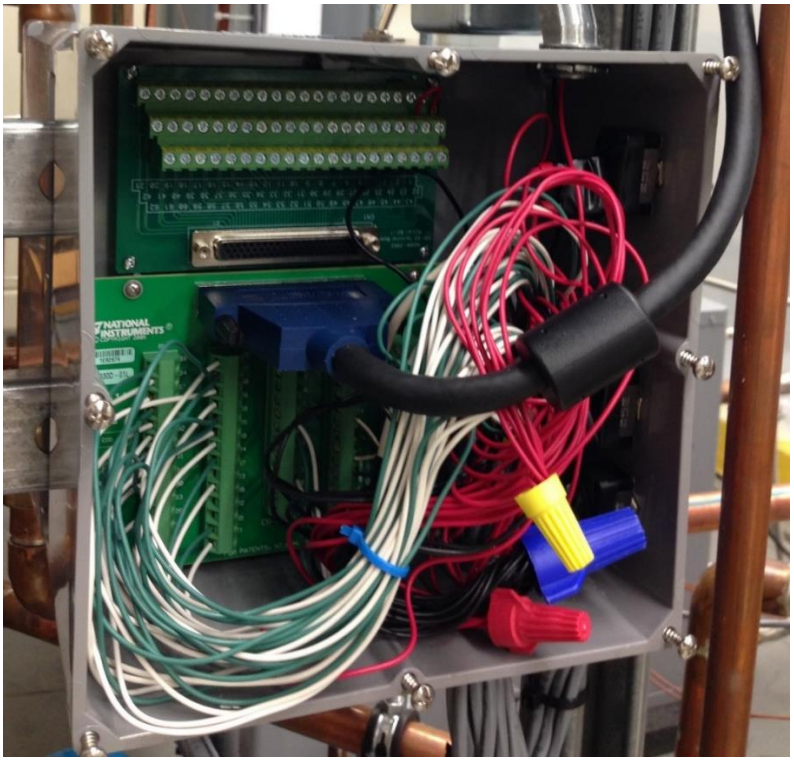

Figure 37: AOM Terminal Wiring

3.3 System Integration

In this section, the integration of experimental apparatus components is presented. Visual aids are used to illustrate the completed design configuration, and LabVIEW programming developed for this project is discussed. Figure 38: Experimental Apparatus Laboratory Set-Up shows the completed laboratory setup of the experimental apparatus. In Figure 39: Experimental Apparatus – Alternate View Showing User Workstation, the installed system is viewed from a second vantage point, including the user workstation for MISAHP system testing with LabVIEW.

Figure 38: Experimental Apparatus Laboratory Set-Up

Figure 39: Experimental Apparatus – Alternate View Showing User Workstation

Figure 40: Experimental Apparatus Equipment Detail combines elements from system diagrams presented in previous sections to offer a comprehensive illustration of all electrical, mechanical, and electromechanical components and their relative positions in the experimental apparatus.

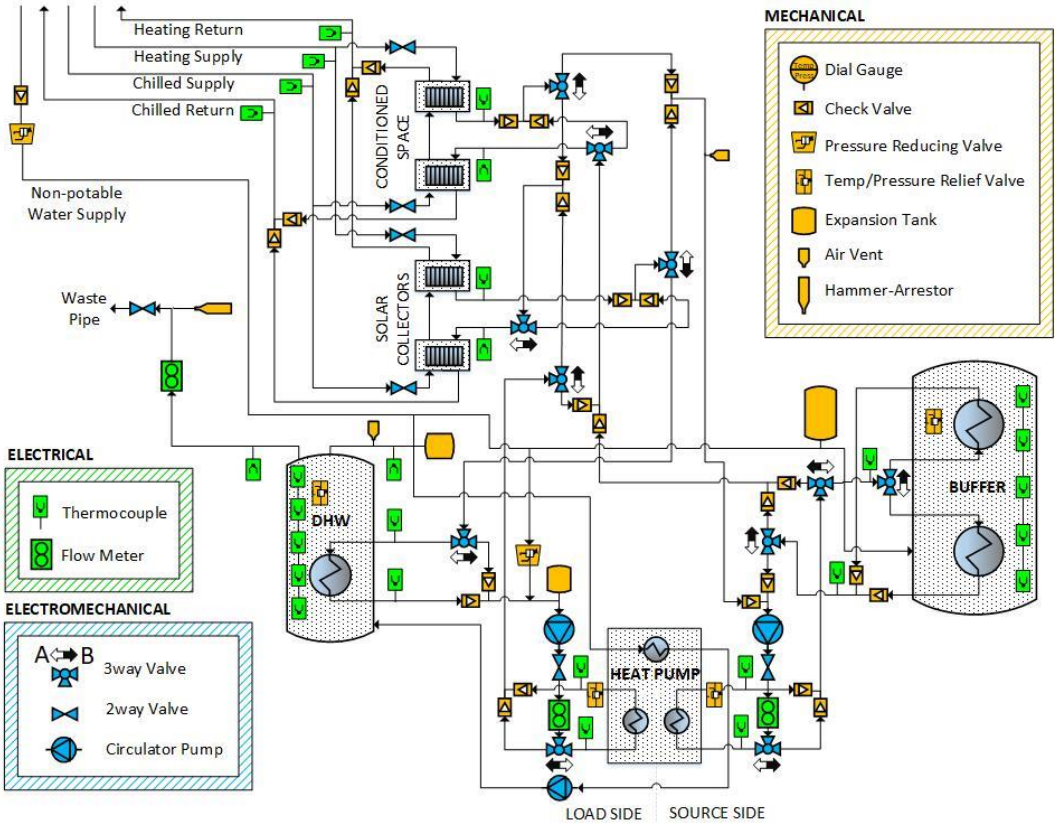

Figure 40: Experimental Apparatus Equipment Detail

NI LabVIEW graphical programming language was used for hardware control and data collection. Modular sub-programs were created in LabVIEW to handle individual tasks, and tested in isolation before incorporation with the main program, beginning with position control for 3-way valves to establish water loops as required for testing of other components.

Figure 41 provides an example of how 3-way valve positions are used to create the desired flow pathways used for Mode 2: Buffer Storage -> Heat Pump -> DHW

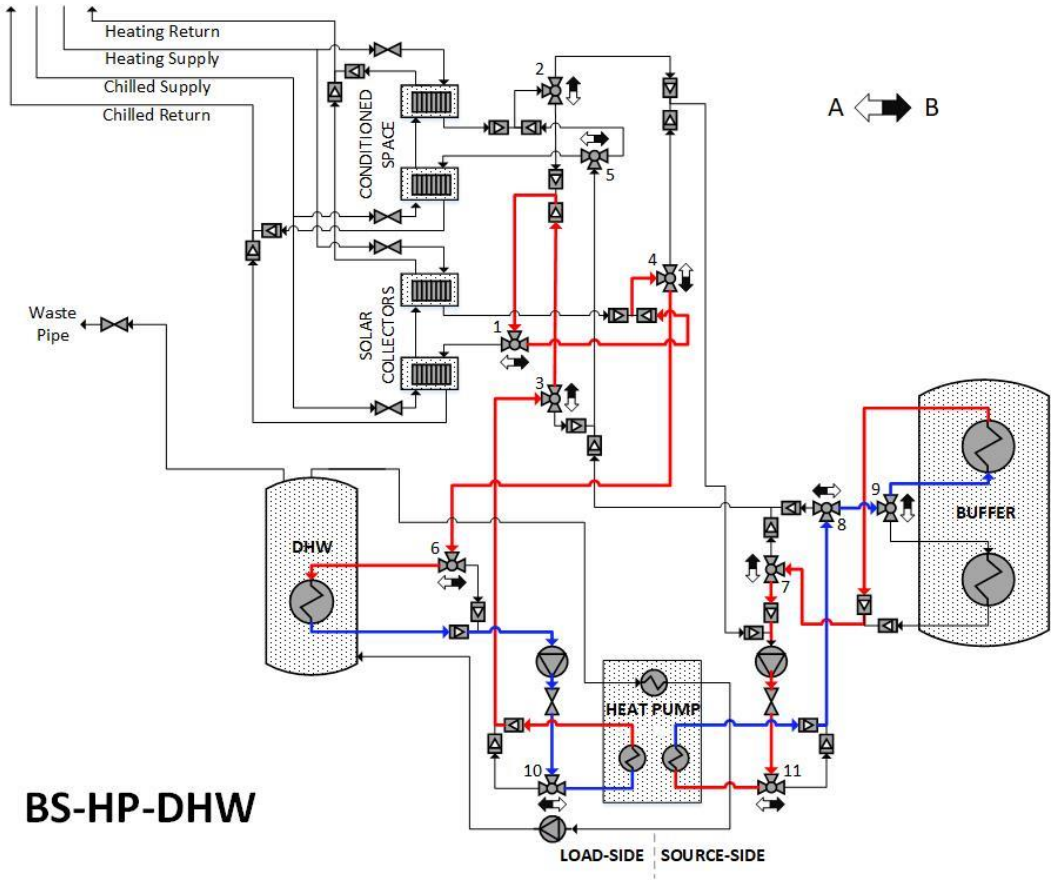

Figure 41: Mode 2: BS-HP-DHW Flow Pathways

3-way Valve positions for each mode are shown in Table 9. Recall from Section 3.2.4 that the A position corresponds to a control signal of 4mA, and the B position corresponds to a control signal of 20mA. A blank entry in the chart designates valves that are not included in active loops for a given mode for ease of reference; however, in practice, inactive valves are sent a control signal for the default (A) position.

Table 9: 3-way Valve Position Schedule

		Valve#/Position (Open Port)										
#	Mode	1	2	3	4	5	6	7	8	9	10	11
1	Collector Array–> DHW	A		B	B		A				B	
2	Buffer Storage -> Heat Pump -> DHW	A		B	B		A	A	A	B	A	A
3	Collector Array -> Conditioned Space	A	A		A	A			B			B
4	Collector Array -> Heat Pump -> Conditioned Space	A	B	B	B	A	B		B		A	A
5	Buffer Storage -> Conditioned Space		B			A		B	A	B		B
6	Buffer Storage -> Heat Pump -> Conditioned	B	A	A	B	A	B	A	A	B	A	A
7	Conditioned Space -> Heat Pump -> DHW Tank	B	B	B	B	A	A		B		A	A
8	Conditioned Space -> Collector Array	A	A		A	A			B			B
9	Conditioned Space -> Heat Pump -> Collector Array	A	B	B	B	A	B		B		A	A
10	Conditioned Space -> Buffer Storage		B			A		B	A	A		B
11	Conditioned Space -> Heat Pump -> Buffer Storage	B	A	A	B	A	B	A	A	A	A	A
12	Collector Array -> Buffer Storage	A	A		A	B		B	A	A		B
13	Collector Array -> Heat Pump -> Buffer Storage	A		B	B		B	A	A	A	A	A
14	Buffer Storage -> Collector Array	A	A		A	B		B	A	B		B
15	Buffer Storage -> Heat Pump -> Collector Array	A		B	B		B	A	A	B	A	A

Data arrays were constructed in LabVIEW with 3-way valve position control signals corresponding to each mode. These signals are output from the AOM to the valve actuators to define the flow paths for operation, allowing sufficient time for valve travel between control signal changes. The response of the valves was verified visually referencing the position of the manual override level on the side of each actuator to confirm that the desired positions were reached in each mode with smooth transitions between modes. In early iterations of the sub-program, control signals were written to the hardware inside a while-loop to create a continuous signal. Some irregularities were detected in actuator response, with two of the valve actuator motors twitching intermittently after reaching position. While this had no appreciable effect on the valve's positions, it was noted that after some time, actuators displaying this behavior began to heat up, raising concerns for eventual damage to the device. Initially, defective hardware seemed to be the most likely explanation given that symptoms were observed for just two out of eleven valves. To move forward with the project, the two problematic valves were manually positioned for testing of other system components. Further observations later in the development of 2-way valve control sub programs indicated that the irregular actuator behavior was a control issue, to be resolved programmatically.

A similar coding structure was implemented for the 2-way valves. The initial response was as expected; however, after repeated sequential execution of 3-way and 2-way valve control sub-programs, more irregularities occurred. The same twitching behavior was exhibited by the 2-way valves, as well as some additional 3-way valves, inconsistently across multiple tests. The while-loop was removed from both subprograms and replaced by sending a single control signal for each position command sent to the valves. This change resolved the twitching behavior but revealed another unexpected difficulty. When the subprograms for valve control were run simultaneously, some valves failed to stop at the desired position. In several instances, running the 3-way valve program triggered the movement of 2-way valves not commanded to change position. Repeated execution of the same commands appeared to compound the issue. For example, while initially a 5V signal sent to any of the 2-way valves resulted in a final position at the center of their range of travel, successive tests showed increasingly disparate results, with different valves stopping at very different positions in response to the same control value.

As described previously, electronic valves are controlled using the AOM. The control signal wire for each valve is connected to a separate output channel, with 3-way valves assigned to current output channels and 2-way valves assigned to voltage output channels. Voltage and current output channels on the AOM are paired to a shared ground terminal. One possible explanation for the irregularities in actuator response is signal interference related to these shared ground terminals; however, the exact nature of this issue remains unknown.

Due to time constraints, a workaround was devised. A third RIB relay was connected to the Relay Controller, and used to switch power between valve groups, with all 3-way valves wired as normally open, and 2-way valves wired as normally closed. In this configuration, power is supplied by default to 2-way valves only. The sub-program for 3-way valve control was updated to include the output of control signals from an available channel on the AOM to the Relay

Controller to close the relay for 35 seconds to allow the 3-way valves to travel from the central "reset" position to the appropriate A or B position, then open the relay, disabling the 3-way valves and returning power to the 2-way valves. This approach ensures that 3-way valves remain in the desired position for the duration of the run cycle, and prevents any interference in control signals sent to 2-way valves for emulation control. AOM voltage output channels used for reference signals sent to the Relay Controller were selected that do not share a ground terminal with an active current output channel to avoid interference issues.

CHAPTER 4: EXPERIMENTAL APPARATUS TESTING AND RESULTS

4.1 Commissioning

Following construction, the experimental apparatus was commissioned with a water pressure test of the system, flushing procedure, individual component testing, and system testing.

The water pressure test was conducted to verify that the pipelines and components could endure the expected operating pressure: 2.8 MPa (40psi) for distribution piping and water tanks, and 1 MPa (15psi) for MISAHP system piping. For this test, an iterative process of systematically filling and pressurizing different parts of the system is used to identify and address any water leakage.

After the water pressure test, the flushing procedure was implemented to remove contaminants including residual solder flux and carbon deposits from soldering to reduce the risk of corrosion and component fouling. Water pressure at the mains was used for flushing, and spent water was discharged into the laboratory waste drain.

3-way valve positions were adjusted using the manual override lever on the actuator to achieve the various flow paths necessary to remove contaminants from all branches of system piping. Additionally, the braided steel hoses at the water connections of the heat pump are uncoupled at the outlet to give special attention to ensure adequate cleaning of the coils. For each element addressed, flushing is performed until water discharged is completely free of visible contaminants. Detailed procedures used for the water pressure test and system flushing are provided in Appendix C and Appendix D.

4.2 Component Testing

With system flushing complete, individual components were tested to verify basic functionality as expected. NI Measurement and Automation Explorer (NI-MAX) was used to generate and acquire analog signals for testing of electromechanical components and instrumentation.

Successful operation was thus confirmed for the relay controller, variable speed circulator pumps, 2-way and 3-way electronic valves, thermocouples and flow meters.

The component tests via NI-MAX identified two major problems. First, unexpected interactions between 2-way and 3-way valve control resulted in abnormal actuator response to control signals, as mentioned previously in describing the necessity of the relay controller (Section 3.3). Second, very low flow rates achieved on source-side water loops, regardless of pump speed, indicated that the commissioning procedure had failed to purge the system of air.

As described in Section 3.2.4, a mechanical air vent was installed at the high point in the MISAHP piping to remove trapped air. The shut-off used to fill the piping of the MISAHP system was opened to supply makeup water, and the source-side circulator pump was set to run at full speed. In multiple stages, 3-way valve positions were manually adjusted to divert the flow path through alternating branches of system piping in an effort to pass air bubbles to the appropriate point for release at the vent. Auditory clues (hissing and gurgling sounds) and a logical approach based on valve positions used in the different operational modes of the system informed a sequence of position changes for the 3-way valves to successfully bleed off the remaining air, however the process was very time-consuming. If the experimental apparatus piping is modified in the future, additional air vents should be strategically installed elsewhere in the system to avoid the reoccurrence of this problem. After all air was removed from the system, flow rates on the source-side loop increased to reasonable levels corresponding to pump speed.

Another test was conducted to verify the operation of the DHW auxiliary resistance heating element. The factory DHW thermostat setting of 49 °C was retained. The DHW auxiliary heating element circuit was energized, and the main program in LabVIEW was used to record temperature data for 2 hours.

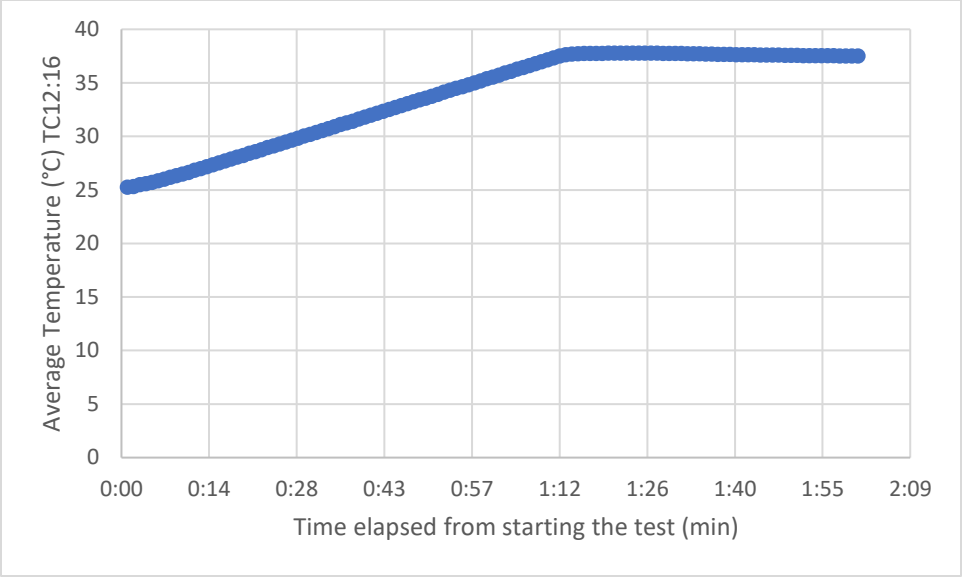

Figure 42: DHW Auxiliary Heating Element Testing

Results from this test verified the basic functionality of the DHW auxiliary heating element, and demonstrated the operation of the thermostatic control mechanism. As shown in Figure 42: DHW Auxiliary Heating Element Testing, the average of measurements from the five DHW in-tank thermocouples increased from 25.25°C to a maximum of 37.78°C after 1 hour and 27 minutes, at which point the temperature began to decrease slowly. It can be inferred from this observation that the heating element was shut off by the thermostat somewhat prematurely. The highest temperature value was 47.42°C (recorded by TC13 after 1 hour and 30 minutes), more than 2 degrees below the setpoint of 49°C.

After basic functional control of individual MISAHP system components was established, system and subsystem testing were conducted. The objectives of these tests were: 1) to debug and verify the functionality of implemented LabVIEW programs, 2) to further verify the functionality of physical components at dynamic boundary conditions, 3) to verify the experimental apparatus, including both hardware and software, can be used to support future research on solar-assisted heat pump systems, and 4) to identify areas for potential improvement and further investigations. These tests were carried out through an iterative process of testing for

the system and each of its subsystems, and the resolution of problems as identified in successive test runs. An in-depth description of the procedures applied to these tests would be cumbersome and of little value, therefore no such discussion is included in this thesis. The following sections will focus on the use of the LabVIEW program for subsequent testing of selected operational modes and system response characteristics.

4.3 LabVIEW Program for System Operations

The main program developed for this thesis to verify system operation features a graphical user interface (GUI) with system controls and indicators on the front panel. These are organized with tabs into five categories including a general run interface tab (Figure 43), a storage tab with waveform charts for monitoring thermal stratification and temperature averages for each tank (Figure 44), a heat pump tab with waveform charts for inlet and outlet temperature readings (Figure 45), a source/load emulation tab with waveform charts for monitoring the inlet and outlet temperature readings of the collector array and conditioned space emulators (Figure 46, Figure 47), and an occupant emulation tab with controls and indicators related to DHW discharge (Figure 48).

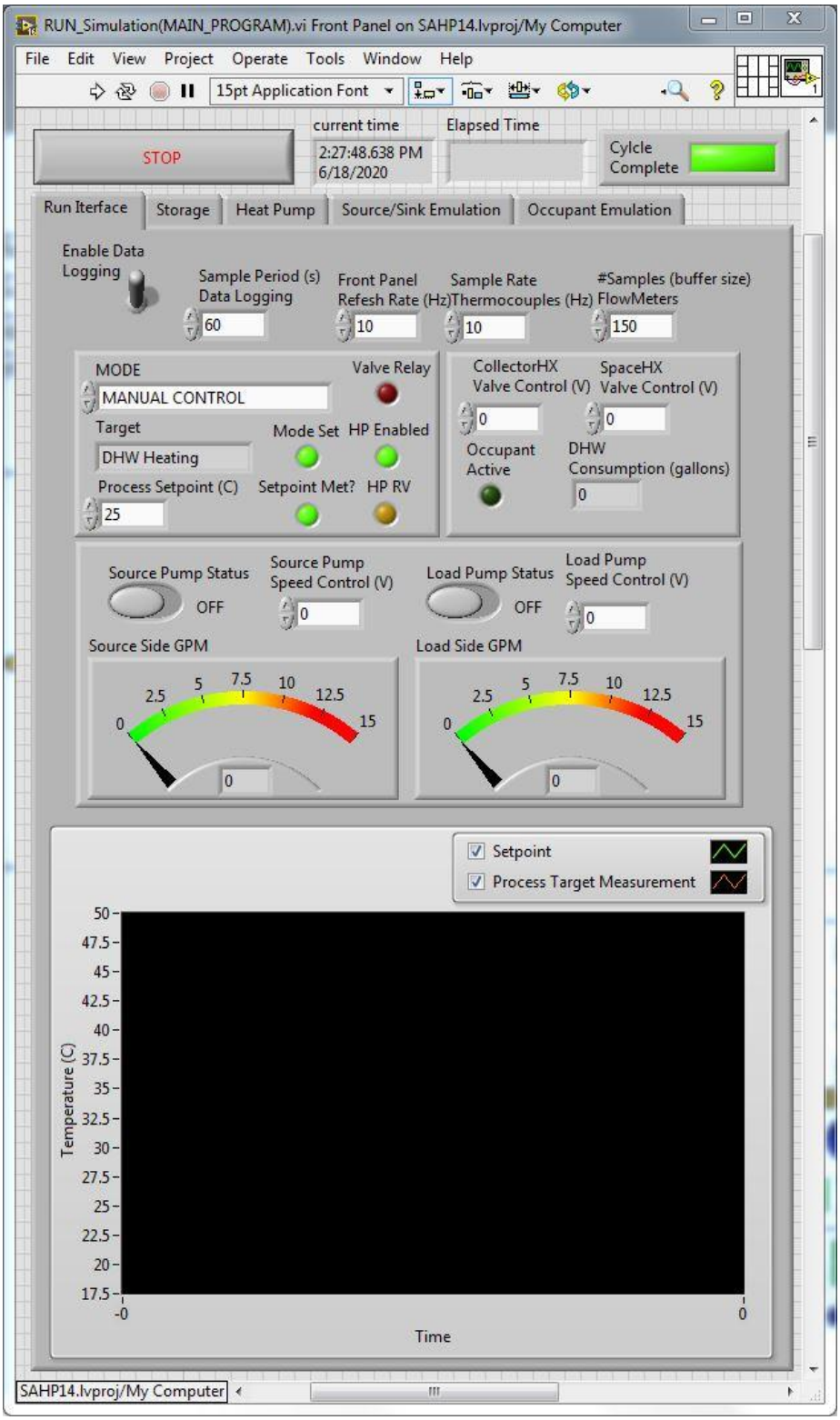

Figure 43: LabVIEW GUI – Run Interface Tab

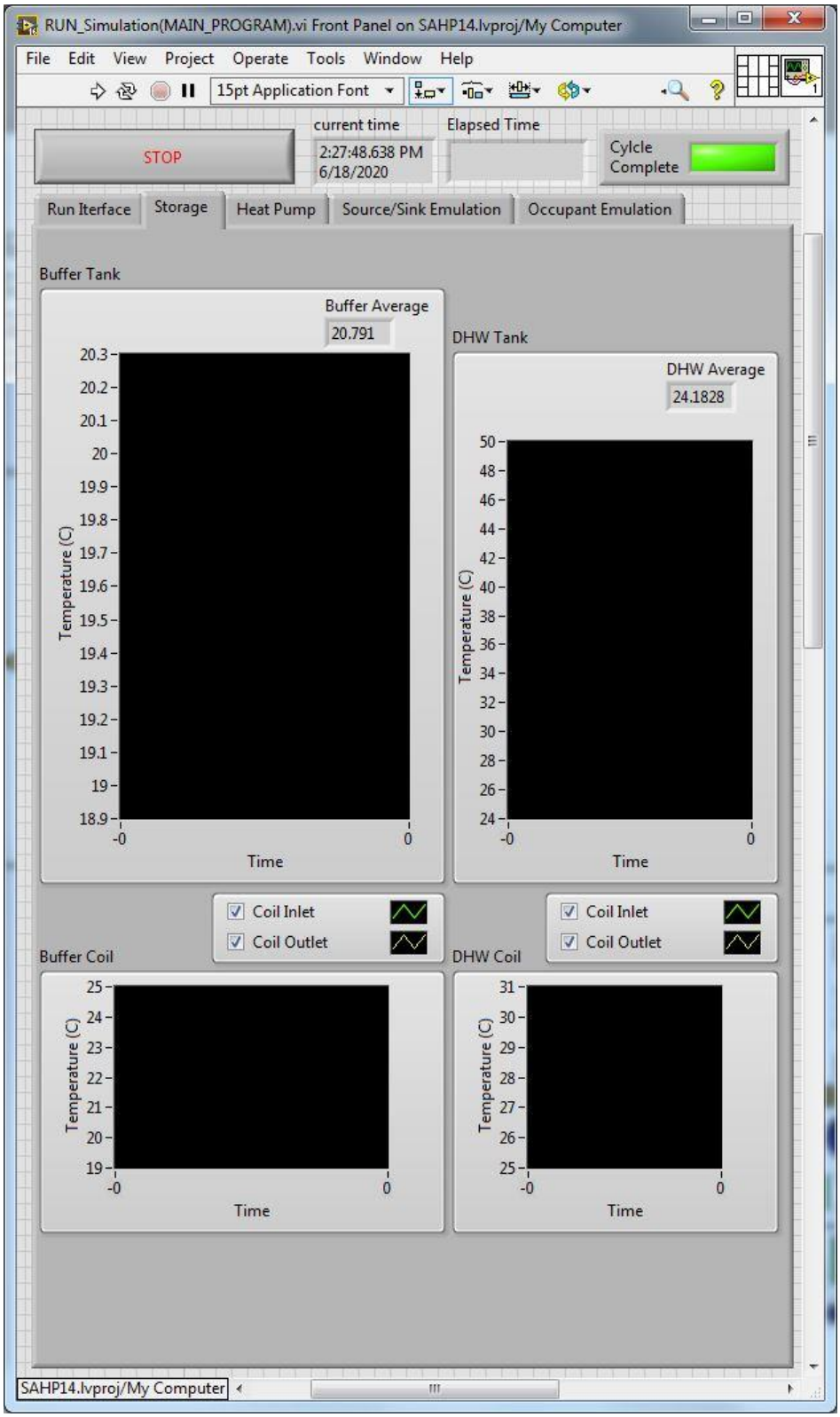

Figure 44: LabVIEW GUI - Storage Tab

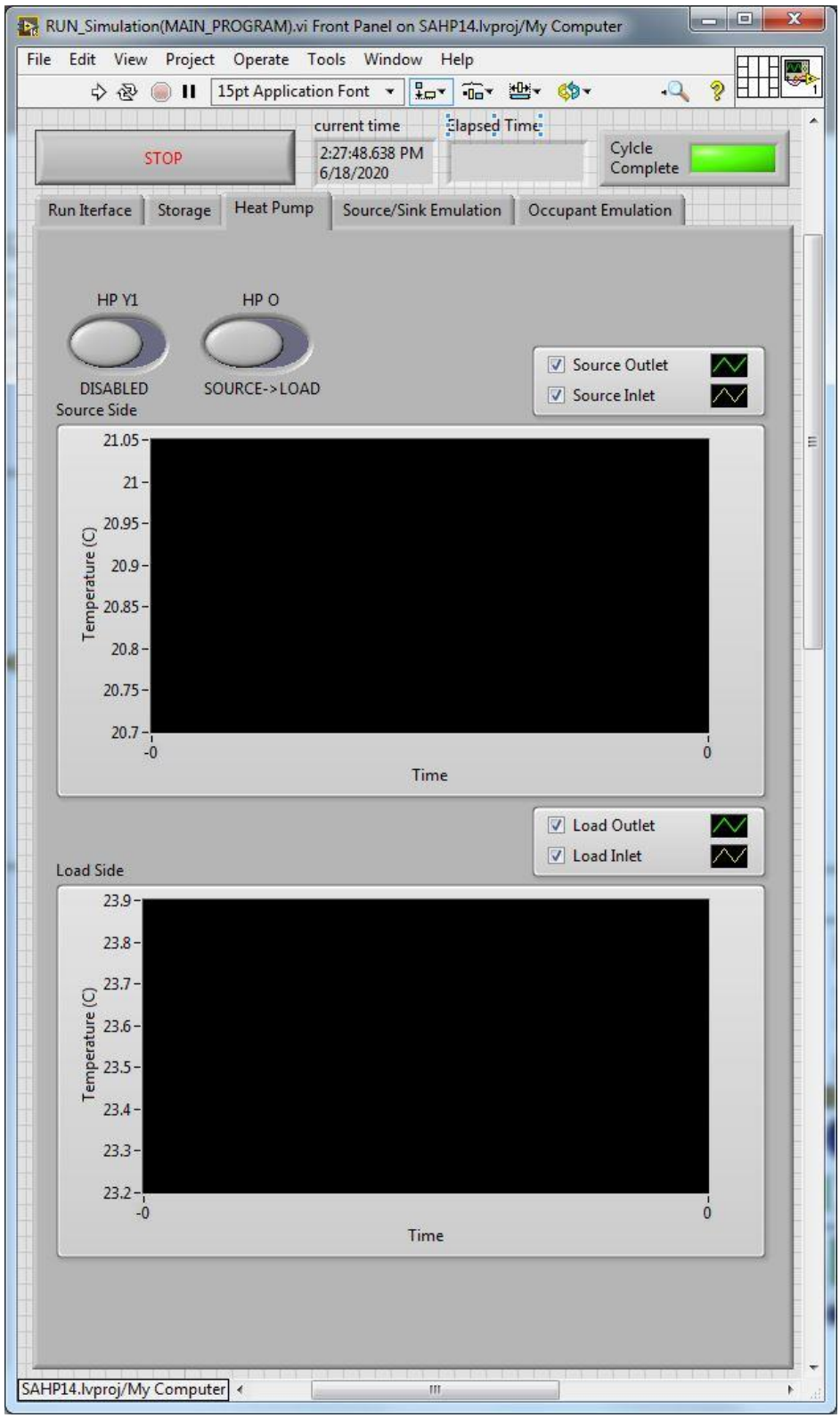

Figure 45: LabVIEW GUI - Heat Pump Tab

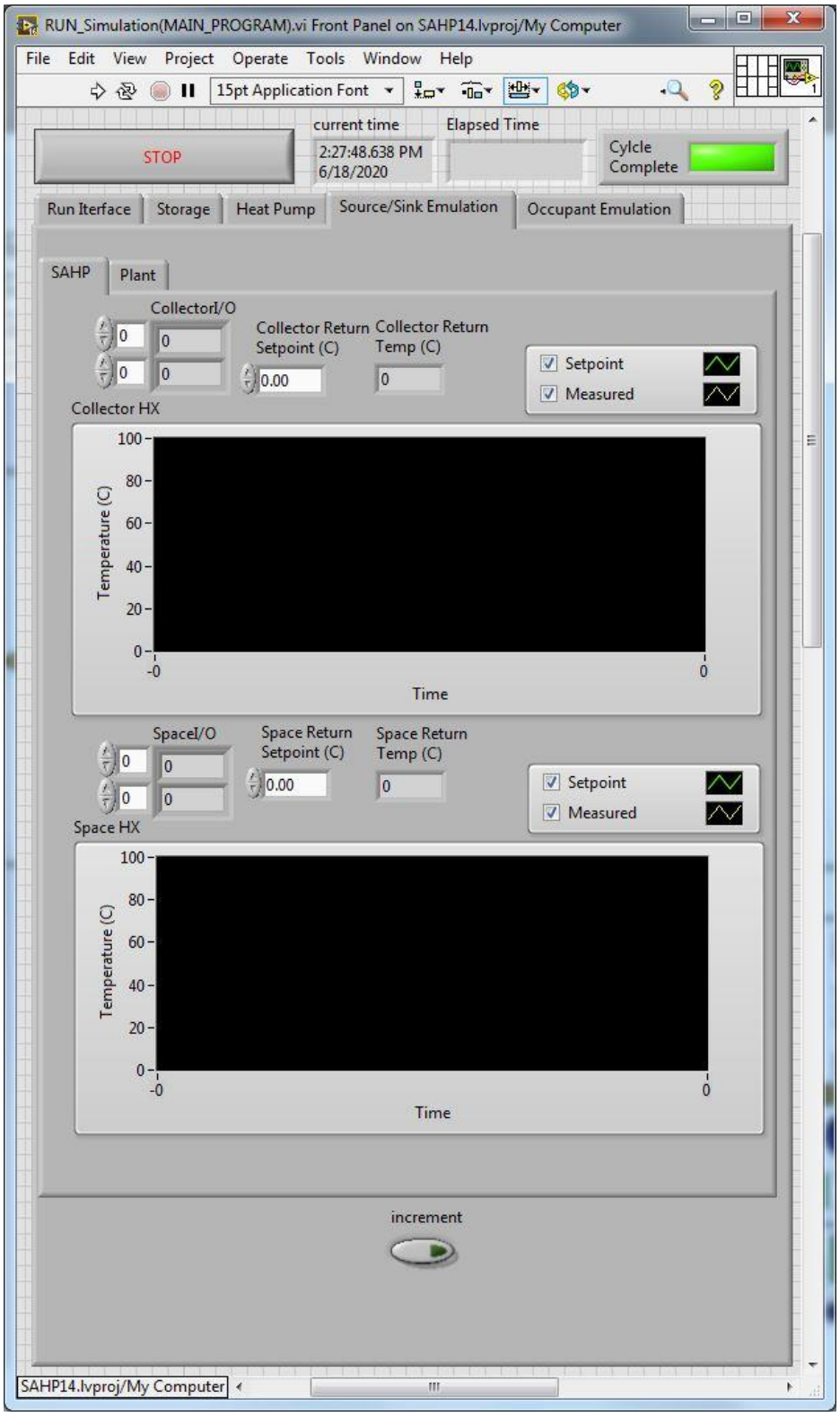

Figure 46: LabVIEW GUI - Source/Sink Emulation Tab, SAHP

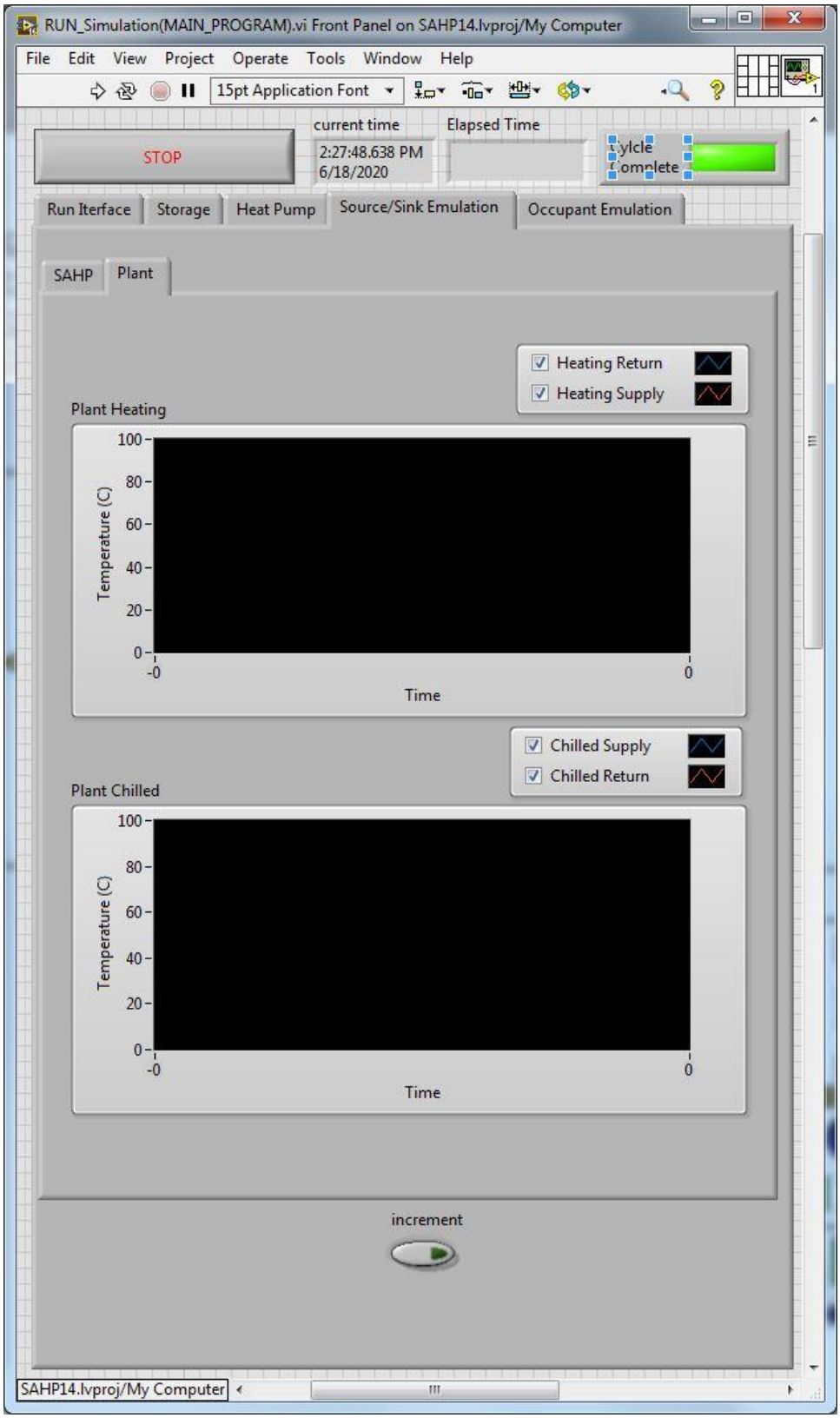

Figure 47: LabVIEW GUI, Source/Sink Emulation Tab, Plant

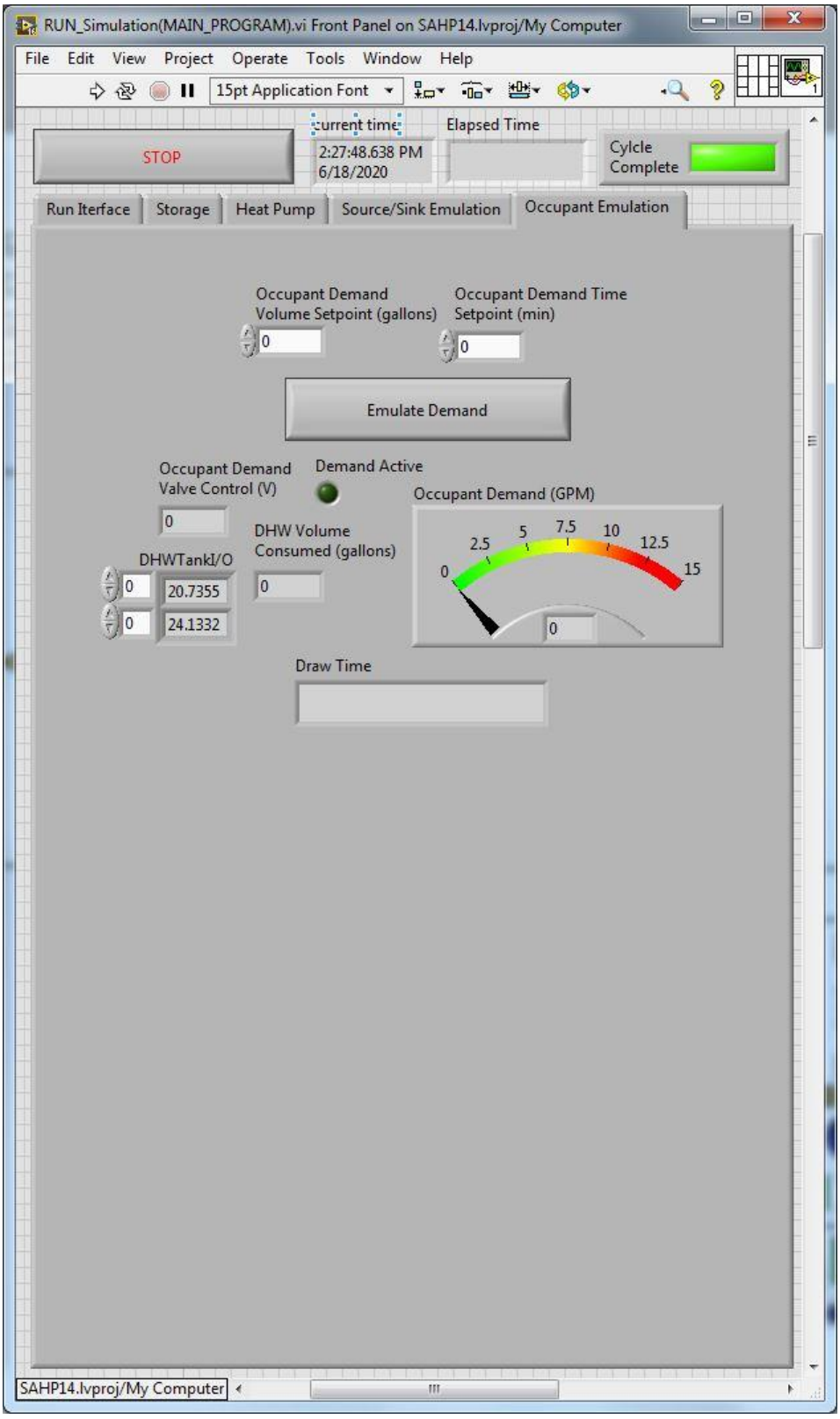

Figure 48:LabVIEW GUI - Occupant Emulation Tab

Before initiating a test run, the user selects operational parameters for the system on the run interface tab, including operational mode, target (process) setpoint, and data sample rates. Sixteen options appear in the mode selection menu corresponding to the 15 operational modes previously described, as well as a manual mode where 3-way valve positions are individually defined by the user (Figure 49).

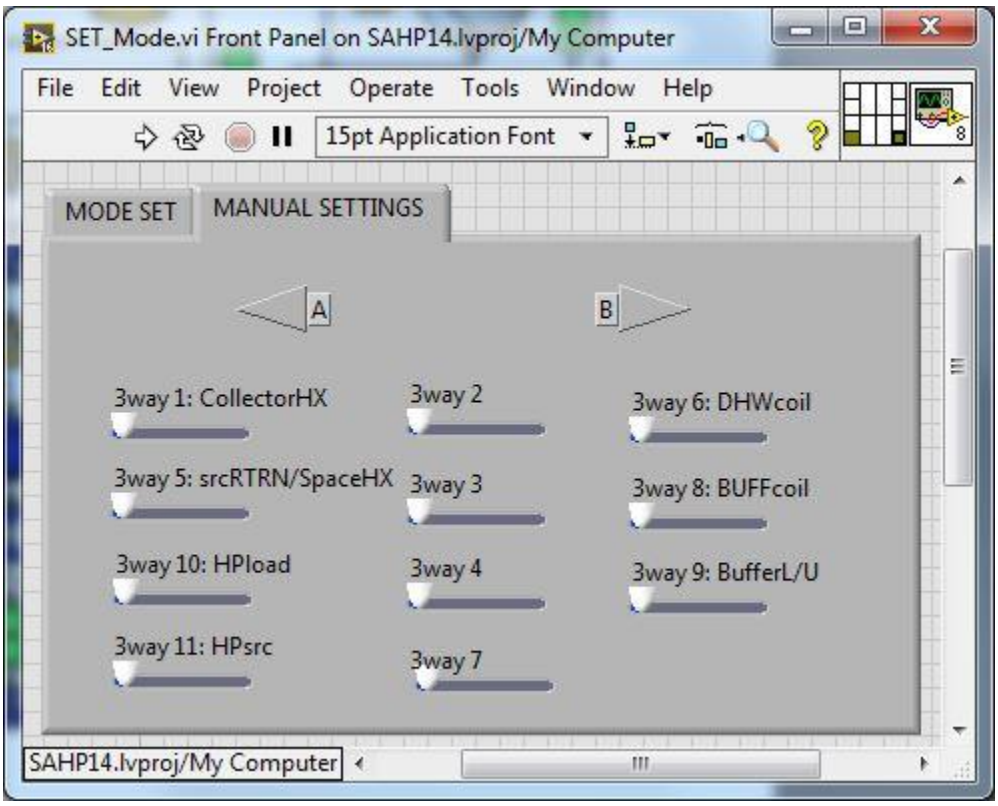

Figure 49: LabVIEW Manual 3-way Valve Position Controls

A the start of the test run, the program references the user-selected operating mode to determine appropriate control actions for 3-way valves and relays and to enable the appropriate hardware for the run cycle, including circulator pumps, 2-way valves, the heat pump compressor and reversing valve. Additionally, mode selection defines the run cycle target, selecting which temperature reading to compare with the user-defined setpoint.

A 2V control signal is sent to the Relay Controller to energize the valve relay, closing the circuit supplying power to the 3-way valves. Position control signals are sent to each of the 3-way

valves, and a timer suspends operation of the program for 35 seconds to allow the valves to travel to their desired positions before sending a 0V signal to the Relay Controller to deenergize the damper valve relay. This action disables the 3-way valves and returns power to the 2-way valves.

After the 3-way valve positions are set and mode parameters are defined, data logging, target monitoring, and boundary emulation are then initiated, and source- and load-side circulator pumps are started as required by the user-selected mode. If the heat pump is required, a 2V control signal is sent to the Relay Controller to energize the compressor relay, which closes the control circuit in the heat pump to start the compressor. The program references the source- and load-side flow meter signals, starting the heat pump only after both report a flow rate greater than 0.32L/s (5gpm). For modes requiring the heat pump to transfer energy from load-side to source-side, an additional 2V signal is sent to the Relay controller to energize the reversing valve relay, closing the control circuit in the heat pump to energize the reversing valve coil. In a typical installation, this would initiate cooling operation for the heat pump, however due to the complex configuration of the system, reverse operation is not necessarily utilized for cooling functions, but rather for modes requiring energy transfer from load-side to source-side. Throughout the run cycle, front panel indicators are updated to provide visual feedback to the user. Hardware status and source and load-side flow rates are displayed prominently on the main run interface tab, and user controls allow for pump speed adjustment and emulator valve position control on the fly. Additionally, at any time while the program is running, the user can define time and volume setpoints for DHW discharge and initiate an occupant demand event. Once initiated, the occupant demand emulation sub-program uses proportional and integral control to regulate the position of the 2-way valve on the DHW outlet, using feedback from the

occupant demand flow meter to approximate the DHW demand profile defined by volume and time duration. Occupant demand emulation can be initiated multiple times in a run cycle.

The program runs in the selected mode until the target setpoint is reached, or until the user clicks the stop button on the front panel. 0V control signals are sent to the Relay Controller to deenergize the compressor and reversing valve relays, initiating the shutoff sequence for the heat pump. Active pumps are stopped and disabled. Data logging is terminated, and the reset sequence begins. Again, a 2V control signal is sent to the Relay Controller to energize the damper valve relay, disabling the 2-way valves and supplying power to the 3-ways. A 0.012mA control signal is sent to all eleven 3-way valves, driving them to a central position in preparation for the next experimental run cycle. The program waits 35 seconds for the valves to reset, then sends a 0V signal to the Relay Controller to deenergize the valve relay, and the program terminates. The main program block diagram is included

APPENDIX F: LABVIEW PROGRAM BLOCK DIAGRAM.

4.4 Testing of Selected Operational Modes and Emulator Functions

In this section, five test scenarios are presented. The general functionality of the experimental apparatus is evaluated for four different operational modes, utilizing all hardware and software components (excluding the desuperheater), and the accuracy of DHW demand emulation is evaluated.

MISAHP Mode 1: Collector Array–> DHW
MISAHP Mode 12: Collector Array -> Buffer Storage
MISAHP Mode 2: Buffer Storage -> Heat Pump -> DHW
MISAHP Mode 13: Collector Array -> Heat Pump -> Buffer Storage
DHW Demand Emulation

Discussions as follow are included to explain the primary objective of each test, the approach to performing the test using the main program in LabVIEW, experimental results, and analysis of test data.

4.4.1 MISAHP Mode 1: Collector Array–> DHW

In this test, water in the DHW tank is heated using the collector array emulator. Figure 50 shows the flow path utilized by this mode, employing the load-side pump to circulate water between the DHW tank coil and the collector array emulator. The main objectives of this test are to demonstrate that the 3-way valves can be controlled to form the desired loop, and to observe the impact of the heating process using the immersed heat exchanger coil on thermal stratification in the DHW tank.

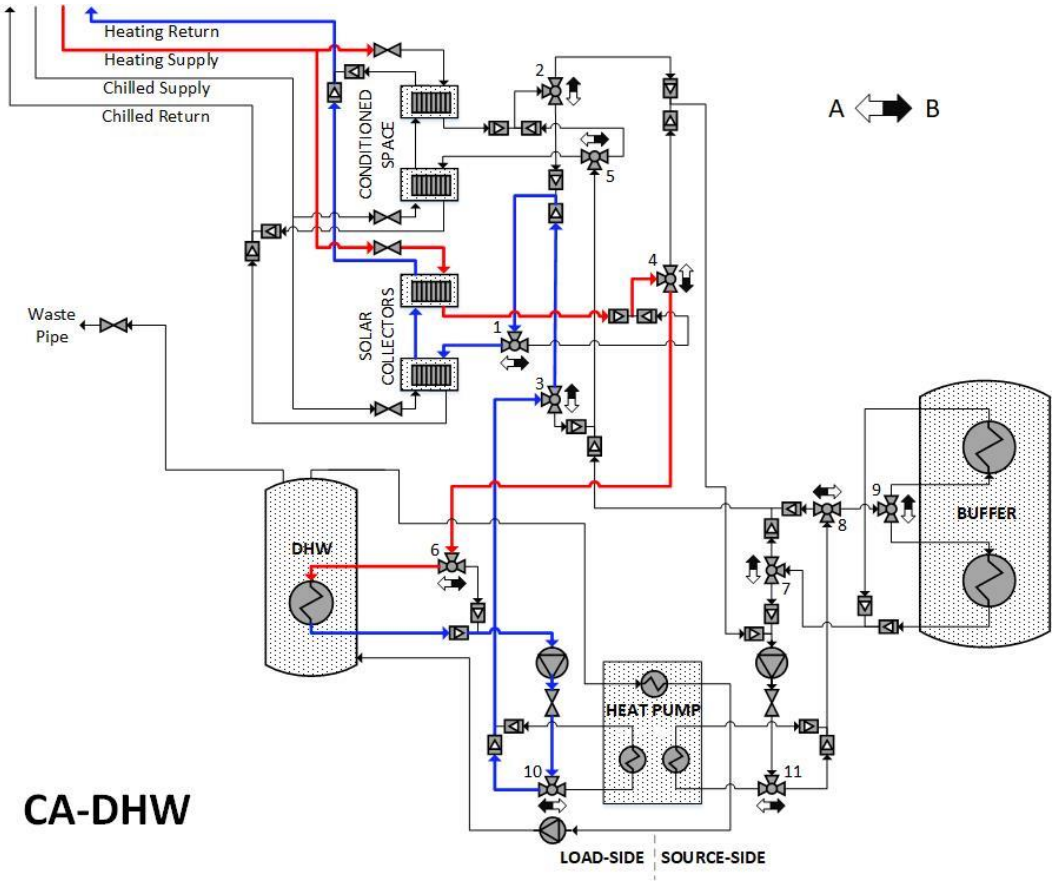

Figure 50: Mode 1: Collector Array -> DHW Tank

Parameters were defined for this test run using controls on the main program's Run Interface panel as shown in Figure 51. COLLECTOR->DHW was selected from the options in the mode control. Additional parameter values were selected by the user, and numerical controls on the Run Interface panel set. A value of 4 was entered for speed control voltage of the load-side pump, and 2.25 was entered for position control voltage of the 2-way valve at the plant heating loop inlet to the collector array emulator. A process setpoint of 50 °C was entered. Data logging was enabled, and the program's default settings for data acquisition were retained to record temperature and flow rate measurements at 1-minute intervals. Additional parameters not relevant for this test were left unchanged on the Run Interface controls. The test run was initiated with the run arrow button on the top left-hand side of the main program window.

Figure 51: CA->DHW - Run Interface

Figure 52 shows the inlet and outlet water temperatures on both sides of the collector array emulator. The temperature of hot water (TC1) supplied from the EPIC building is constant at about 71°C. After exchanging heat with the relatively cold water from the DHW tank, the plant water temperature (TC0) dropped to 54°C at the 4th minute and 61°C at the 28th minute at the test end. As expected, the temperature drop (TC1-TC0) decreases as the inlet temperature (TC7) on the MISAHP side of the collector array emulator increases. Based on the recorded data, the average effectiveness of the heat exchanger is calculated to be 64.4%, without considering the heat loss to the surrounding. Note that in the first 3 minutes, the measured temperatures of TC0 and TC7 drop significantly due to the thermal mass of the heat exchanger.

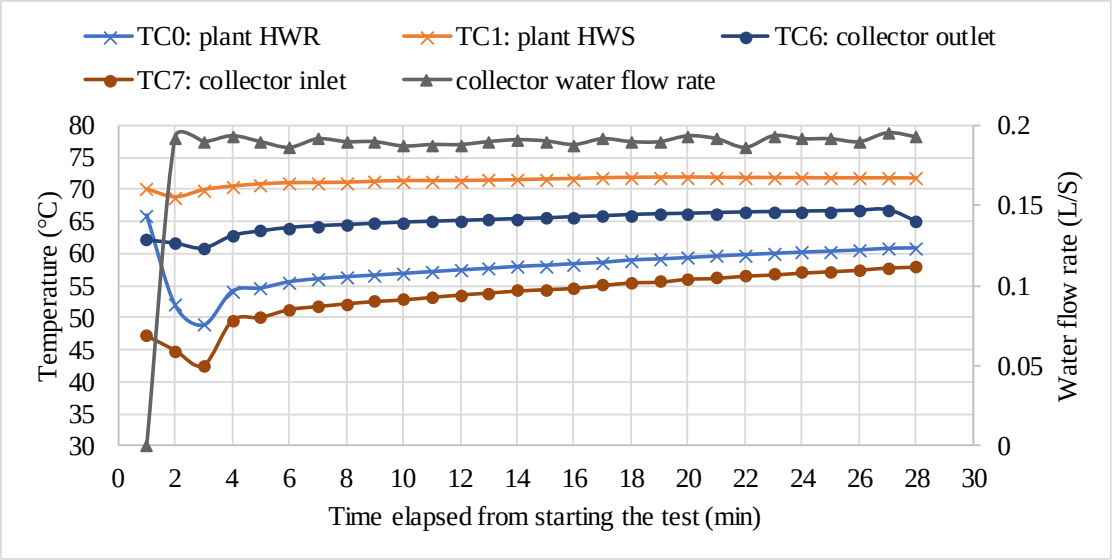

Figure 52: CA-DHW Temperature Readings

Figure 53 shows the five temperature readings recorded from the vertical thermocouple probe installed in the DHW tank. Over the 28 minute run time of this test, the water temperature reading at the bottom of the tank (TC16) increased by 10.2°C from 36°C to 46.2°C whereas the other four temperatures increased by 11.2°C from 39.5°C to 50.7°C. Several interesting phenomena can be observed:

- The temperature sensor (TC12) located on the top has slightly (~1°C) lower temperature than the three sensors at the intermediate heights. This observation indicates that the topmost water layer does not have the highest temperature because of the heat losses through the tank top surface.
- The three temperature sensors placed in the middle of the tank have almost identical temperature readings.
- DHW heating via the immersed heat exchanger has a negligible impact on thermal stratification.

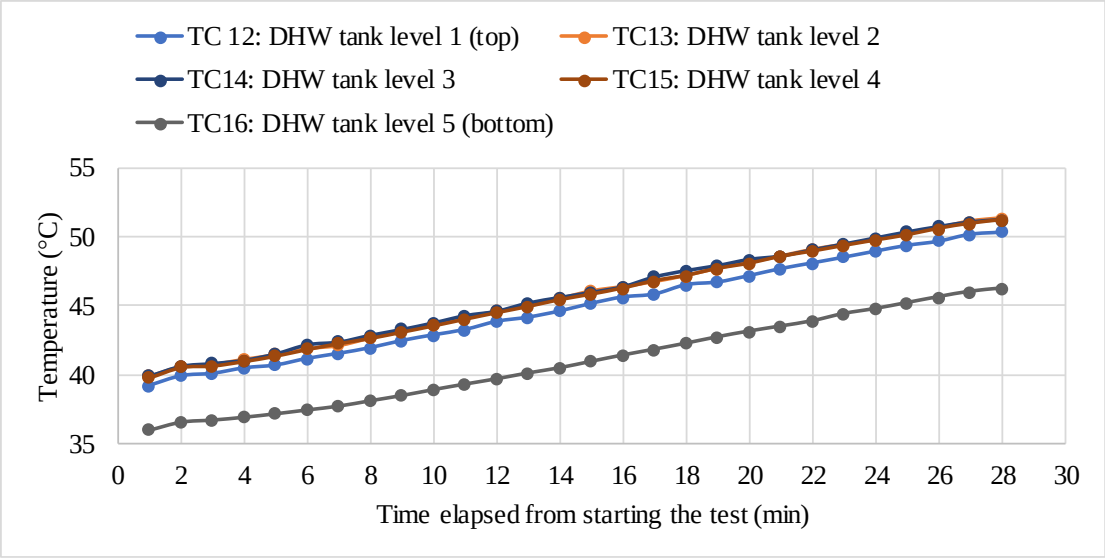

Figure 53: CA->DHW – DHW Tank Vertical Thermocouple Probe Temperature Readings

4.4.2 MISAHP Mode 12: Collector Array -> Buffer Storage

In this test, water in the buffer storage tank is heated using the collector array emulator. Figure 54: Mode 12: Collector Array -> Buffer Storage shows the flow path utilized by this mode, employing the source-side pump to circulate water between the lower coil of the buffer storage tank and the collector array emulator. The main objectives in this test are the following: 1) to verify that the 3-way valves are controlled correctly according to the schedule in Table 9: 3-way Valve Position Schedule for this mode and the desired flow paths are achieved, 2) to investigate the behavior of the 2-way valve to a range of control signal values as it relates to flow regulation of plant heating water and outlet temperatures from the collector array emulator, and 3) to investigate the impacts on thermal stratification in the buffer storage tank during the heating process using the lower immersed coil.

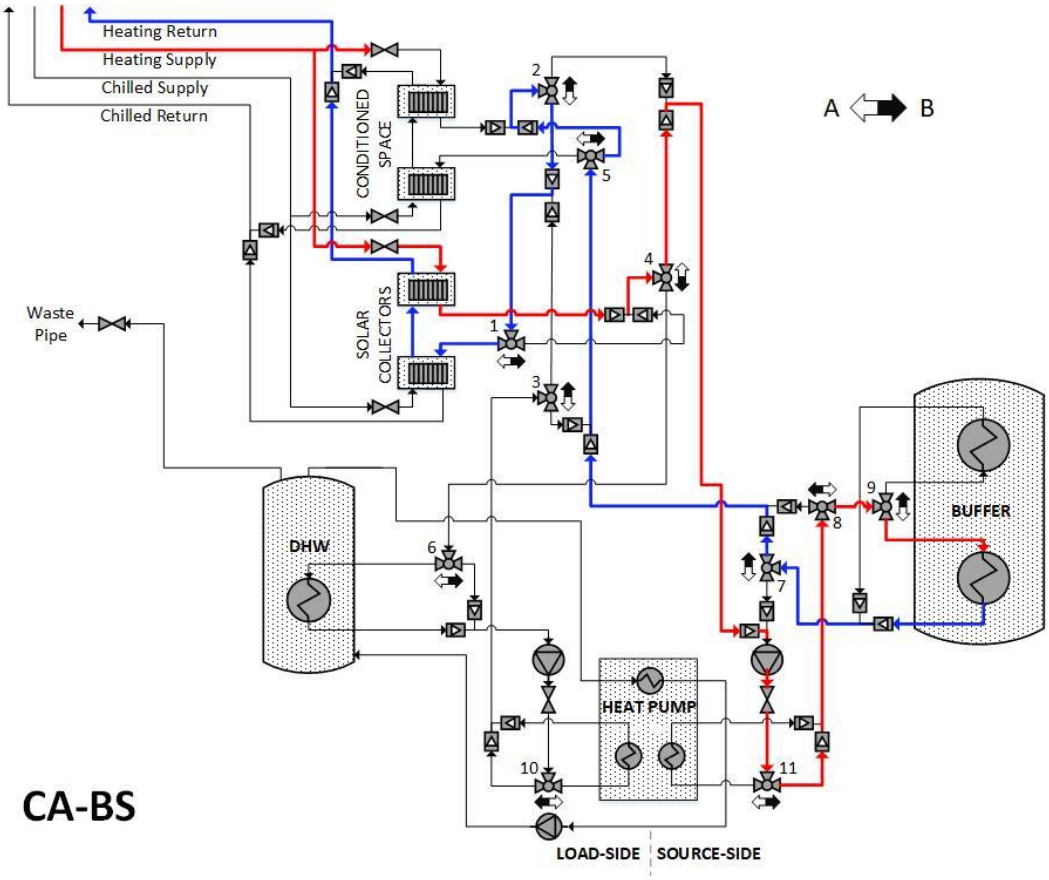

Figure 54: Mode 12: Collector Array -> Buffer Storage

As before, parameters were defined for this test run using controls on the main program's Run Interface tab. COLLECTOR->BUFFER was selected from the options in the mode control. A value of 7.5 was entered for the speed control voltage of the source-side pump. Process setpoint monitoring was disabled from the control on the global variables panel to allow the program to run continuously until stopped by the user. Data logging was enabled, an data acquisition settings were adjusted to record temperature and flow rate measurements at 5-second intervals. Additional parameters not relevant for this test were left unchanged on the Run Interface controls. On the source/sink panel tab, a Boolean control added specifically for this test was used to enable automated adjustment of position control values sent to the 2-way valve on the plant heating water inlet to the collector array emulator. This control value was thus gradually increased from an initial value of 0 in 0.1 V increments at 30-second intervals. The

test run was initiated with the run arrow button on the top left-hand side of the main program window.

Figure 55 and Figure 56 show the inlet and outlet temperatures of the two water streams of the collector array emulator. Figure 55 includes the recorded flow rate on the MISAHP side of the emulator, and Figure 56 includes the 2-way valve control signal value. Because no flow meter is installed on the building plant side, the relative flow rate of plant heating water must be inferred from inlet and outlet temperature value change. Observations of interest are as follows:

The water flow rate on the apparatus side was maintained at about 0.25L/s (4gpm) over the entire test, as expected for the constant pump speed control value.

Temperature values recorded from the thermocouple on the plant heating supply (TC1) remained very close to the ambient air temperature in the laboratory at around 21 °C until approximately 18 minutes (220*5 seconds) into the test run, at the time when the incremented control voltage had increased to a value of 1.8. This observation indicates that the valve inlet port remains closed when the control signal is less than 1.8 V. Prior to the 18-minute mark, with the valve inlet closed off, there was no flow of plant heating water flowing through emulator, and therefore no heat was transferred to the MISAHP side of the heat exchanger.

The temperature reading at the plant heating supply (TC1) increased between the 18th minute (220*5 seconds) and the 22nd minute (270*5 seconds, valve control signal at 2.2 V) of testing. The most probably explanation is that the volume of water passed by the valve was insufficient to raise the overall temperature of water in the pipe at low flow rates.

As the 2-way valve was increasingly open, the outlet water temperature on the apparatus side (TC6) demonstrated a trend of approximating the plant water inlet temperature (TC1).

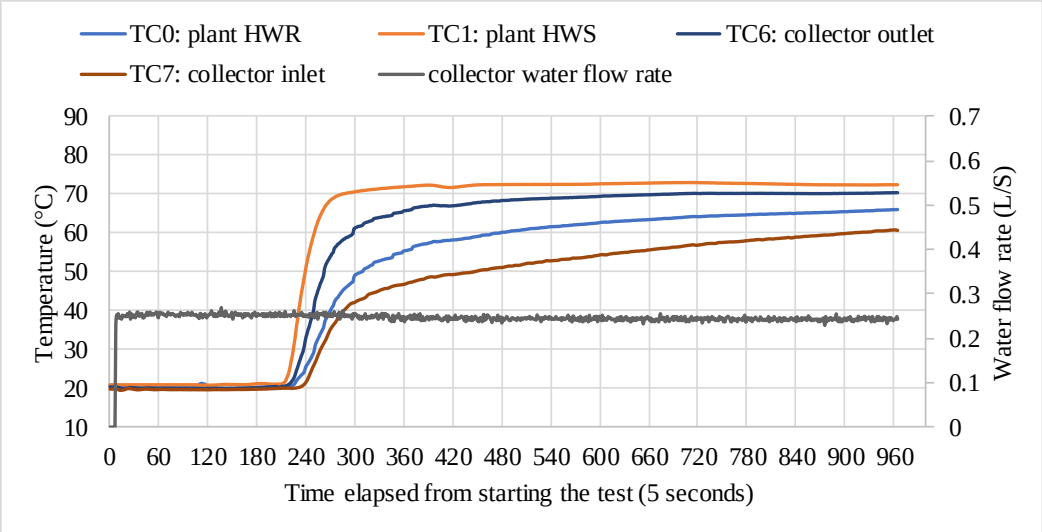

Figure 55: CA->BS Collector Emulator I/O Temperatures and Source-Loop Flow Rate

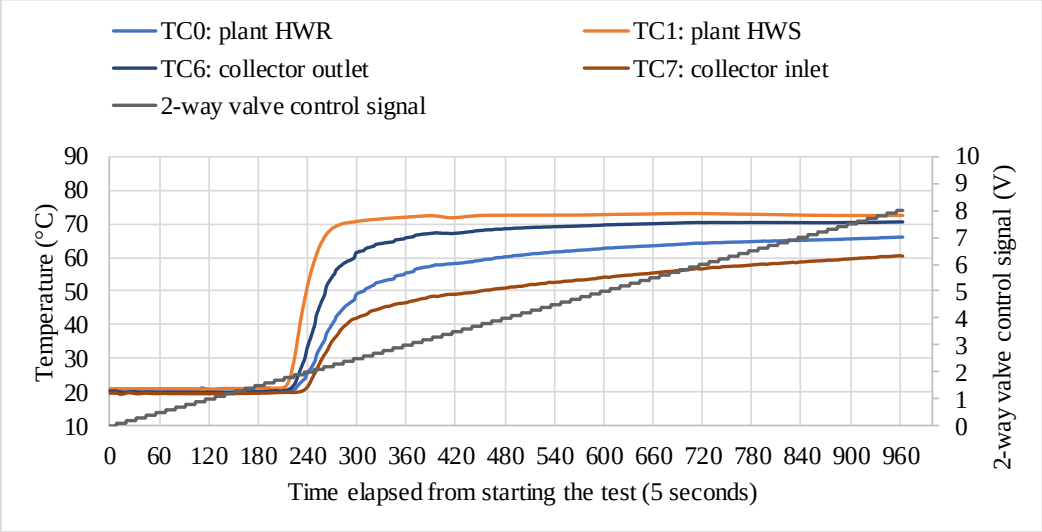

Figure 56: CA->BS Collector Array Emulator I/O Temperature and 2-way Valve Control Value

Figure 57 shows the temperature profiles measured by the five thermocouples in the storage tank. The initial temperature of water in the tank was around 19°C. During the heating process, the first four thermocouples (TC23-TC26) had reported very close temperature readings. The value for the thermocouple at the highest position on the probe did not read the highest temperature value. These observations are consistent with those found from the DHW tank heating in the previous test.

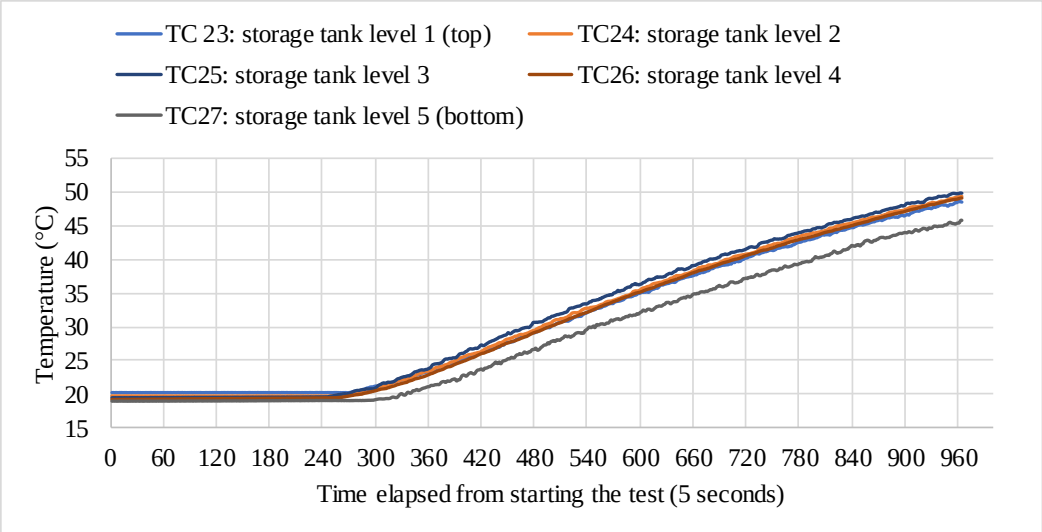

Figure 57: CA->BS - Buffer Storage Temperature Readings

4.4.3 MISAHP Mode 2: Buffer Storage -> Heat Pump -> DHW

In this test, the heat pump was used to heat water in the DHW tank utilizing the buffer storage tank as an energy source. The main objectives of this test were 1) to verify the control of the 3-way valves to achieve the desired flow paths as shown in Figure 58 to verify the functionality of the heat pump in heating mode and observe the temperature change of the water through the source- and load-side coils and 3) to observe the performance of the system with relatively a low-temperature energy source to better understand the limits of the heat pump as installed in the MISAHP system.

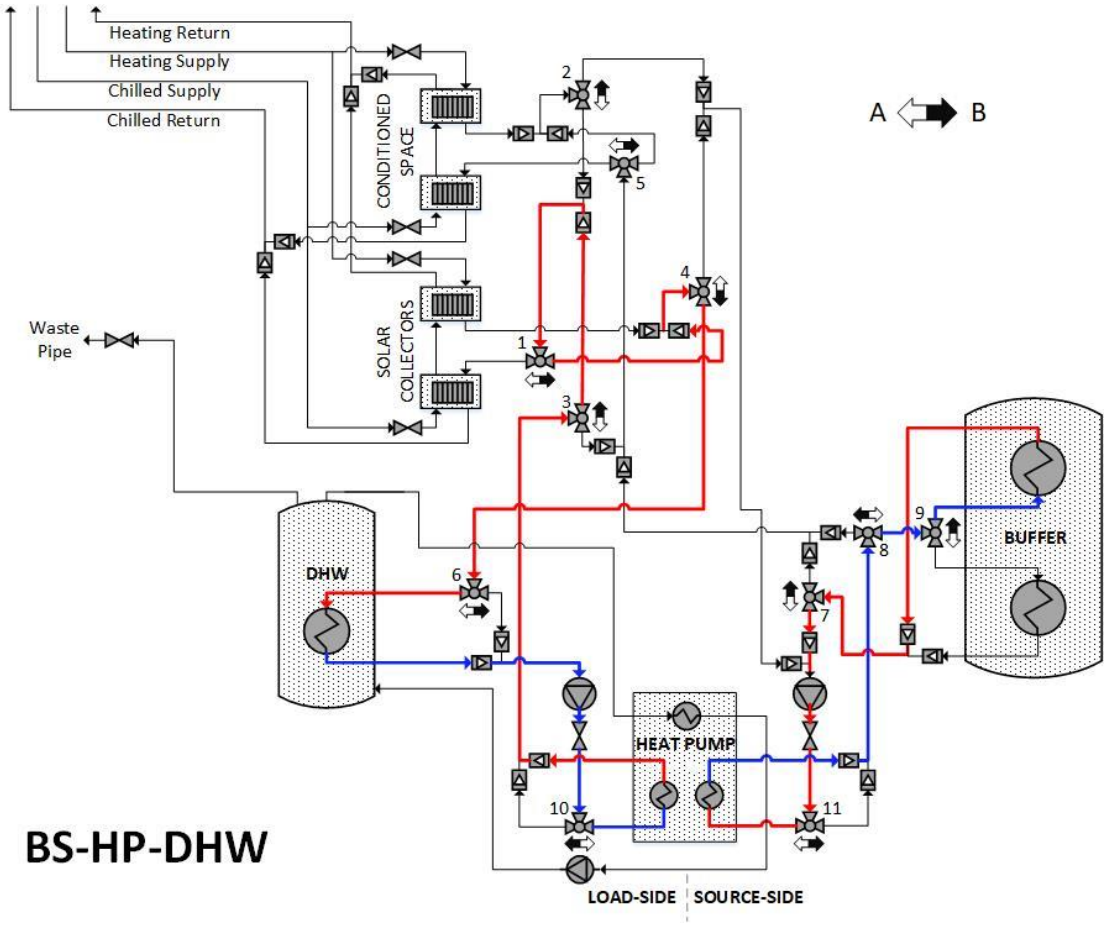

Figure 58: Mode 2: Buffer Storage -> Heat Pump -> DHW Tank

Again, parameters were defined for this test run using controls on the main program's Run Interface tab. BUFFER->HP->DHW was selected from the options in the mode control. Speed control values were set to the maximum of 10V for the source- and load-side circulator pumps. Data logging was enabled, and the program's default settings for data acquisition were retained to record temperature and flow rate measurements at 1-minute intervals. Additional parameters not relevant for this test were left unchanged on the Run Interface controls. The test run was initiated with the run arrow button on the top left-hand side of the main program window.

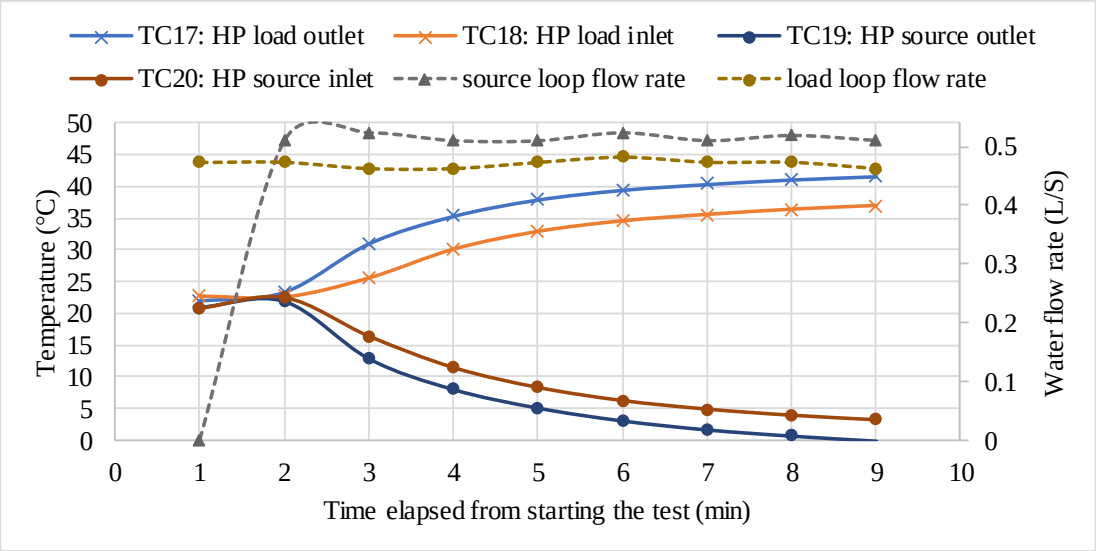

Figure 59: BS->HP->DHW - Heat Pump I/O Temperatures and Source/Load-side Flow Rates

Figure 59 shows the water temperature and flow rates as measured in the source- and load-side water loops. The flow rate of the water averaged roughly 0.51 L/s (8.15gpm) and 0.47 L/s (7.46gpm) for the source- and load-side loops respectively. While the heat pump compressor was active, the temperature readings at the inlet and outlet of the heat pump source coil (TC19 and TC20) decreased rapidly at first, then at a slower rate, reaching an appreciably diminished rate of decline after about 6 minutes. Temperature readings at the inlet and outlet of the heat pump load coil (TC17 and TC18) followed a similar trend, increased rapidly in the beginning, then continuing to rise at a substantially reduced rate. The temperature change of the water in the heat pump coils between the inlet and outlet averaged at -3.3°C on the source-side and 5.0°C on the load-side.

Results from this test demonstrated successful control of the heat pump compressor, with an average heating output of approximately 10 kW (34120 Btu/hr). Temperature readings from the vertical thermocouple probes installed for each tank showed a 2.4°C decrease in average water temperature in the buffer storage tank, and a 3.5 °C increase in temperature for the DHW tank. This finding confirms that the MISAHP system performed its intended function in this mode,

using the heat pump for transfer of energy from buffer storage to the DHW tank; however, troubling temperature trends observed in the source-side water loop give cause for additional consideration of this mode.

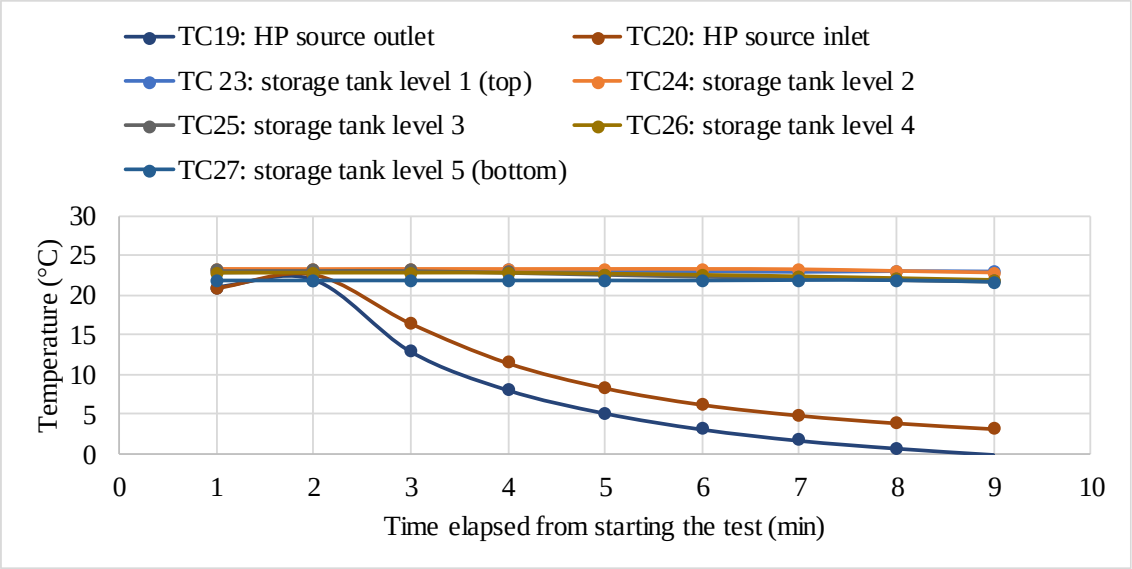

Figure 60: BS->HP->DHW – Source-Side Loop and Buffer Storage Temperature Readings

In the 9th minute of the test, a negative temperature measurement was recorded at the source-side outlet of the heat pump, as shown in Figure 60. While a field-installed version of this MISAHP system would, in most climates, utilize a glycol-based working fluid for freeze protection, the experimental apparatus is filled with water, and is at risk of failure or damage if ice formation were to occur. Furthermore, the test was stopped after just 12 minutes, with water temperatures in the source-side loop continuing to decline. It seems reasonable to expect that continued operation under these conditions could exceed the safe operating limits of the heat pump, which specifies a minimum entering source temperature of -6.7 °C.

Results from this test suggest that the thermal mass of the source-side water loop for this mode, and surface area of the lower coil of the buffer storage tank were not appropriately matched to the capacity of the heat pump. This problem could be addressed with an alternative tank design

and piping configuration for direct circulation of the water held in buffer storage; however, this would undoubtedly lead to increased disruption of thermal stratification in the tank.

The experimental apparatus was constructed with flexibility as a primary design consideration, and presented the option for an additional test scenario using both the upper and lower coils of the buffer storage tank to investigate the potential improvement of operation through the addition of thermal mass and surface area for heat transfer. The subprogram used for 3-way valve control was minimally revised for this purpose, with the addition of a Boolean control to modify position control value array. If the control is setting is true, a value of 0.012 replaces the array element corresponding to the 3-way valve responsible for selecting between flow paths through the upper or lower coils of the buffer storage tank. The substituted control value positions the valve at the halfway point, leaving both A and B ports open, thus including both heat exchangers in the source-side water loop for modes with thermal exchange to or from the buffer tank. The revised flow path is designated BS*->HP->DHW, and illustrated by Figure 61. Apart from the new Boolean control (set as true), all run parameter settings were retained from the previous test run.

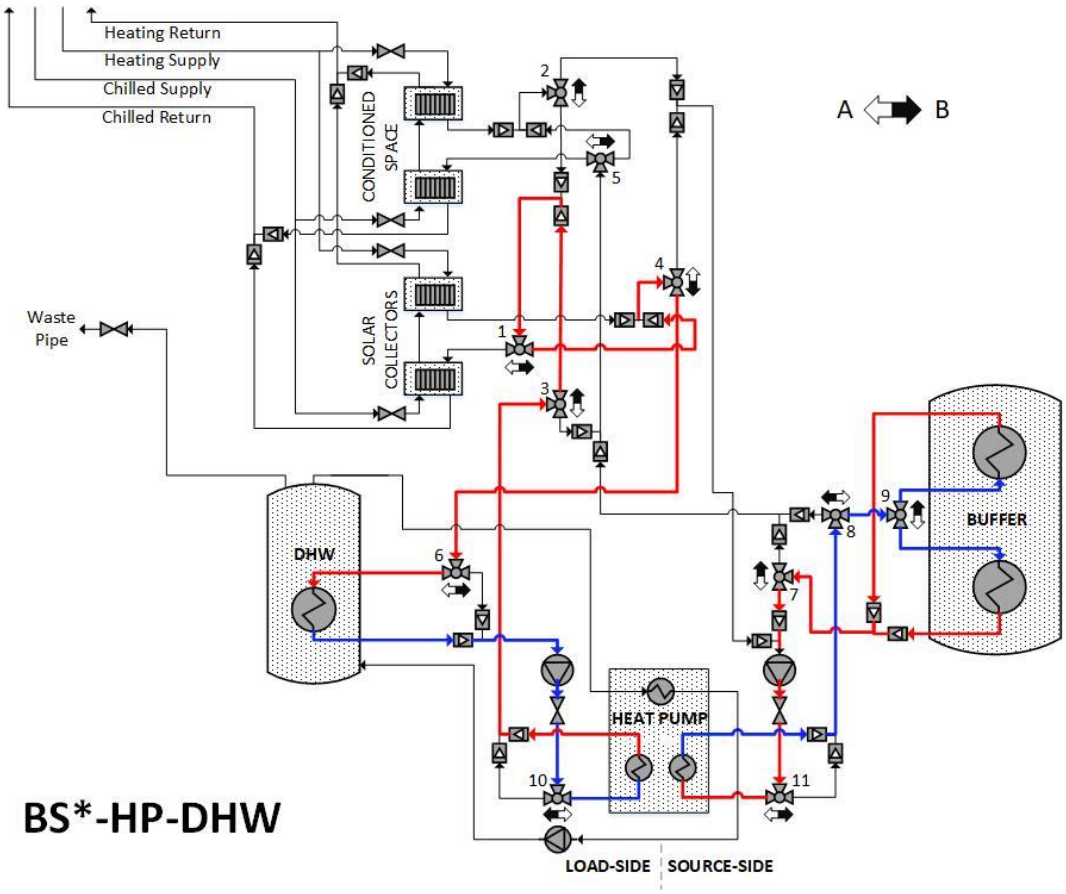

Figure 61: Mode 2 with Buffer Storage Parallel Coil Configuration

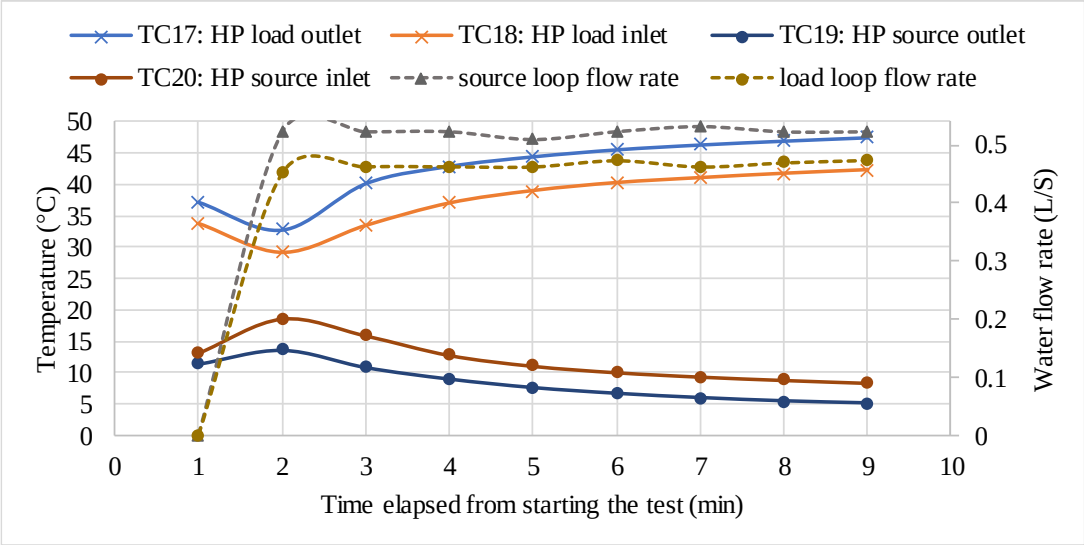

Figure 62: BS->HP->DHW - Heat Pump I/O Temperatures and Source/Load-side Flow Rates*

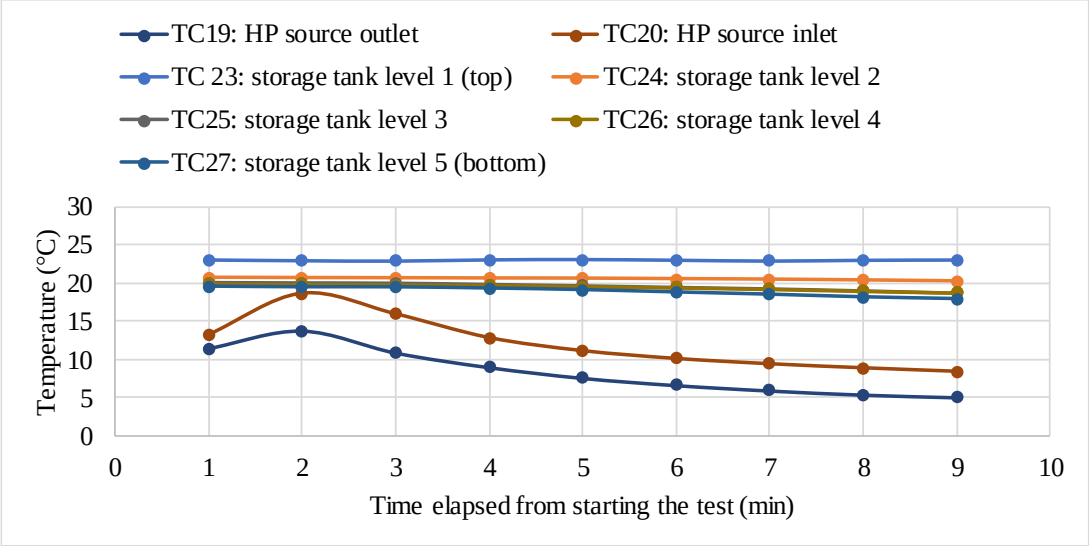

Figure 63:BS->HP->DHW – Source-Side Loop and Buffer Storage Temperature Readings*

Results from this test are shown in Figure 62 and Figure 63. A comparison of Figure 60 and Figure 63 illustrates that for similar source coil inlet temperatures, measurements from the second test run demonstrated substantially higher source loop temperatures, despite lower temperature readings in the buffer storage tank. As expected, the increased surface area for heat transfer and additional thermal mass provided by this configuration produced operating conditions more comfortably within the operating limits of the equipment.

4.4.4 MISAHP Mode 13: Collector Array -> Heat Pump -> Buffer Storage

By convention, a typical heat pump moves energy from source to load for heating, and from load to source for cooling (Note that the source- and load-side designations are consistent with labels on the equipment – see Figure 2: Water-To-Water Geothermal Heat Pump). As employed in the MISAHP system concept, however, adherence to this convention would add substantial complexity to the piping necessary to support all operational modes, as described in section 3.1. As a solution to this design challenge, the heat pump's reversing valve is exploited to deliver the desired function irrespective of the source/load designation assigned to the coils.

Mode 13: CA->HP->BS provides an example of this operational premise in use. In this mode, the heat pump is used for heating of the buffer storage load, with the collector array acting as the energy source. The piping configuration of the MISAHP system as built does not allow for a pathway to couple these components in their roles as the source and load to the heat pump coils designated by convention. Instead, the reversing valve is energized, and the heat pump is run in cooling mode to deliver a heating function, moving energy from the load-side loop to the source-side loop. Figure 64 shows the flow pathways utilized in this mode.

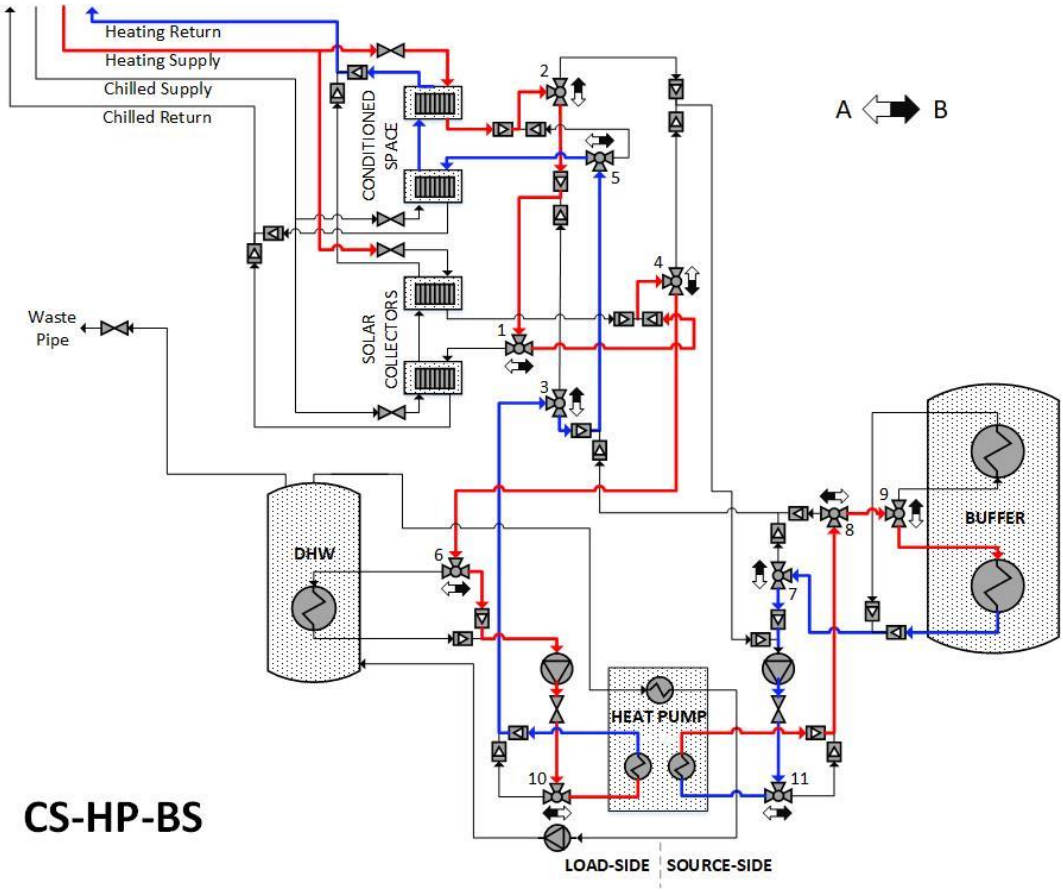

Figure 64: Mode 13: Collector Array -> Heat Pump -> Buffer Storage

Run parameters were defined for this test run using controls on the main program's Run Interface tab. COLLECTOR->HP-BUFFER was selected from the options in the mode control. Data logging was enabled, and the program's default settings for data acquisition were retained to record temperature and flow rate measurements at 1-minute intervals. Additional parameters not relevant for this test were left unchanged on the Run Interface controls. The test run was initiated with the run arrow button on the top left-hand side of the main program window. Figure 65 reports water temperatures and flow rate as measured on both sides of the heat pump, and clearly illustrates the successful transfer of energy from the heat pump source-side loop to the load-side loop, confirming the ability of the system to deliver a heating function to elements coupled to the source coil by virtue of the reversing valve and "cooling" operation of

the heat pump. Note that the temperature values observed at the beginning of this test were a result of conditions developed in the preceding test run cycle.

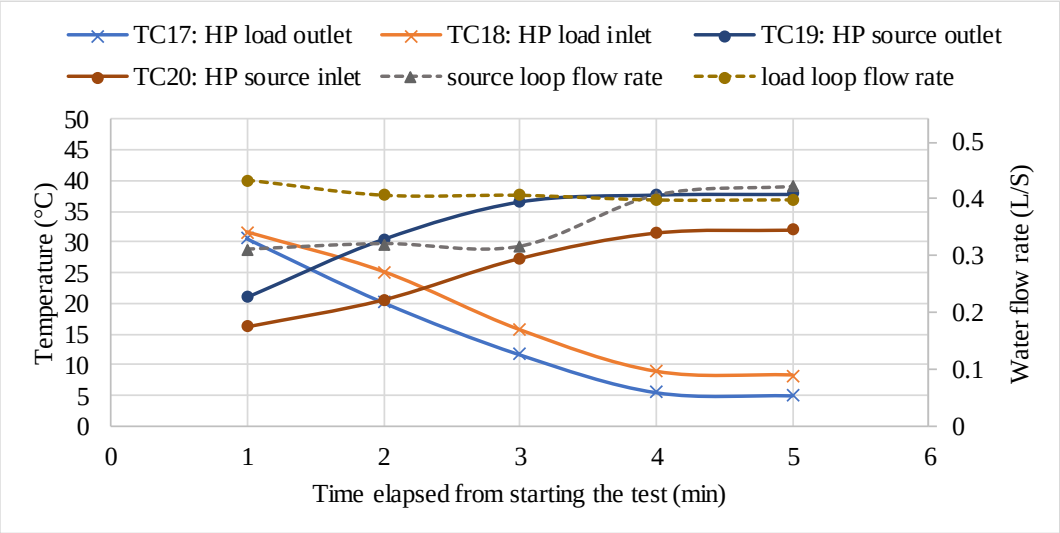

Figure 65: CA-HP-BS - Heat Pump I/O Temperatures and Source/Load-side Flow Rates

4.4.5 DHW Demand Emulation

In the context of HIL simulation for solar-assisted heat pump systems, the DHW consumption profile is usually provided. This profile specifies the amount of hot water consumption within a particular time window. For this project, the emulation of DHW consumption is performed through the controlled discharge of hot water from the DHW tank into the laboratory waste drain. A target flow rate is calculated by the program to determine the average flow rate required to discharge the correct volume in the specified period. Proportional-integral (PI) control is implemented to modulate the position of the 2-way valve on the DHW discharge pipe in response to feedback from the associated flow meter.

In preliminary trials of the control strategy, precise regulation of discharge rate presented some challenges, due in large part to a delayed response by the 2-way valve to changes in control signals. To account for the slow response time of the actuator, the sub-program used to control

the 2-way valve was designed to begin closing the valve before the measured volume of discharge reaches the setpoint volume to avoid overshoot.

Early iterations of this strategy proved ineffective due to the limitations of the flow meters, which are not capable of accurate measurement for flow rates below 0.03L/s (0.52gpm). The counter channel configuration used for reading signal pulse-frequency in LabVIEW returns an error for any instance where 0 signal pulses are detected in a sample period. The sub-program for reading flow measurements includes a workaround to this problem, canceling the error and outputting a value of zero.

As a result, a problem occurred when the flow rate dropped below the threshold of accuracy for the flow meters before the value required to begin closing the valve was registered. In these instances, the 2-way valve opened on command, and position control delivered a flow rate reasonably close to the target but failed to close the valve completely after the specified volume of discharge. This effect was because, despite the valve being partially open and continuing to allow discharge, a reported flow rate value of zero prevented the counter from advancing. Control parameters governing valve closing were adapted to correct this problem, incorporating a period of fixed control value at the end of the demand event to ensure a detectable flow rate until control signals are sent to close the valve.

Because the purpose of DHW withdrawal is to emulate the DHW load, emulating the total volume of water in a demand event is more critical than the accurate withdrawal rate. Therefore, additional accommodations are made for demand profiles with low average flow rates. A minimum flowrate of 0.75 GPM is used for all demand events, and withdrawal time is simply shortened to deliver the specified volume of discharge at the adjusted flow rate.

Following several nominal trial runs with the revised control strategies, this final test was performed to demonstrate the performance of the DHW demand emulation mechanism in

producing a specified withdrawal profile, and to investigate any negative impact on flow regulation due to elevated pressure conditions occurring as a result of large temperature changes in the DHW tank.

Run parameters were defined for this test run using controls on the main program's Run Interface tab. As operational mode selection had no relevance for the objective of this test, and COLLECTOR->DHW was chosen arbitrarily from the options in the mode control, and the circulator pumps remained inactive, with speed control values were set to 0. Data logging was enabled, and the program's default settings for data acquisition were retained to record temperature and flow rate measurements at 1-minute intervals. Additional parameters not relevant for this test were left unchanged on the Run Interface controls.

As shown in Figure 66, the Occupant Emulation tab was used to define the parameters of DHW demand events emulated for this test: numerical controls for volume and withdrawal time setpoints were adjusted for each of the events in succession. The test run was initiated with the run arrow button on the top left-hand side of the main program window.

At the start of the test, DHW tank water pressure was measured at 0.28 MPa (40psi) using the mechanical dial gauge installed on the outlet. Four different emulated occupant demand events were initiated in sequence, and measured values for water volume discharged and time duration of discharge were recorded. Pressure change was investigated as a potential source of error for DHW demand emulation control, considering that the close of pressure specified by the valve manufacture in only slightly higher than water pressure at the mains, and some degree of thermal expansion is expected after a significant temperature rise. The DHW tank auxiliary heating element was energized, and the average in-tank temperature was increased to 37.5°C. DHW tank water pressure was measured at 0.32 MPa (46psi) using the mechanical dial gauge. Two additional emulated occupant demand events were initiated in sequence. Emulation

parameters were specified to match settings used for the 1st and 4th demand events, and measured values for water volume discharged and time duration of discharge were recorded.

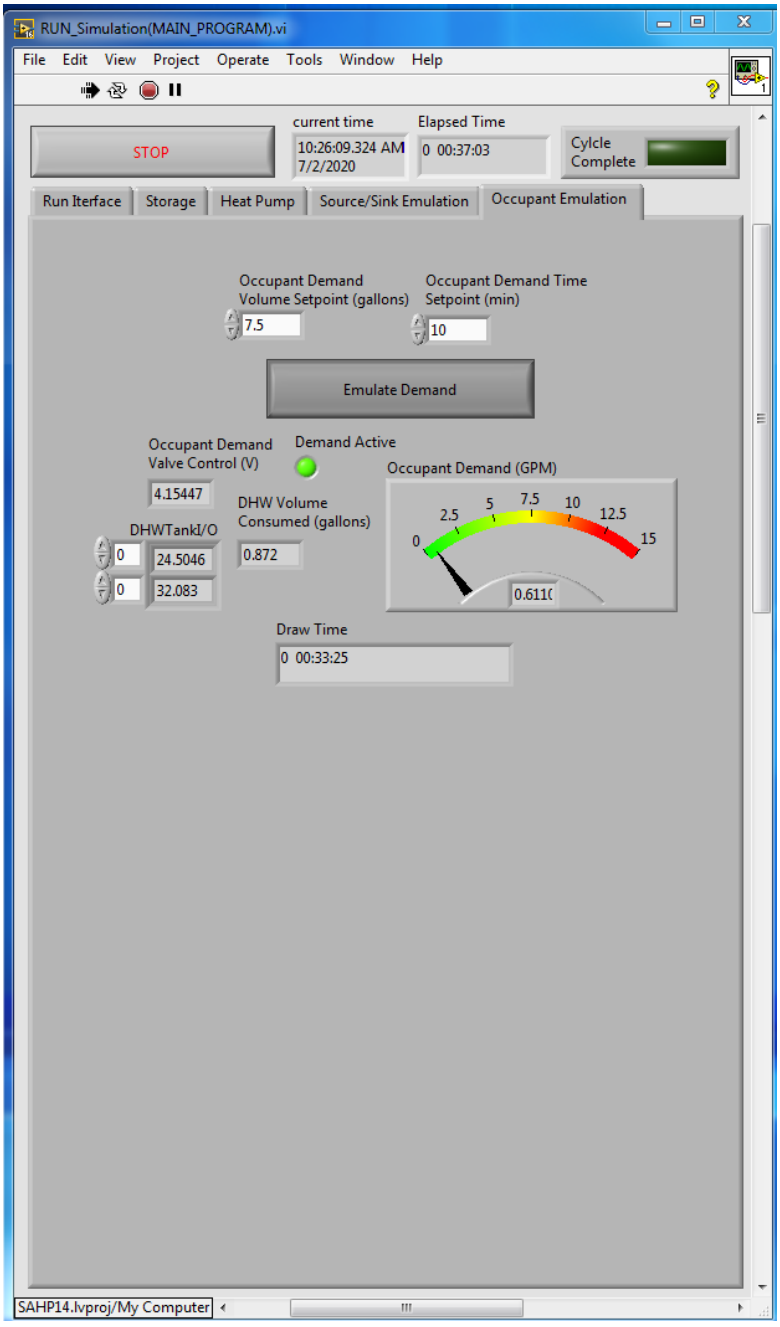

Figure 66: Occupant Demand Emulation Control Tab

Results from this test demonstrated the performance of the DHW demand emulator. Although measured flow rates were observed to be inconsistent with calculated flow rate targets, the

total measured volume of discharge for all six demand emulation events were very closely matched to corresponding target volumes specified, as reported in Table 10. No adverse effects were observed for the 5th demand event which was intentionally triggered after temperature rise caused an increase in water pressure in the DHW Tank.

Table 10: DHW Demand Emulation

Demand Event #	Target volume of DHW withdrawal (L)	Actual volume of DHW withdrawal (L)
1	76	74.2
2	152	150.9
3	28.5	25.4
4	19	15.5
5	76	68.9
6	19	17.5

CHAPTER 5: CONCLUSION, DISCUSSION AND RECOMMENDATIONS FOR FUTURE WORK

As discussed, the objective of this thesis is to support future research of solar-assisted heat pump systems using the hardware-in-loop simulation approach. The experimental apparatus was designed and constructed in the interest of flexibility and range of functionalities. In this thesis, basic functionality of the control and operation was verified through testing of four out of fifteen operation modes as described in section 3.1, and domestic hot water withdrawal emulation. Functionality and basic control of all essential components in the design concept were investigated and confirmed. Due to the similarities in function shared among modes, including valve position control, pump configuration, and heat pump operations, it is reasonable to expect that the other modes not tested in this thesis would deliver basic functionality as well. Still, several improvements are necessary to address the challenges identified in testing before the full potential of this system is realized for HIL testing as desired. Due in large part to time constraints, critical factors affecting the performance of the apparatus in the emulation of boundary conditions and effective range of operation as intended have yet to be addressed. Furthermore, as the reduction of energy consumption achieved by the MISAHP system is the primary measure of its value against other building system technologies, the supplementation of instrumentation with additional equipment for power consumption monitoring would be an essential next step in the pursuit of these goals.

The capabilities of the heat pump and circulators for MODBUS RTU communication offer an appealing option for power monitoring; however, the implementation of this approach has yet to be investigated in earnest. Alternatively, simple current and voltage transducers should be supplied for appropriate equipment including the heat pump compressor, three circulator pumps, and the DHW tank auxiliary heating element.

In preparation for control testing, it may be desirable to allow for automated switching of the power supply to some components to avoid any inopportune operation, in particular the DHW auxiliary electric heating element. An appropriately sized power relay, controlled from either the relay controller or the AOM, is a straightforward solution for this purpose.

As a non-essential element in the MISAHP system, the desuperheater subsystem, including the associated piping, circulator, and thermostatic switch, was not commissioned or tested in this thesis. Care must be taken to “burp” the desuperheater pump before operation to remove air from the impeller cavity by breaking the seal at the housing with the water loop under pressure as specified in the installation guidelines from the manufacturer.

In-tank temperature readings recorded during testing demonstrated reasonable retention of vertical temperature stratification in both storage tanks as desired, however the temperature reading from the thermocouples at the top of both tanks were generally lower than temperature readings from the sensor just below, which may suggest that they are positioned above the top of the storage compartment in the tank’s insulation layer. A simple investigation could reveal if this explanation holds; removal of the temperature wells and a cross-check of measurements for the well depth and sensor spacing against the dimensional drawing and specifications for each of the tanks. If an error in assembly is confirmed, instrumentation should be adjusted accordingly. It is also possible that heat dissipated from penetrations in the insulation at the top of the tanks contributed to the phenomenon as observed.

Although the second test of Mode 2: BS->HP->DHW (utilizing both heat exchanger coils in parallel) demonstrated an improvement from earlier test runs in avoiding conditions outside of the safe operating limits of the equipment, these results are not to be interpreted as a resolution to the problem observed. Because the MISAHP system was designed to utilize the two heat exchanger coils in the buffer tank for separate functions, parallel operation of the coils

is not optimized for thermal charging or discharging in the upper or lower portions of the tank volume as intended. Instead, the water enters through two ports near the middle of the tank, and moves through the coils in opposite directions, exiting near the top and bottom of the tank. For this reason, the parallel configuration is not an ideal solution to the issues encountered in the second test. Additionally, only a single, short-duration iteration of this test was conducted. There is no reason to assume that operation in this mode under different conditions, or in other modes involving the heat pump could produce a similar problem. Possible alternatives include reconfiguration for direct circulation in the buffer tank (without the use of internal heat exchanger coils) to take advantage of increased thermal mass; however, the best solution would likely be replacement or modification of the heat pump to include a variable speed compressor to modulate capacity with demand.

Occupant emulation testing was limited in scope, and although volume discharge targets were met with reasonable accuracy and results were deemed satisfactory for purposes of this thesis, further tuning of the control gains could undoubtedly improve flow regulation and reduce the oscillations created by the corrective action of the controller.

Collector Array and Conditioned Space emulation control strategies will require significant revision before this system can be utilized for real-time HIL testing. While rapid heat exchange is easily achieved with the current setup, several factors impede successful emulation of more moderate temperatures, as are expected to be common, if ubiquitous in the simulation of realistic boundary conditions. The high capacity of the emulator heat exchangers, temperature intensities of the plant water loops, as well as the slow valve actuator response, and inconsistent results observed for very low flow rates all contribute to ineffective regulation of the emulator outlet temperature as intended. General observations in trial and testing seemed

to indicate that a single control strategy is unlikely to perform appropriately for the full range of operating conditions that will occur in the simulation of a real house and collector array.

CS->CA, CA->CS, CS->HP-CA and CA->HP->CS will perhaps be the most challenging modes to emulate, because these require the emulation of two boundary conditions at the same time in a system where the response to changes in conditions for one variable has a dynamic effect on the resulting behavior of the other. The development of effective control strategies for this application will be reliant on the achievement of balanced interaction between emulators to avoid overshoot, and on the definition of control parameters appropriate to the requirements of individual scenarios under test.

One potential strategy that seems to hold some promise for resolution of these issues would be to utilize both plant heating and chilled water loops simultaneously for an individual emulator, employing the thermal potential in one plant loop for tempering the energy transferred by the other. This method would involve more intermediate valve positions, which observations suggested could improve the consistency of regulation on the plant water rate of flow. Given that the existing hardware configuration could accommodate this approach without any change, the idea seems worthy of investigation.

Under the changes as discussed, this system could be of considerable value for future studies. Topics of interest may include integration with electrical storage and PVT panels, latent heat storage using phase-change materials, and utilization of thermal storage for load shifting to minimize peak consumption, both in an individual structure and on a distributed scale.

REFERENCES

AOSmith. 2020. Residential Electric Indirect Solar Booster Water Heaters. Available online: https://www.hotwater.com/lit/spec/solar/AOSQE50000.pdf (accessed 26 July 2020).

Aijazi, Arfa, and Gail Brager. 2018. "Understanding Climate Change Impacts on Building Energy Use." *ASHRAE Journal* VOL 60 NO 10.

Bridgeman, Andrew George 2010. "Experimental Analysis of an Indirect Solar Assisted Heat Pump for Domestic Water Heating."

Chow, T. T. 2010. "A review on photovoltaic/thermal hybrid solar technology." *Applied Energy* 87 (2):365-379. doi: https://doi.org/10.1016/j.apenergy.2009.06.037.

Chu, Jenny, and Cynthia A. Cruickshank. 2014. "Solar-assisted heat pump systems: A review of existing studies and their applicability to the canadian residential sector." *Journal of Solar Energy Engineering, Transactions of the ASME* 136 (4). doi: 10.1115/1.4027735.

Chua, K. J., S. K. Chou, and W. M. Yang. 2010. "Advances in heat pump systems: A review." *Applied Energy* 87 (12):3611-3624. doi: https://doi.org/10.1016/j.apenergy.2010.06.014.

Demirel, Yasar 2016. *Energy Production, Conversion, Storage, Conservation and Coupling*: Springer International.

EIA. 2015. Residential Energy Consumption Survey. Accessed October 19th, 2019.

Hadorn, J. C. 2015. *Solar and Heat Pump Systems for Residential Buildings*. Edited by J. C. Hadorn: Ernst & Sohn.

IEA. 2018. Global Energy & CO2 Status Report. Accessed October 1st 2019.

Laveyne, Joannes I., Brecht Zwaenepoel, Greet Van Eetvelde, and Lieven Vandevelde. 2014. "Increasing economic benefits by load-shifting of electrical heat pumps." *Chemical Engineering Transactions* 39 (Special Issue):1513-1518. doi: 10.3303/CET1439253.

McQuiston, Faye C. , Jerald D. Parker, and Jeffrey D. Spitler. 2005. *Heating, Ventilating, and Air Conditioning*. 6th ed: John Wiley & Sons, Inc.

Pérez-Lombard, Luis, José Ortiz, and Christine Pout. 2008. "A review on buildings energy consumption information." *Energy and Buildings* 40 (3):394-398. doi: https://doi.org/10.1016/j.enbuild.2007.03.007.

Ruschenburg, Jörn, Sebastian Herkel, and Hans-Martin Henning. 2013. "A statistical analysis on market-available solar thermal heat pump systems." *Solar Energy* 95:79-89. doi: https://doi.org/10.1016/j.solener.2013.06.005.

Sarbu, Ioan, and Calin Sebarchievici. 2017a. "Chapter 3 - Solar Collectors." In *Solar Heating and Cooling Systems*, edited by Ioan Sarbu and Calin Sebarchievici, 29-97. Academic Press.

Sarbu, Ioan, and Calin Sebarchievici. 2017b. "Chapter 4 - Thermal Energy Storage." In *Solar Heating and Cooling Systems*, edited by Ioan Sarbu and Calin Sebarchievici, 99-138. Academic Press.

Schiffer, Hans-Wilhelm, Tom Kober, and Evangelos Panos. 2018. "World Energy Council's Global Energy Scenarios to 2060." *Zeitschrift für Energiewirtschaft* 42 (2):91-102. doi: 10.1007/s12398-018-0225-3.

Sun, Xingshu, Yubo Sun, Zhiguang Zhou, Muhammad Ashraful Alam, and Peter Bermel. 2017. "Radiative sky cooling: fundamental physics, materials, structures, and applications." *Nanophotonics* 6.

Thygesen, Richard, and Björn Karlsson. 2013. "Economic and energy analysis of three solar assisted heat pump systems in near zero energy buildings." *Energy and Buildings* 66:77-87. doi: https://doi.org/10.1016/j.enbuild.2013.07.042.

Xu, Xiaolong, Runping Niu, and Feng Guohui. 2015. "An Experimental and Analytical Study of a Radiative Cooling System with Flat Plate Collectors." *Procedia Engineering* 121:1574-1581. doi: 10.1016/j.proeng.2015.09.180.

040 - Performance Data

Cooling Capacity

Source			Load Flow-5 GPM							Load Flow-7.5 GPM							Load Flow-10 GPM						
EST °F	Flow GPM	ELT °F	LLT °F	TC MBTUH	Power kW	HR MBTUH	EER	LST °F		LLT °F	TC MBTUH	Power kW	HR MBTUH	EER	LST °F		LLT °F	TC MBTUH	Power kW	HR MBTUH	EER	LST °F
30	5	50	34.0	38.7	1.38	43.4	28.0	47.9		37.8	39.8	1.39	44.5	28.7	48.4		41.6	40.9	1.39	45.6	29.4	48.8	
		70	54.5	37.5	1.27	41.8	29.4	47.2		58.3	38.0	1.26	42.3	30.4	47.4		62.0	38.6	1.23	42.8	31.4	47.6	
		90	75.1	36.2	1.17	40.2	31.1	46.6		78.8	36.2	1.12	40.0	32.6	46.5		82.5	36.2	1.06	39.9	34.1	46.4	
		110	95.6	35.0	1.06	38.6	33.0	45.9		99.3	34.5	0.98	37.8	35.3	45.6		103.0	33.9	0.90	37.0	37.7	45.2	
	7.5	50	34.5	37.7	1.32	42.2	28.6	43.2		38.2	38.6	1.33	43.1	29.1	43.5		41.9	39.4	1.33	43.9	29.6	43.8	
		70	55.1	36.2	1.23	40.4	29.6	42.6		58.7	36.7	1.21	40.8	30.3	42.8		62.3	37.1	1.19	41.2	31.2	42.9	
		90	75.7	34.7	1.13	38.6	30.7	42.1		79.3	34.8	1.09	38.5	31.9	42.1		82.8	34.9	1.05	38.5	33.1	42.0	
		110	96.3	33.2	1.04	36.7	32.1	41.6		99.8	32.9	0.98	36.2	33.7	41.4		103.3	32.6	0.92	35.7	35.6	41.2	
	10	50	34.9	36.7	1.26	41.0	29.1	38.5		38.5	37.3	1.27	41.6	29.5	38.6		42.2	37.9	1.27	42.2	29.8	38.7	
		70	55.6	34.9	1.18	38.9	29.7	38.0		59.1	35.3	1.17	39.3	30.3	38.1		62.6	35.7	1.16	39.6	30.9	38.2	
		90	76.3	33.2	1.09	36.9	30.3	37.6		79.7	33.3	1.07	37.0	31.2	37.6		83.1	33.5	1.04	37.1	32.1	37.6	
		110	97.1	31.4	1.01	34.8	31.1	37.2		100.3	31.4	0.97	34.7	32.4	37.1		103.5	31.3	0.93	34.5	33.7	37.1	
50	5	50	33.3	35.7	1.76	41.7	21.6	67.2		38.6	37.4	1.76	43.4	22.6	67.9		41.9	39.2	1.76	45.2	23.5	68.6	
		70	53.4	40.2	1.73	46.1	24.5	69.0		57.3	41.5	1.72	47.4	25.5	69.5		61.2	42.8	1.71	48.6	26.4	70.1	
		90	73.5	44.8	1.71	50.6	27.4	70.9		76.0	45.6	1.69	51.4	28.5	71.2		80.4	46.4	1.66	52.1	29.5	71.5	
		110	89.6	49.4	1.68	55.1	30.4	72.7		94.7	49.7	1.65	55.3	31.7	72.8		99.7	50.1	1.62	55.6	33.0	72.9	
	7.5	50	34.1	35.3	1.69	41.0	20.9	62.8		38.8	36.9	1.68	42.6	21.9	63.3		42.1	38.5	1.68	44.2	22.9	63.8	
		70	57.8	39.2	1.65	44.8	23.7	64.0		58.7	40.3	1.64	45.9	24.5	64.4		63.4	41.5	1.63	47.1	25.4	64.7	
		90	76.5	43.0	1.62	48.6	26.5	65.2		77.8	43.8	1.60	49.2	27.3	65.4		80.8	44.5	1.59	49.9	28.1	65.7	
		110	95.2	46.9	1.59	52.3	29.5	66.5		95.4	47.2	1.56	52.5	30.2	66.5		100.2	47.5	1.54	52.7	30.9	66.6	
	10	50	42.8	34.9	1.61	40.4	23.0	58.3		38.9	36.4	1.61	41.9	23.8	58.6		42.2	37.9	1.61	43.3	24.7	58.9	
		70	62.1	38.1	1.57	43.5	25.3	59.0		60.1	39.1	1.57	44.5	26.1	59.2		61.7	40.2	1.56	45.5	26.9	59.4	
		90	81.5	41.3	1.54	46.5	27.6	59.6		79.6	41.9	1.52	47.1	28.4	59.7		81.2	42.6	1.51	47.7	29.1	59.8	
		110	100.8	44.5	1.50	49.6	30.0	60.2		96.2	44.7	1.48	49.7	30.8	60.3		100.7	44.9	1.46	49.9	31.5	60.3	
70	5	50	36.6	32.6	2.14	39.9	15.2	86.5		39.4	35.0	2.14	42.3	16.4	87.4		42.3	37.4	2.13	44.7	17.6	88.4	
		70	52.3	43.0	2.19	50.5	19.6	90.8		56.3	45.0	2.20	52.5	20.5	91.6		60.3	47.0	2.20	54.5	21.4	92.5	
		90	68.0	53.3	2.25	61.0	23.7	95.2		73.2	55.0	2.26	62.7	24.4	95.8		78.3	56.6	2.26	64.3	25.0	96.5	
		110	Operation not recommended																				
	7.5	50	36.5	32.9	2.05	39.8	16.0	82.3		39.4	35.2	2.04	42.2	17.2	83.1		42.2	37.6	2.04	44.5	18.5	83.8	
		70	56.9	42.1	2.08	49.2	20.2	85.3		58.7	44.0	2.08	51.1	21.2	85.9		60.5	45.9	2.08	52.9	22.1	86.5	
		90	73.9	51.4	2.11	58.6	24.3	88.4		76.4	52.7	2.12	59.9	24.9	88.8		78.8	54.1	2.12	61.3	25.5	89.3	
		110	Operation not recommended																				
	10	50	36.4	33.1	1.96	39.8	16.9	78.2		39.3	35.5	1.96	42.1	18.2	78.7		42.2	37.8	1.94	44.4	19.5	79.2	
		70	61.5	41.2	1.97	48.0	20.9	79.9		61.1	43.0	1.96	49.7	21.9	80.2		60.8	44.7	1.96	51.4	22.8	80.6	
		90	79.8	49.4	1.98	56.1	24.9	81.6		79.6	50.5	1.98	57.3	25.5	81.8		79.4	51.6	1.97	58.3	26.1	82.0	
		110	86.3	57.5	1.99	64.3	28.9	83.3		92.1	58.0	1.99	64.8	29.1	83.4		97.9	58.5	1.99	65.3	29.4	83.5	
90	5	50	38.0	29.1	2.74	38.4	11.4	105.8		40.6	30.9	2.74	40.3	12.2	106.6		43.2	32.8	2.74	42.2	13.0	107.4	
		70	53.8	39.2	2.80	46.8	15.0	110.1		57.5	41.1	2.81	50.7	15.7	110.9		61.1	43.0	2.81	52.6	16.4	111.7	
		90	69.6	49.4	2.86	59.1	18.4	114.4		74.3	51.3	2.87	61.1	19.0	115.2		79.0	53.3	2.88	63.1	19.6	116.0	
		110	Operation not recommended																				
	7.5	50	41.0	29.2	2.65	38.3	11.0	101.8		40.6	31.1	2.64	40.1	11.8	102.4		43.2	33.0	2.64	42.0	12.5	103.0	
		70	57.9	38.9	2.68	48.1	14.5	104.9		59.6	40.8	2.68	49.9	15.2	105.5		61.2	42.7	2.68	51.8	15.9	106.1	
		90	74.9	48.6	2.71	57.9	17.9	108.0		77.0	50.5	2.71	59.7	18.6	108.6		79.2	52.3	2.71	61.6	19.3	109.2	
		110	Operation not recommended																				
	10	50	43.9	29.4	2.55	38.1	12.3	97.9		40.5	31.3	2.54	40.0	13.4	98.2		43.1	33.3	2.54	41.9	14.3	98.6	
		70	62.0	38.7	2.56	47.4	16.2	99.8		61.7	40.5	2.55	49.2	17.0	100.1		61.3	42.3	2.54	51.0	17.8	100.5	
		90	80.1	47.9	2.56	56.6	19.8	101.7		79.8	49.6	2.56	58.4	20.6	102.0		79.4	51.4	2.55	60.1	21.3	102.4	
		110	Operation not recommended																				
110	5	50	38.5	25.5	3.34	36.9	7.6	125.2		41.8	26.9	3.33	38.3	8.0	125.8		44.2	28.2	3.33	39.6	8.4	126.3	
		70	55.4	33.5	3.41	47.1	10.4	129.4		58.7	37.3	3.42	48.9	10.9	130.2		61.9	39.1	3.42	50.8	11.4	130.9	
		90	Operation not recommended																				
		110																					
	7.5	50	39.4	25.6	3.24	36.7	7.9	121.4		41.8	27.0	3.24	38.1	8.3	121.8		44.1	28.5	3.24	39.5	8.8	122.2	
		70	59.0	35.8	3.28	46.9	10.9	124.5		60.4	37.6	3.28	48.8	11.5	125.1		61.9	39.5	3.28	50.7	12.1	125.7	
		90	Operation not recommended																				
		110																					
	10	50	39.4	25.7	3.14	36.4	8.2	117.5		41.7	27.2	3.14	37.9	8.7	117.8		44.1	28.7	3.13	39.4	9.2	118.1	
		70	62.6	36.1	3.14	46.8	11.5	119.6		62.2	38.0	3.14	48.7	12.1	120.0		61.8	39.9	3.13	50.6	12.8	120.4	
		90	Operation not recommended																				
		110																					

8/09/09

040 - Performance Data cont.

Heating Capacity

Source		Load Flow-5 GPM							Load Flow-7.5 GPM						Load Flow-10 GPM					
EST °F	Flow GPM	ELT °F	LLT °F	HC MBTUH	Power kW	HE MBTUH	COP	LST °F	LLT °F	HC MBTUH	Power kW	HE MBTUH	COP	LST °F	LLT °F	HC MBTUH	Power kW	HE MBTUH	COP	LST °F
25	7.5	60	Operation not recommended																	
		80																		
		100																		
		120																		
	10	60	72.2	29.7	1.83	23.5	4.76	20.2	68.2	29.7	1.78	23.6	4.89	20.1	66.1	29.6	1.72	23.7	5.04	20.1
		80	91.9	28.8	2.42	20.6	3.50	20.8	87.9	28.8	2.36	20.7	3.58	20.7	85.9	28.7	2.29	20.9	3.67	20.7
		100	111.5	28.0	3.00	17.7	2.73	21.5	107.7	27.9	2.94	17.9	2.78	21.5	105.7	27.8	2.87	18.0	2.84	21.3
		120	131.2	27.1	3.59	14.8	2.21	21.9	127.4	27.0	3.52	15.0	2.25	21.9	125.5	26.9	3.44	15.2	2.29	21.9
30	5	60	72.7	30.9	1.84	24.6	4.92	19.8	69.5	30.8	1.79	24.7	5.06	19.8	66.3	30.7	1.73	24.8	5.20	19.8
		80	92.4	30.0	2.42	21.8	3.64	21.0	89.3	30.0	2.36	21.9	3.73	21.0	86.2	29.9	2.30	22.0	3.81	20.9
		100	112.0	29.2	2.99	19.0	2.85	22.2	109.0	2.91	2.93	19.1	2.91	22.1	106.0	29.0	2.86	19.3	2.97	22.1
		120	131.7	28.3	3.57	16.1	2.32	23.4	128.7	28.3	3.50	16.3	2.37	23.3	125.8	28.2	3.43	16.5	2.41	23.2
	7.5	60	73.3	32.3	1.84	26.0	5.14	22.1	70.0	32.2	1.78	26.1	5.29	22.1	66.6	32.2	1.73	26.3	5.46	22.0
		80	92.8	31.0	2.43	22.7	3.74	23.1	89.6	31.0	2.36	23.0	3.85	23.0	86.4	31.1	2.29	23.2	3.97	22.9
		100	112.3	29.8	3.02	19.5	2.90	24.0	109.2	2.99	2.94	19.9	2.98	23.9	106.2	30.0	2.86	20.2	3.07	23.9
		120	131.8	28.6	3.61	16.3	2.32	25.0	128.9	28.7	3.52	16.7	2.39	24.9	125.9	28.9	3.43	17.1	2.46	24.8
	10	60	73.9	33.6	1.84	27.3	5.35	24.4	70.4	33.6	1.78	27.5	5.54	24.3	66.9	33.6	1.72	27.7	5.72	24.3
		80	93.2	32.0	2.44	23.7	3.85	25.1	89.9	32.1	2.37	24.1	3.99	25.0	86.6	32.2	2.29	24.4	4.12	25.0
		100	112.6	30.5	3.04	2.01	2.94	25.9	109.5	30.7	2.95	20.6	3.05	25.8	106.4	30.9	2.86	21.1	3.16	25.6
		120	131.9	28.9	3.64	16.5	2.33	26.6	129.0	29.2	3.54	17.1	2.42	26.5	126.1	29.5	3.43	17.8	2.52	26.3
50	5	60	76.9	41.1	1.88	34.7	6.37	35.7	72.7	40.8	1.81	34.7	6.61	35.7	68.4	40.6	1.74	34.6	6.84	35.7
		80	96.3	39.5	2.47	31.1	4.67	37.2	92.2	39.3	2.39	31.1	4.82	37.2	88.1	39.1	2.30	31.2	4.97	37.1
		100	115.6	37.9	3.06	27.4	3.61	38.7	111.7	37.7	2.96	27.6	3.72	38.6	107.8	37.6	2.87	27.8	3.84	38.5
		120	134.9	36.3	3.65	23.8	2.90	40.2	131.2	36.2	3.54	24.1	2.99	40.1	127.5	36.2	3.44	24.4	3.06	39.9
	7.5	60	77.7	43.0	1.86	36.6	6.77	38.9	73.2	42.7	1.80	36.5	6.95	38.9	68.7	42.3	1.74	36.4	7.15	38.9
		80	96.9	41.1	2.46	32.7	4.89	40.1	92.7	40.9	2.38	32.7	5.03	40.0	88.4	40.7	2.30	32.8	5.18	40.0
		100	116.1	39.1	3.06	28.7	3.75	41.3	112.1	3.91	2.97	29.0	3.86	41.2	108.0	39.0	2.87	29.2	3.98	41.1
		120	135.4	37.2	3.66	24.7	2.98	42.4	131.5	37.3	3.55	25.2	3.08	42.3	127.7	37.4	3.44	25.6	3.19	42.2
	10	60	78.5	44.9	1.84	38.6	7.14	42.0	73.8	44.5	1.79	38.4	7.29	42.1	69.1	44.1	1.74	38.2	7.43	42.1
		80	97.6	42.6	2.45	34.3	5.08	42.9	93.1	42.5	2.38	34.3	5.23	42.9	88.7	42.3	2.30	34.4	5.37	42.9
		100	116.7	40.4	3.07	30.0	3.85	43.8	112.5	40.4	2.97	30.3	3.99	43.8	108.3	40.4	2.87	30.6	4.13	43.7
		120	135.8	38.2	3.68	25.6	3.03	44.7	131.9	38.4	3.56	26.3	3.16	44.6	128.0	38.6	3.44	26.9	3.29	44.5
70	5	60	81.2	51.3	1.92	44.7	7.83	51.5	75.8	50.9	1.83	44.6	8.16	51.6	70.4	50.4	1.74	44.5	8.49	51.7
		80	100.2	48.9	2.52	40.3	5.69	53.4	93.1	48.6	2.42	40.4	5.91	53.4	90.0	48.3	2.31	40.4	6.13	53.3
		100	119.2	46.6	3.12	35.9	4.37	55.2	114.4	46.4	3.00	36.1	4.54	55.1	109.5	46.2	2.88	36.4	4.70	55.0
		120	138.2	44.2	3.72	31.5	3.48	57.0	133.7	44.2	3.59	31.9	3.65	56.8	129.1	44.1	3.45	32.3	3.75	56.7
	7.5	60	82.1	53.7	1.88	47.3	8.37	55.6	76.5	53.1	1.81	46.9	8.58	55.7	70.8	52.5	1.75	46.5	8.82	55.8
		80	101.1	51.1	2.49	42.6	6.00	57.1	93.7	50.7	2.40	42.5	6.18	57.1	90.4	50.3	2.31	42.4	6.38	57.1
		100	120.0	48.5	3.11	37.9	4.57	58.5	115.0	48.3	2.99	38.1	4.73	58.4	109.9	48.1	2.88	38.3	4.90	58.4
		120	138.9	45.9	3.72	33.2	3.61	59.9	134.2	45.9	3.58	33.6	3.75	59.8	129.5	45.9	3.45	34.1	3.90	59.6
	10	60	83.1	56.1	1.84	49.8	8.93	59.7	77.2	55.4	1.80	49.2	9.04	59.9	71.3	54.6	1.75	48.6	9.14	60.0
		80	102.0	53.2	2.47	44.8	6.32	60.8	96.4	52.8	2.39	44.6	6.47	60.8	90.8	52.5	2.31	44.4	6.62	60.8
		100	121.0.8	50.4	3.09	39.8	4.77	61.8	115.5	50.2	2.99	40.0	4.93	61.8	110.3	50.0	2.88	40.2	5.09	61.7
		120	139.6	47.5	3.72	34.8	3.74	62.8	134.7	47.6	3.58	35.4	3.90	62.7	129.8	47.7	3.44	36.0	4.06	62.6
90	5	60	85.4	65.5	1.99	54.7	9.05	67.4	78.5	59.0	1.88	52.5	9.20	68.3	71.6	56.4	1.77	50.4	9.34	69.2
		80	104.5	59.4	2.56	50.7	6.79	69.1	97.8	56.7	2.44	48.3	6.80	7.01	91.1	53.9	2.32	46.0	6.80	71.0
		100	Operation not recommended																	
		120																		
	7.5	60	86.2	63.7	2.01	56.8	9.30	72.6	79.0	60.4	1.89	53.9	9.37	73.5	71.8	57.1	1.77	51.0	9.44	74.3
		80	105.5	61.9	2.58	53.1	7.03	73.8	98.4	58.3	2.45	49.9	6.97	74.7	91.3	54.7	2.33	46.8	6.90	75.6
		100	124.8	60.1	3.15	49.3	5.59	75.0	117.8	56.2	3.01	45.9	5.47	76.0	110.8	52.4	2.88	42.6	5.33	76.9
		120	Operation not recommended																	
	10	60	87.1	65.8	2.02	58.9	9.54	77.9	79.5	61.8	1.90	55.3	9.55	78.6	71.9	57.7	1.77	51.7	9.55	79.3
		80	106.5	64.3	2.59	55.4	7.27	78.6	99.0	59.9	2.46	51.5	7.13	79.4	91.5	55.6	2.33	47.6	7.00	80.2
		100	125.9	62.7	3.16	51.9	5.82	79.3	118.4	58.1	3.02	47.8	5.62	80.2	111.0	53.4	2.88	43.6	5.43	81.0
		120	Operation not recommended																	

8/12/09

APPENDIX B: IN-TANK VERTICAL SENSOR WELL AND THERMOCOUPLE PROBES - DESIGN AND CONSTRUCTION

1) A section of ½ inch copper pipe is cut to a length slightly greater the height of the tank to which it is installed. This pipe will form the walls of the sensor well to be immersed in the tank. To avoid any risk of damaging the anticorrosive tank linings, measurements used are intended to leave roughly 1.3 cm (½ inch) of clearance between the installed sensor well and the bottom of the tank.

2) A cap is soldered to one end of the pipe section (Figure 67: Sensor Well Construction - Soldered End Cap)

Figure 67: Sensor Well Construction -Soldered End Cap

3) A ½ inch marvel adapter and brass threaded reducing bushing are soldered to the opposite end of the pipe section, completing the sensor well (Figure 68: Sensor Well Construction - Soldered Marvel Adapter and Brass Reducing Bushing).

Figure 68: Sensor Well Construction - Soldered Marvel Adapter and Brass Reducing Bushing

4) The sensor well is installed in the designated port at the top of the tank. Threads are sealed with Teflon. For the buffer storage tank, the sensor well is connected to the 1-inch hot water outlet port centered on the top of the tank using soldered copper fittings. For the DHW tank, factory-installed temperature and pressure relief valve, centered on the top of the tank, is removed and relocated to an unused port on the side of the tank, and the sensor well is connected to the newly vacant port with a threaded brass nipple and coupling (Figure 29).

5) A 3/8 inch threaded rod is cut to a length slightly greater than the depth of the finished sensor well. Tank outer dimensions and reported insulation thickness are used to estimate measurements for attaching five evenly spaced thermocouples.

6) 10 3/8 inch hex nuts are threaded onto the rod in pairs to the 5 positions measured for thermocouple placement. The hex nut pairs are counter-tightened in place, and grooves are cut using a grinding wheel to create space for the thermocouple wires. The hex nuts are just small enough to be inserted into the sensor well, and assist in centering the probe (Figure 69).

Figure 69: Thermocouple Probe Construction – Counter Tightened Guide Nuts

7) ¼-inch adhesive-backed foam weatherproofing strips are wrapped around the rod just beneath each hex nut pair (Figure 70).

8) 5 Type T glass insulated thermocouples are tightly fastened to the rod with tape, with one junction positioned on each of the foam strips, completing the thermocouple probe (Figure 70, Figure 71).

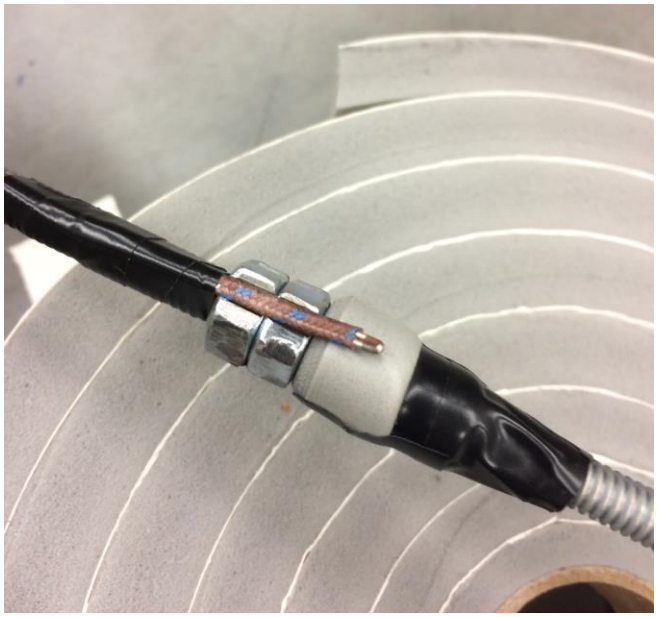

Figure 70: Thermocouple Probe Construction - Transition Joint Fitment

Figure 71: Assembled In-Tank Thermocouple Probe

9) The thermocouple probe is carefully slid into the sensor well (Figure 72: Thermocouple Probe Installation) until the tip contacts the capped end of the copper pipe. The foam strips are compressed as the probe is inserted into the well. This creates outward pressure on each of the thermocouple junctions, ensuring contact with the inner walls of the copper tube, and creating a thermally conductive link to the liquid in the tank for temperature readings.

Figure 72: Thermocouple Probe Installation

APPENDIX C: OPERATIONAL MODE FLOW PATHWAYS

MODE 1: Collector Array–> DHW

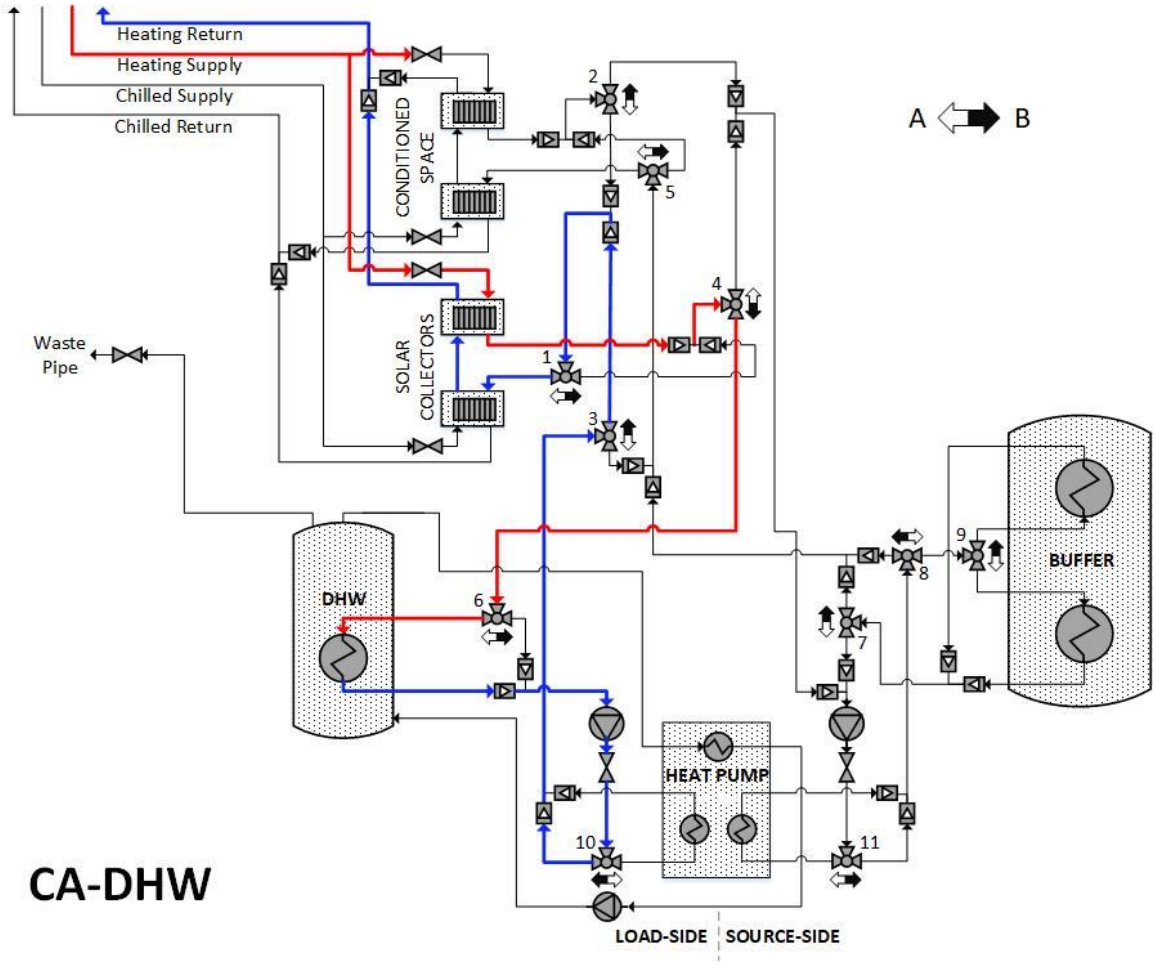

MODE 2: Buffer Storage -> Heat Pump -> DHW

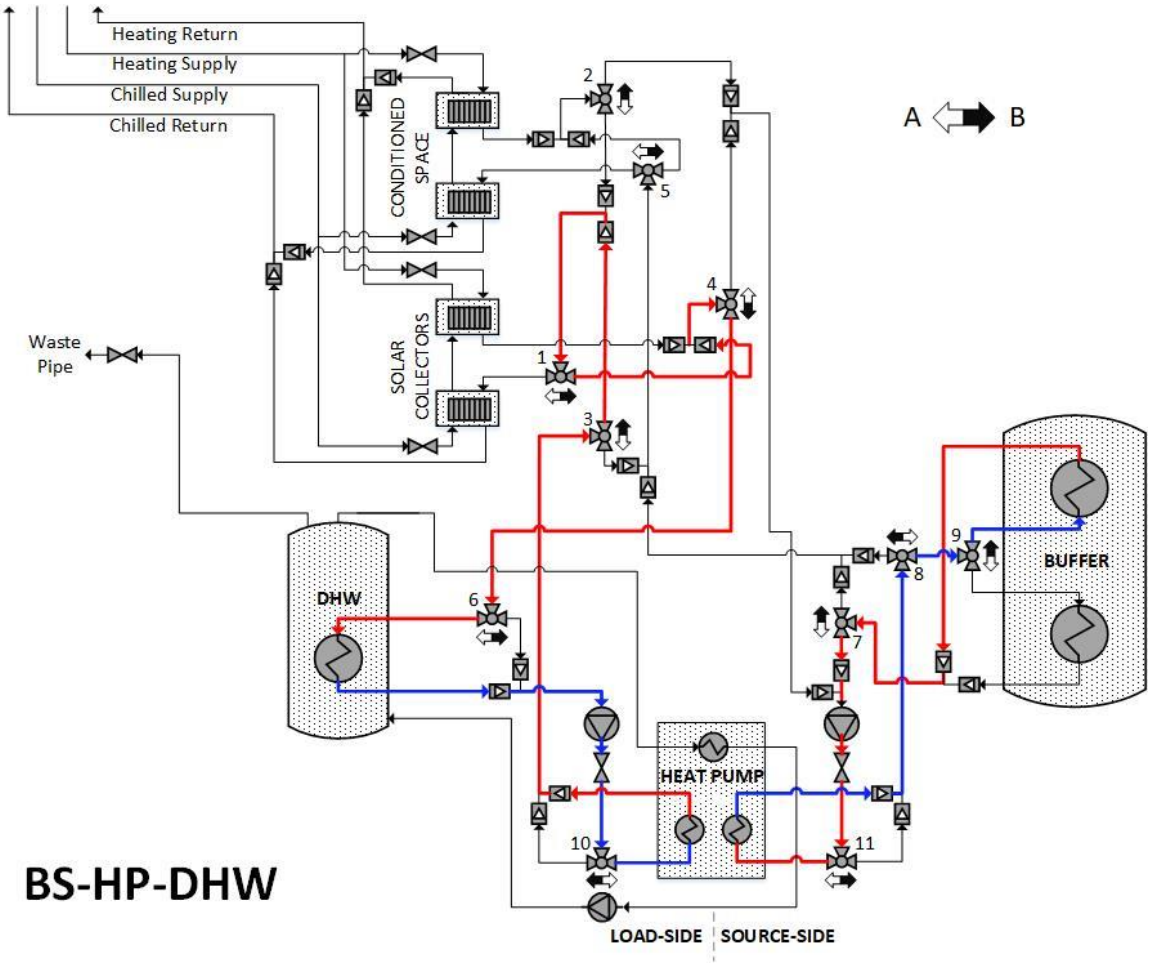

MODE 2*: Buffer Storage *-> Heat Pump -> DHW

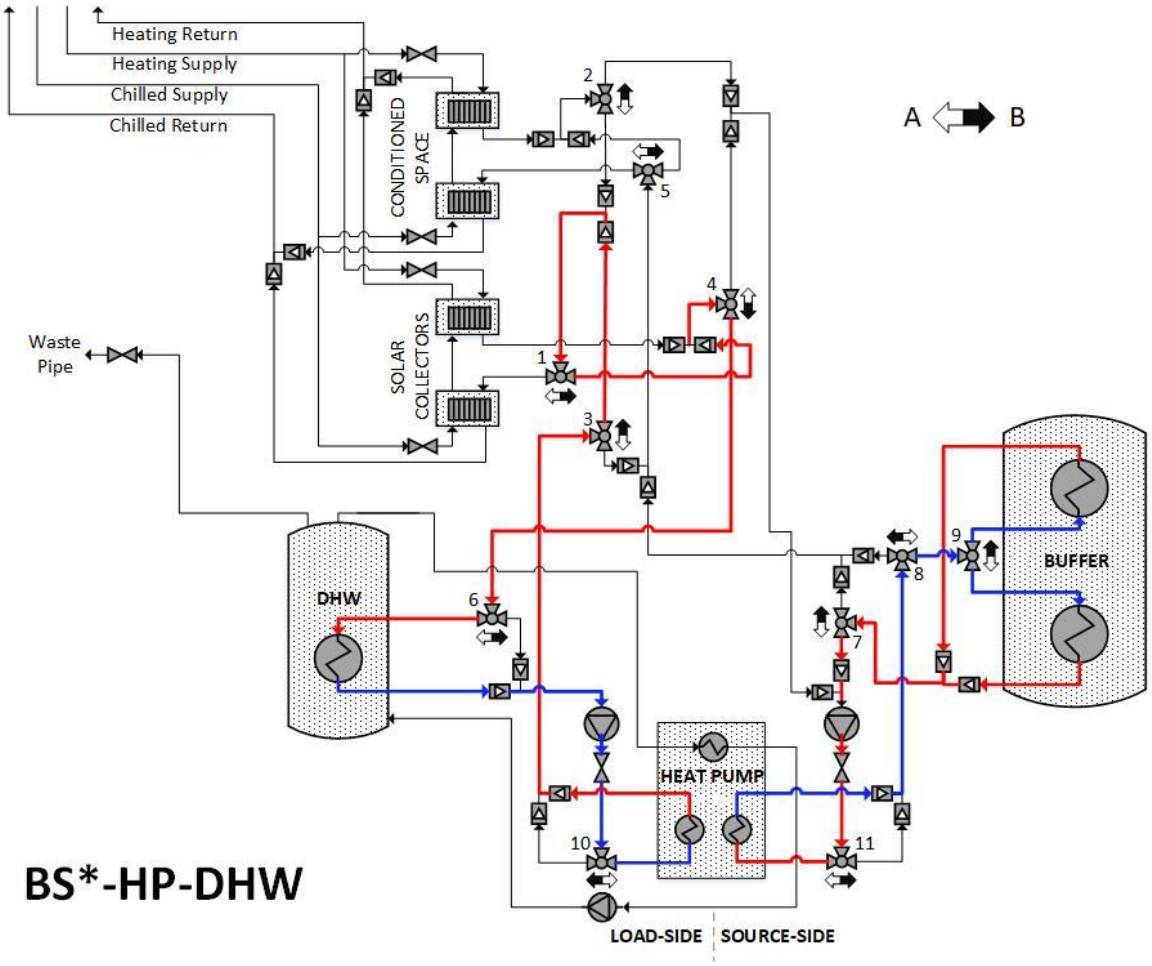

MODE 3: Collector Array -> Conditioned Space

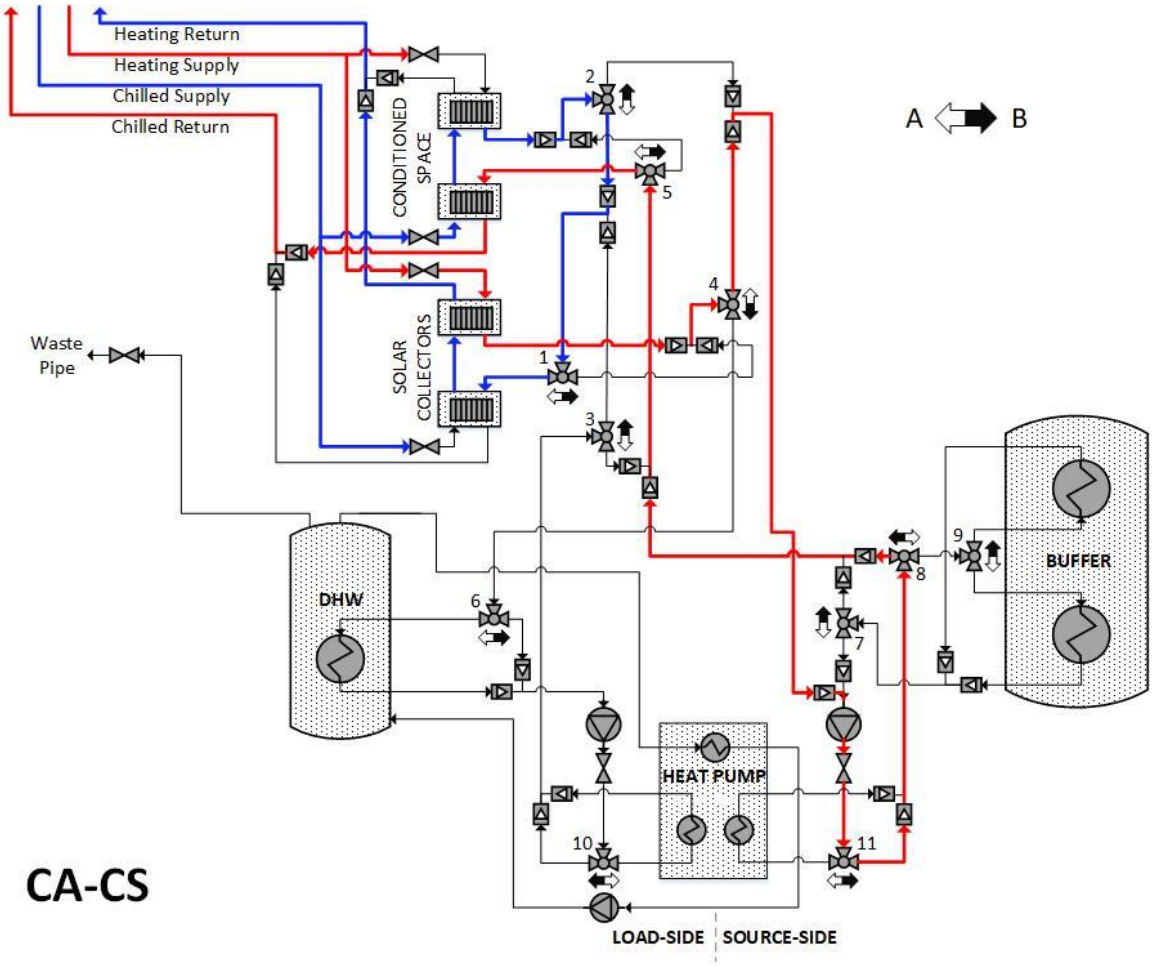

MODE 4: Collector Array -> Heat Pump -> Conditioned Space

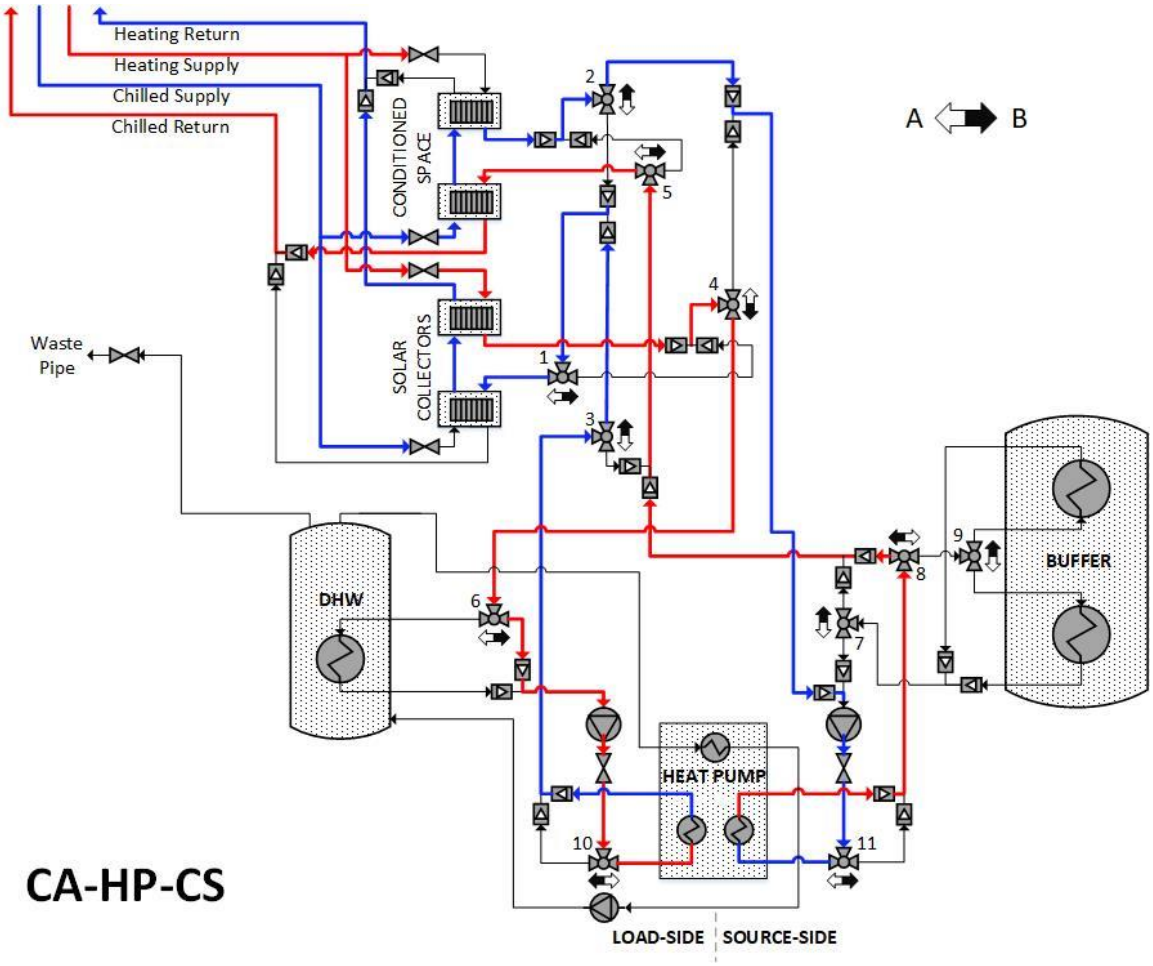

MODE 5: Buffer Storage -> Conditioned Space

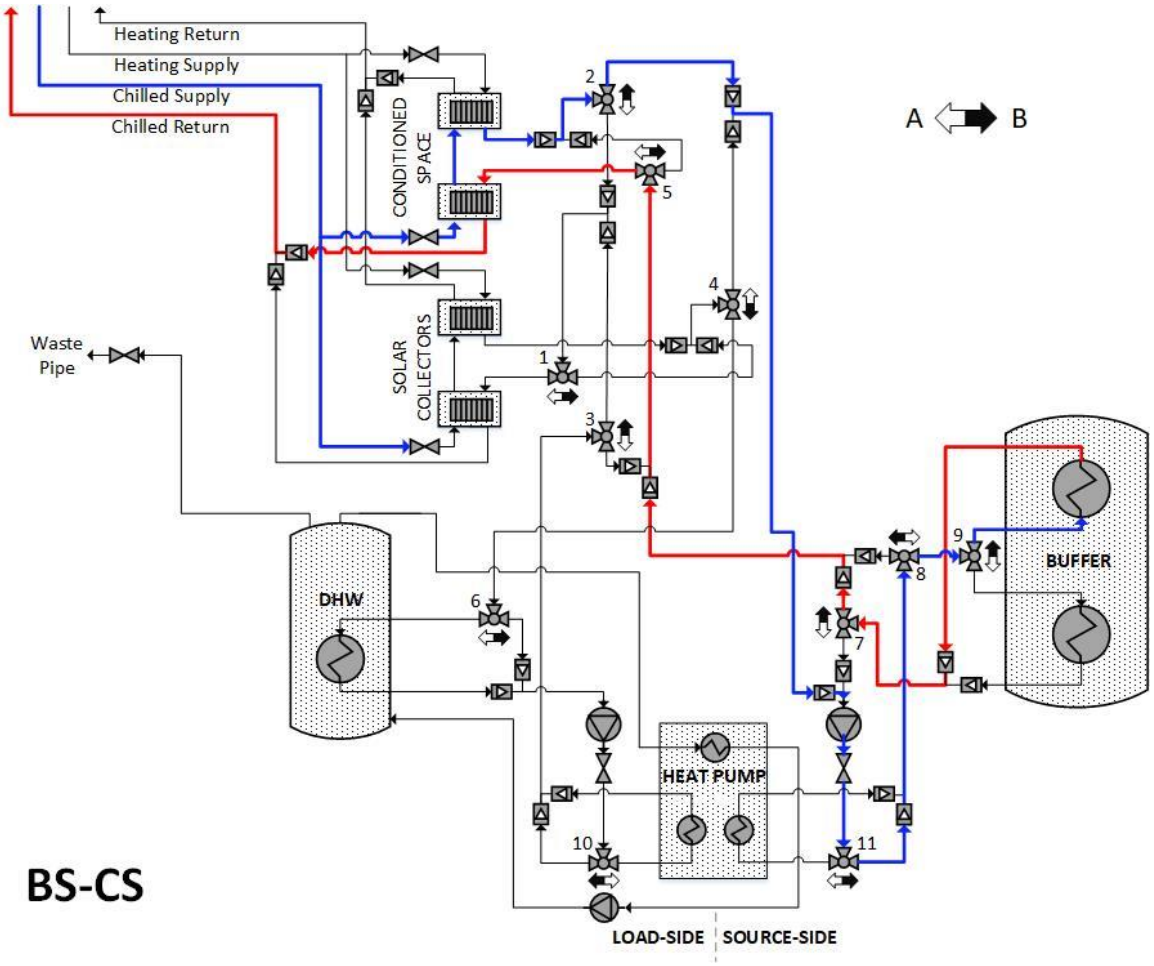

MODE 6: Buffer Storage -> Heat Pump -> Conditioned Space

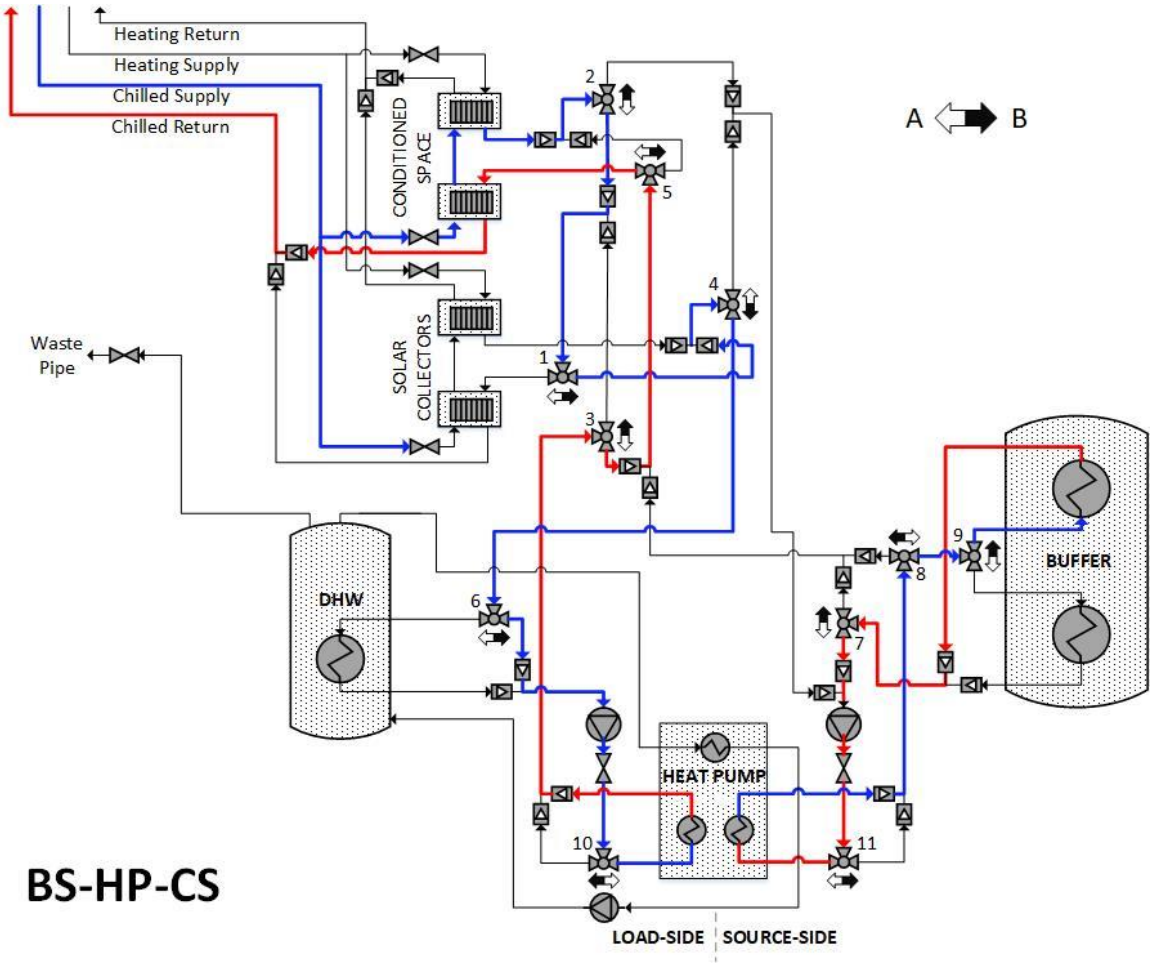

MODE 7: Conditioned Space -> Heat Pump -> DHW

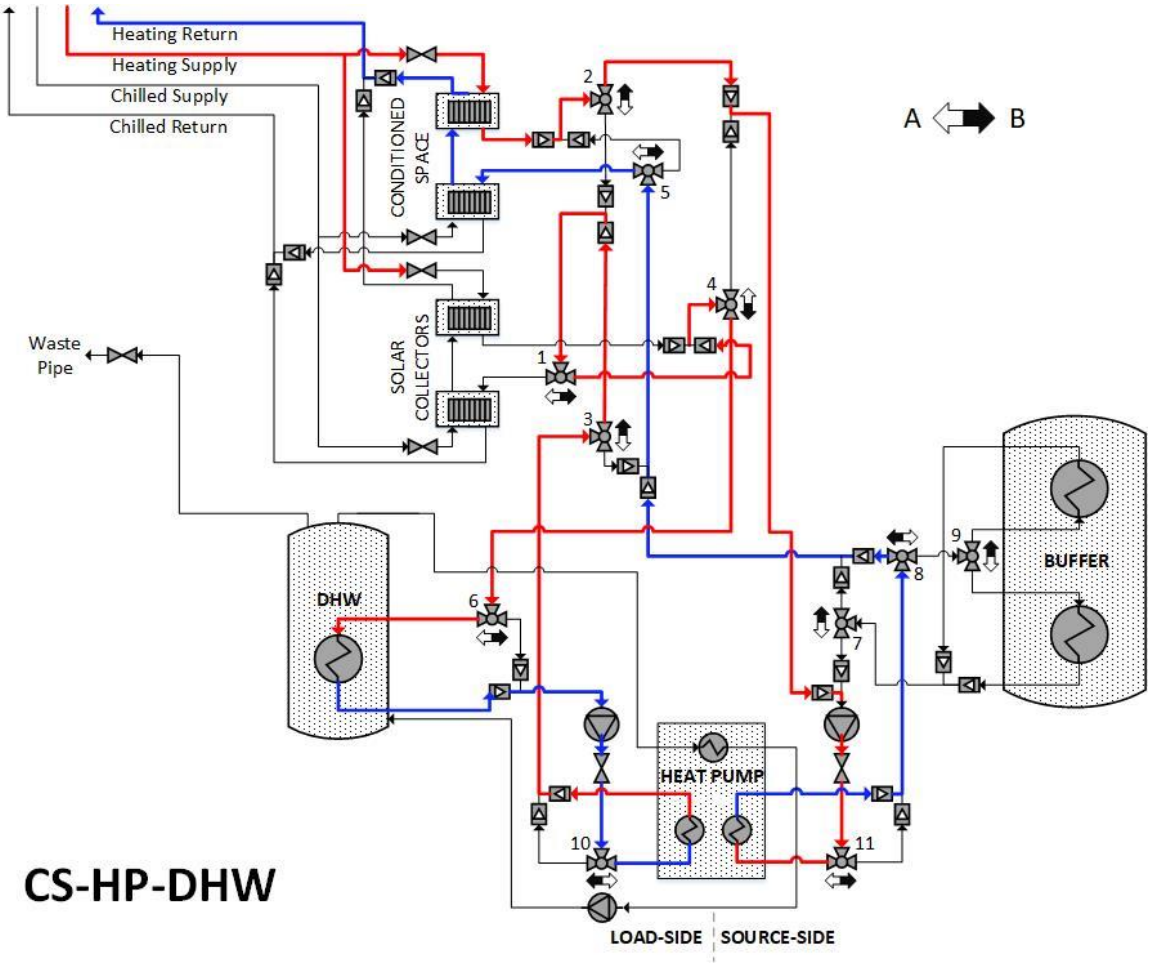

MODE 8: Conditioned Space -> Collector Array

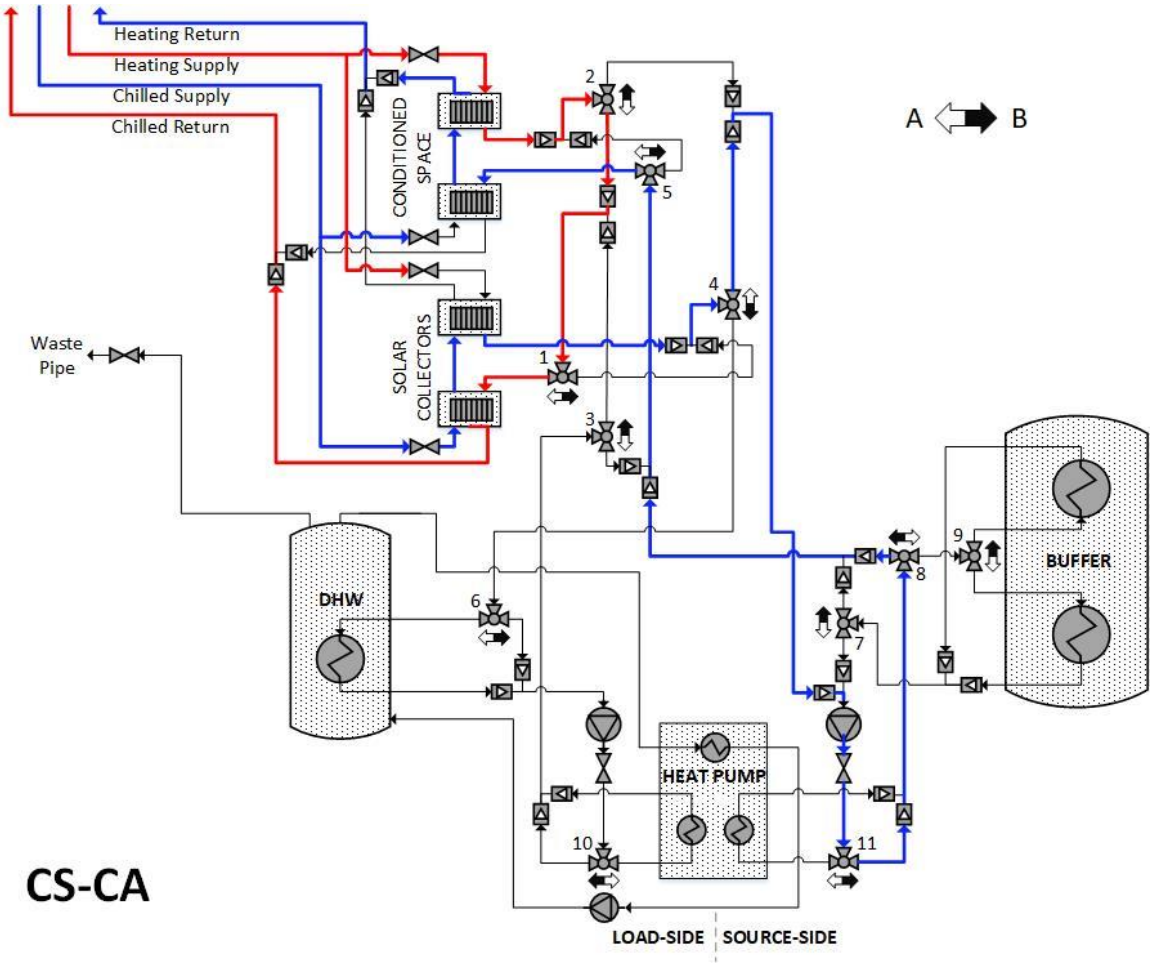

MODE 9: Conditioned Space -> Heat Pump -> Collector Array

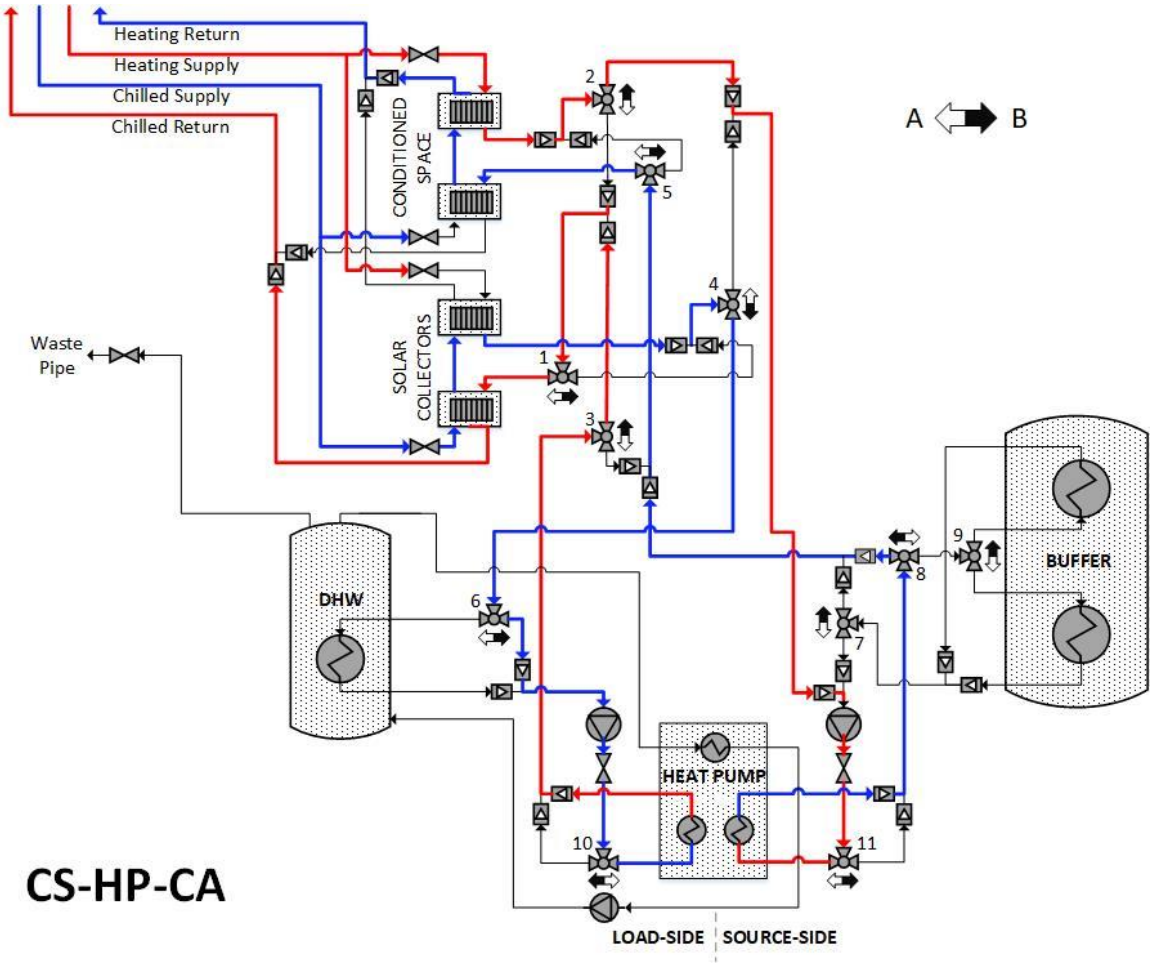

MODE 10: Conditioned Space -> Buffer Storage

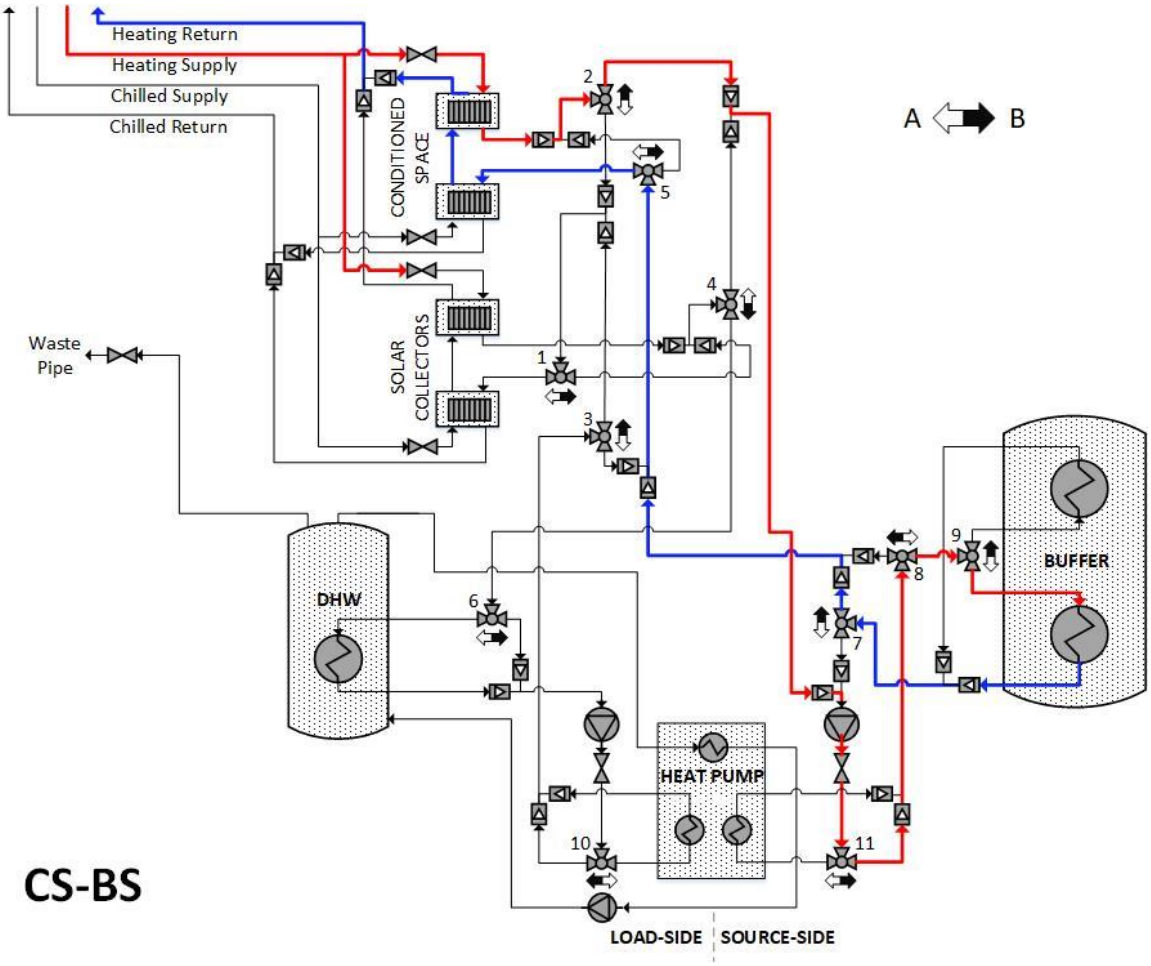

MODE 11: Conditioned Space -> Heat Pump -> Buffer Storage

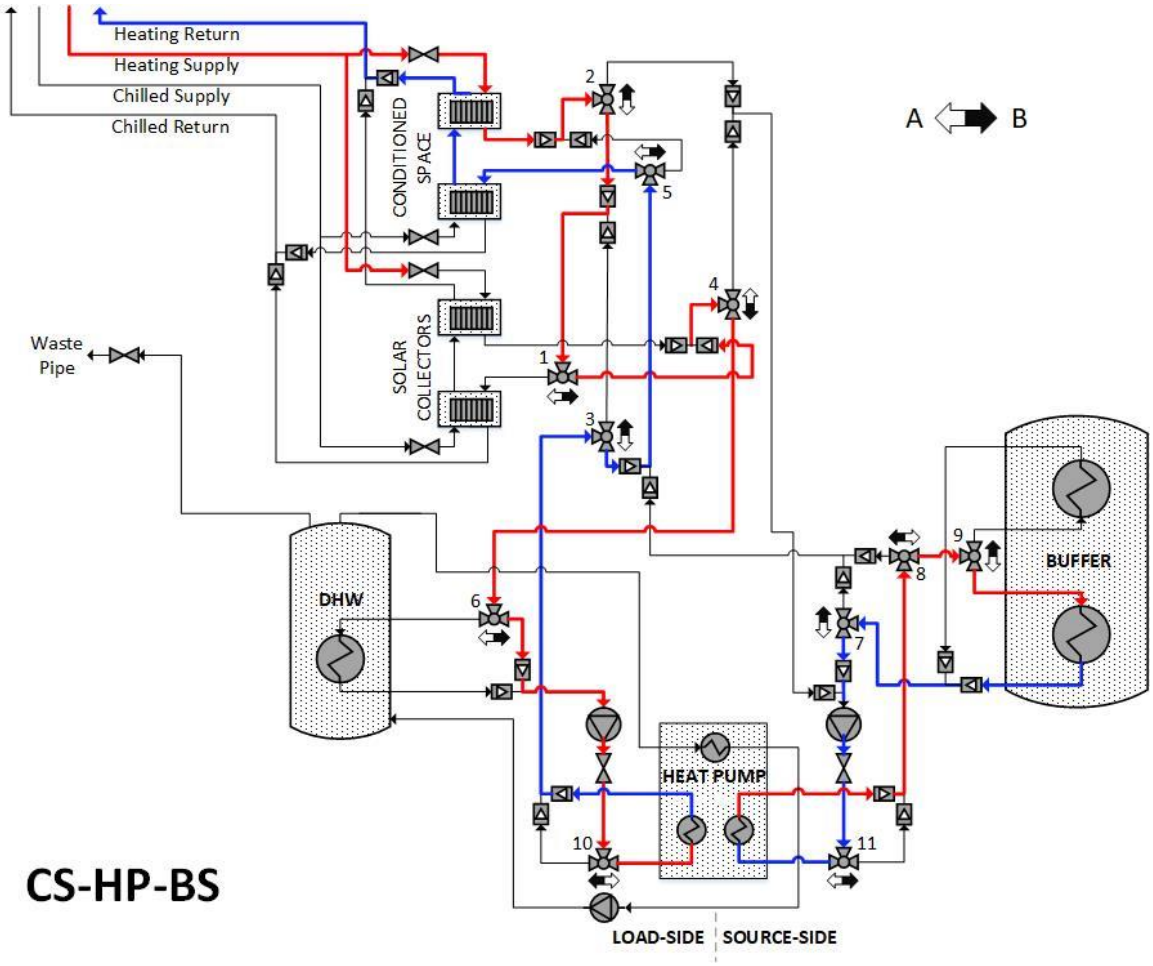

MODE 12: Collector Array -> Buffer Storage

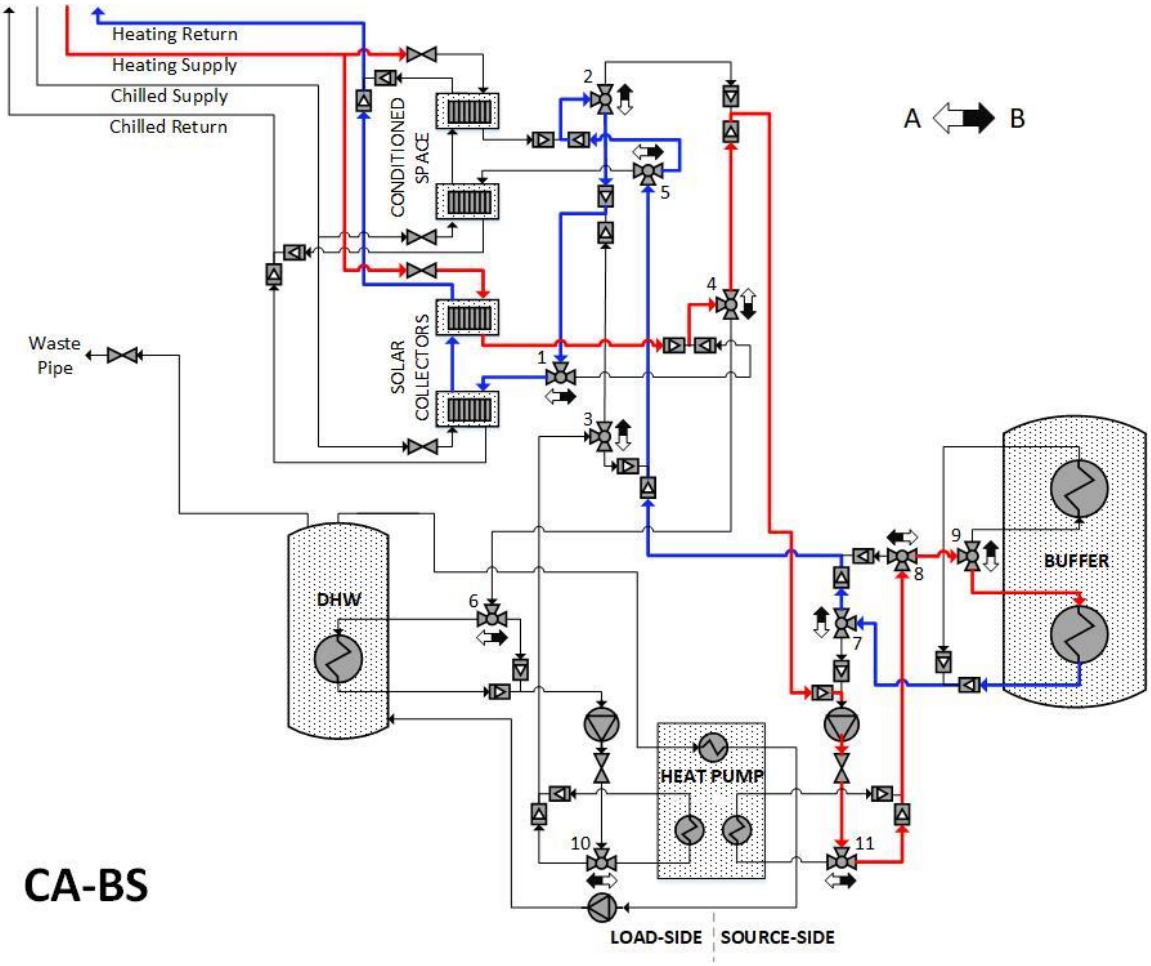

MODE 13: Collector Array -> Heat Pump -> Buffer Storage

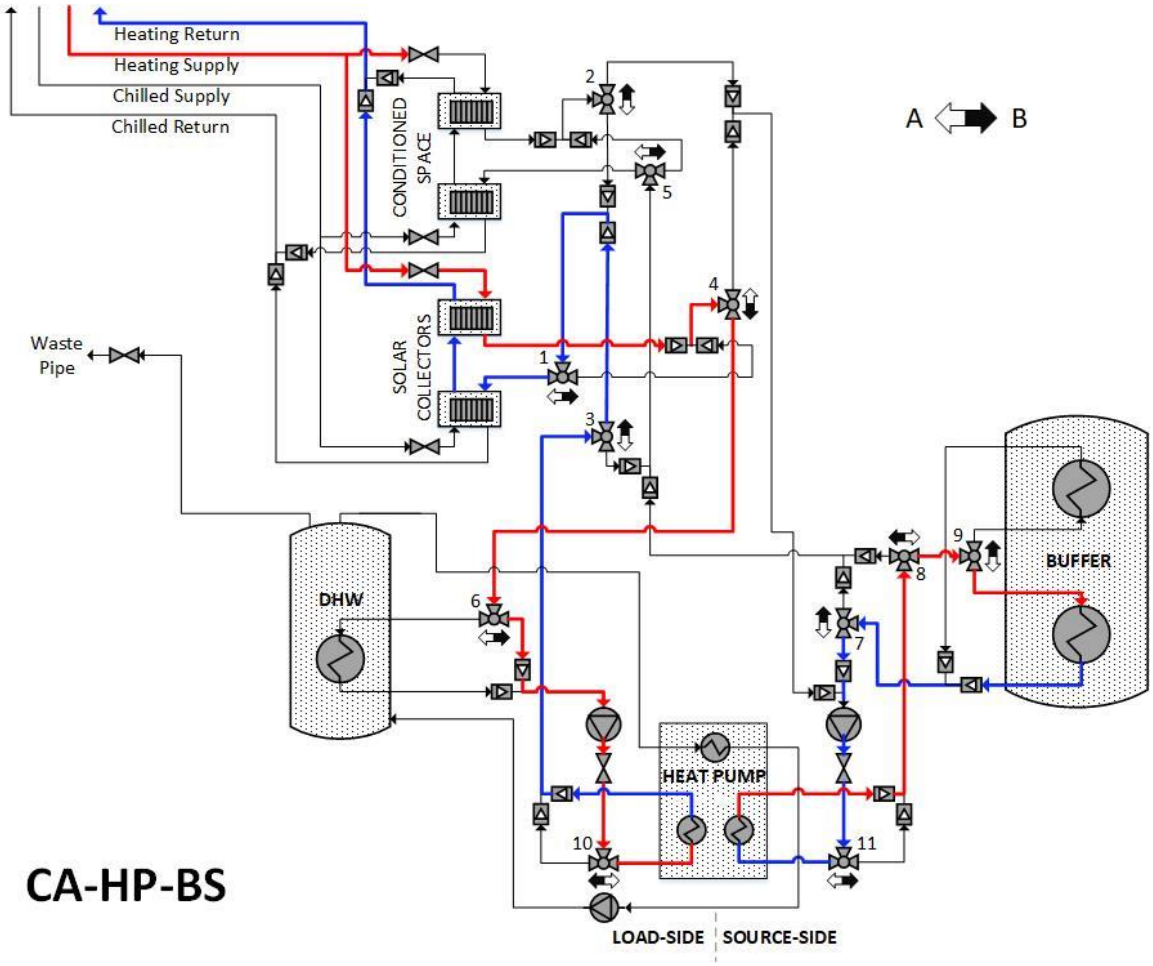

MODE 14: Buffer Storage -> Collector Array

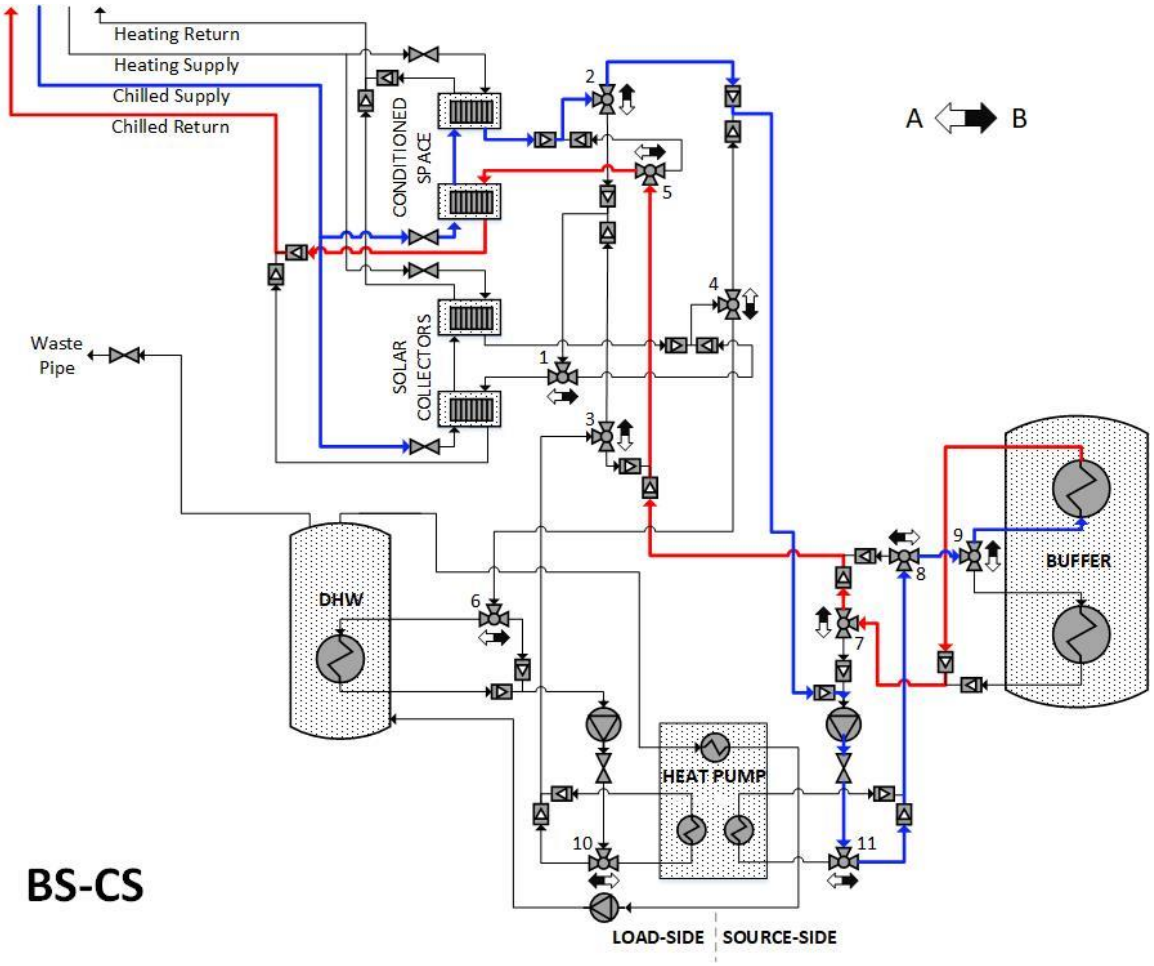

MODE 15: Buffer Storage -> Heat Pump -> Collector Array

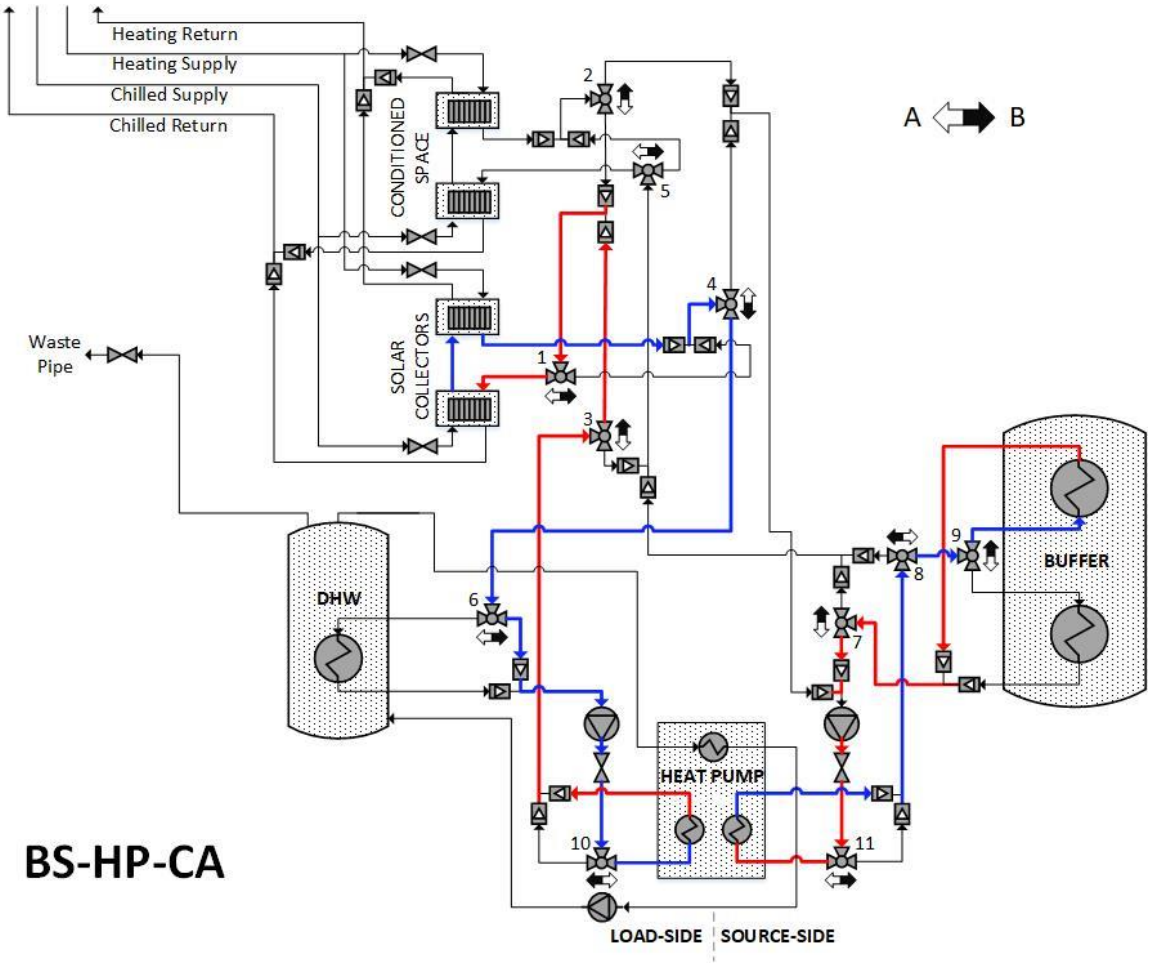

APPENDIX D: EXPERIMENTAL APPARATUS PRESSURE TEST AND FILL PROCEDURE

1. Close all manual valves (S1-S14, D1-D5)
2. Disconnect and remove heat exchangers
3. Manually set electronic 3-way valves to bypass heat exchangers and all major components 1:B, 5:B, 6:B, 8:B, 10:B, 11:B
4. Manually set electronic 2-way valve (16) at DHW discharge to partially open to allow air removal
5. Open non-potable supply valve (S1)
6. Open DHW supply valve (S6) to fill DHW tank
7. When full, manually close DHW discharge valve (16)
8. Open Buffer supply valve (S9) to fill Buffer tank
9. When full, close buffer supply valve (S9), install vertical temperature well, and re-open buffer supply valve (S9)
10. Manually set MISAHP system electronic 3-way valves to isolate pump loops from components (1:B, 5:B, 6:B, 8:B, 10:B, 11:B)
11. Open MISAHP supply valve (S8) to fill pump loop
12. Manually set MISAHP system electronic valve 6:A
13. Manually set MISAHP system electronic valve 8:A
14. Adjust pressure regulators and bleed off excess pressure at drain valves (D1-5) as necessary to set supply distribution to 40psi, and MISAHP piping network to 15psi.
15. Close all ball valves and manually set electronic valves 1:B, 5:B, 6:B, 8:B, 10:B, 11:B

APPENDIX E: EXPERIMENTAL APPARATUS FLUSHING PROCEDURE

1. Connect hose to drain valve (D2) on DHW tank to discharge into laboratory waste pipe
2. Open non-potable supply valve (S1), DHW supply valve (S6)
3. Open DHW drain valve (D2), allow water to flow until discharge is clean
4. Close DHW drain valve (D2)
5. Connect hose to drain valve on Buffer tank (D5) to discharge into laboratory waste pipe
6. Open Buffer supply valve (S9)
7. Open Buffer drain valve (D5), allow water to flow until discharge is clean
8. Close Buffer drain valve (D5).
9. Connect hose to drain valve on MISAHP source side (D4) to discharge into laboratory exit drain
10. Open MISAHP system supply valve (S8)
11. Manually set electronic valve 6:A
12. Open source loop drain valve (D4)
13. Manually set electronic valve 8:A
14. Allow water to flow until discharge is clean
15. Close source loop drain valve (D4)
16. Close MISAHP system supply valve (S8)
17. Connect hose to drain valve on MISAHP load side (D3) to discharge into laboratory exit drain
18. Open MISAHP system supply valve (S8)
19. Manually set electronic valve 8:A
20. Open load side drain valve (D3)
21. Allow water to flow until discharge is clean
22. Close load side drain valve (D3)

APPENDIX F: LABVIEW PROGRAM BLOCK DIAGRAM